TECHNISCHE UNIVERSITÄT MÜNCHEN

Institut für Theoretische Chemie

New aspects of the Jahn-Teller effect in tetrahedral systems: high-order expansions of the electrostatic Hamiltonian and relativistic Jahn-Teller couplings

Daniel Opalka

Vollständiger Abdruck der von der Fakultät für Chemie
der Technischen Universität München zur Erlangung des akademischen Grades eines

Doktors der Naturwissenschaften

genehmigten Dissertation.

Vorsitzender:	Univ.-Prof. Dr. Lukas Hintermann
Prüfer der Dissertation:	1. Univ.-Prof. Dr. Wolfgang Domcke
	2. Univ.-Prof. Moniek Tromp, Ph. D.
	3. apl. Prof. Dr. Ulrich Boesl-von Grafenstein

Die Dissertation wurde am 29.09.2011 bei der Technischen Universität München eingereicht und durch die Fakultät für Chemie am 28.11.2011 angenommen.

Contents

1 Introduction

The Jahn-Teller (JT) effect is intimately connected to the concept of potential-energy (PE) surfaces, which has its origin in the Born-Oppenheimer approximation [1, 2]. In 1937, based on the concept PE surfaces, H. A. Jahn and E. Teller formulated the Jahn-Teller theorem [3, 4]:

> "A configuration of a polyatomic molecule for an electronic state having an orbital degeneracy cannot be stable with respect to all displacements of the nuclei unless in the original configuration the nuclei all lie on a straight line."

As is well known, this theorem and its consequences play an eminently important role in molecular and solid-state physics [5]. The JT effect is an essential concept in coordination chemistry, for example, to explain static distortions in transition metal complexes. The modern interpretation of the JT effect summarizes all symmetry-related vibronic coupling phenomena in molecules, molecular complexes and solids under the terms JT and pseudo-JT effect. Despite its venerable history of more than 70 years [3, 6], the JT effect continues to be an active area of research in chemistry and solid-state physics [5–9].

In the context of vibronic coupling theory, the Jahn-Teller effect can be considered as a special case of conical intersections (CIs) which are induced by the high spatial symmetry of a molecule [3]. Some of the key dynamical processes in photochemistry and photobiology are related to CIs. Radiationless energy conversions in polyatomic molecules generally proceed through CIs [10]. Since the construction of complete multi-dimensional PE surfaces including CIs in large molecules is often infeasible due to the complexity of the electronic-structure problem, theoretical descriptions usually resort to vibronic coupling and JT models [11], which are based on low-order Taylor expansions of the potentials at a reference geometry of high symmetry. According to standard JT theory [5], the JT Hamiltonians arise from a polynomial expansion of the PE surface in symmetry-adapted coordinates up to second order.

Because of the simple mathematical structure of the JT Hamiltonians, they are often employed for the simulation of non-adiabatic quantum dynamics in molecular spectroscopy and photochemistry [9]. For example, standard JT theory has been successfully applied in the analysis of a vast number of molecular photoelectron spectra. Important developments during recent decades have been the computation of linear and quadratic JT coupling constants from first principles [11–15] and the systematic treatment of multi-mode JT couplings [11, 16, 17].

The description of very pronounced JT distortions and large-amplitude motions requires PE surfaces with a large range of validity. The best investigated example is the $E\times e$ JT effect in molecules with three identical atoms in an equilateral triangular arrangement. In this case, the degeneracy of a doubly degenerate electronic state of E symmetry is lifted by a nuclear coordinate of the same symmetry. The first systematic treatment of the $E \times e$ JT problem with explicit consideration of large-amplitude motions was developed by Viel and Eisfeld [18] for the ammonia cation. It was shown that a systematic expansion of the electronic potentials to higher order can significantly improve the quality of JT PE surfaces [18]. This approach is limited to dihedral point groups and cannot be applied to JT systems of tetrahedral and cubic symmetry, which exhibit a particularly rich variety of JT phenomena.

The methane cation in its T_2 electronic ground state, for example, exhibits a very strong $T_2 \times (e + t_2 + t_2)$ JT effect [19–21]. He I photoelectron spectra of CH_4 have been reported by Rabalais et al. [22] and Potts and Price [23]. Although both groups published almost identical spectra, there are remarkable differences in the assignments. Recent experiments using pulsed-field-ionization zero-kinetic-energy spectroscopy revealed an extremely high spectral line density and indicated that the hydrogen atoms exchange by tunneling on a picosecond timescale [24, 25]. A theoretical analysis of the photoelectron spectrum of methane thus requires a PE surface including at least the eight JT active degrees of freedom. Additionally, it is particularly important for quantum dynamical simulations to take symmetry constraints into account, that is, the PE surface must be invariant under exchange of the hydrogen atoms. It is a goal of the present work to devise a method for the systematic construction of multi-sheeted JT PE surfaces, taking into account the invariance under permutation of identical nuclei.

In solid-state physics, the JT effect in cubic symmetry is of utmost importance. Contrary to molecular systems, large-amplitude motions are often of minor importance, since distortions and vibrational amplitudes of the atomic centers in crys-

tals are usually small. On the other hand, cooperative effects such as spin phase-transitions and magnetism arise from the periodic structure of solids. The microscopic origin of the electron-phonon coupling in doped rare earth perovskites, which exhibit colossal magnetoresistance, is considered to be a consequence of the JT effect [26, 27]. Another example of technological importance which may involve the JT effect is the high-temperature superconductivity in cuprates and alkali-metal doped fullerides [5, 28]. A currently evolving research field, which combines molecular electronics and spintronics, are molecular magnets [29]. Molecular magnets are typically composed of one or a cluster of metal atoms, embedded in an organic shell. The goal is to control the alignment of the electronic spin for the construction of molecular devices [29, 30]. Besides the JT effect, the electronic spin plays a crucial role in all these examples and it is an open question, how the vibronic coupling effects interfere with the electronic spin.

Recently, JT Hamiltonians including spin-orbit (SO) coupling beyond the zeroth order in the vibrational normal mode expansion have been developed for tetrahedral and cubic systems [31–33]. Based on these model Hamiltonians, the influence of SO coupling on vibronic spectra can be addressed beyond the zeroth-order approximation for the first time. A well-suited series of tetrahedral systems with increasing SO coupling are the $X_4{}^+$ (X = P, As, Sb, Bi) cluster cations of the fifth main group. It has been found that the ionized clusters exhibit very strong JT effects, involving the e and t_2 modes in the ^2E ground state and the $^2T_2$ first excited state of the radical cations. Depending on the electronic state, there exist $E \times t_2$, $E \times t_2$, $T_2 \times e$ and $T_2 \times t_2$ JT effects in these systems exhibiting PE surfaces of considerable topographical complexity. In addition, effects of (zero-order) SO splittings were identified in the spectra of As_4^+ and Sb_4^+ [34–38].

The material in the following chapters of this thesis is organized as follows: The purpose of the second chapter is to introduce the most important concepts for the construction of symmetry-invariant polynomials and Hamiltonians, the description of relativistic SO coupling in JT systems and the treatment of nuclear dynamics for the simulation of photoelectron spectra. The third chapter is devoted to the development of high-order expansions of JT PE surfaces in tetrahedral systems using the algebraic methods from Chapter 2. A prototypical example of a tetrahedral JT system is the methane cation discussed in Chapter 4. The work encompasses all steps of the *ab initio* construction of a symmetry-adapted PE surface for the methane cation in its triply degenerate ground state. In Chapter 5, a systematic study

of relativistic SO coupling effects in X_4^+ (X = P, As, Sb, Bi) clusters is presented. Effects of vibronic coupling and SO coupling in photoelectron spectra are analyzed on the basis of *ab initio* calculations.

2 Theoretical background and methods

In this chapter, the fundamental problem of analytic representations of potential-energy (PE) surfaces is addressed. Accurate PE surfaces are an essential requirement for a quantum dynamical description of the nuclear motion in molecules. Modeling multi-sheeted PE surfaces in more than three dimensions of nuclear motion still represents a major challenge in theoretical chemistry. In all stages of the development of PE surfaces and their applications, the choice of the coordinates to represent the molecular geometry is of outstanding importance. The present theoretical approach focuses, apart from the inevitable discussion of appropriate coordinates, on the treatment of symmetry, using concepts from group theory and the theory of invariant polynomials. The theory of spin-orbit coupling in Jahn-Teller systems and an efficient wave-packet propagation scheme, which has been used for the simulation of photoelectron spectra, are described in the last two sections.

2.1 The Born-Oppenheimer approximation

Potential-energy surfaces arise from the Born-Oppenheimer (BO) approximation in the mathematical formulation of quantum mechanics. The BO approximation is the most important approximation in computational electronic-structure theory [1, 2]. The fundamental idea of the BO approximation and its variants is the separation of the motions of nuclei and electrons. This is motivated by the large difference of masses between electrons and nuclei and is generally interpreted as instantaneous relaxation of the electronic structure under displacements of the nuclei. Though widely attributed to the initial work of Born and Oppenheimer [1], modern formulations of the BO approximation usually follow the derivation Born and Huang published more than 30 years later [2]. According to the BO approximation, PE surfaces can be understood as functions of the nuclear coordinates corresponding to

the total energy of the system in one particular electronic state. The nuclei of a given molecule may be considered to move on one (or several) of these surfaces.

The molecular Schrödinger equation can be written as the eigenvalue problem

$$H\Psi_j(\mathbf{r},\mathbf{R}) = E_j\Psi_j(\mathbf{r},\mathbf{R}) \qquad j = 1, 2\ldots \tag{2.1}$$

where j enumerates the electronic/vibrational/rotational eigenstates and $\mathbf{r}$ and $\mathbf{R}$ denote the electronic and nuclear coordinates, respectively. On the nonrelativistic level of theory, the Hamiltonian operator H is the sum of five operators,

$$H = T_{\mathrm{nu}} + T_{\mathrm{el}} + V_{\mathrm{nn}} + V_{\mathrm{ee}} + V_{\mathrm{ne}}, \tag{2.2}$$

where T_{nu} and T_{el} are the kinetic-energy operators acting on the nuclear and electronic coordinates, respectively. The symbols V_{nn}, V_{ee} and V_{ne} denote the (Coulomb) electron-electron, nucleus-nucleus and nucleus-electron interaction operators. It is the term V_{ne}, which prevents the exact separation of H into an electronic (H_{el}) and a nuclear (H_{nu}) Hamiltonian and thus solutions of the form $\Psi(\mathbf{r},\mathbf{R}) = \chi(\mathbf{R})\psi(\mathbf{r})$ do not exist.

Instead of solving Eq. (2.1), virtually all electronic-structure algorithms compute approximate solutions of the *electronic* Schrödinger equation

$$\begin{aligned} H_{\mathrm{el}}\psi_i(\mathbf{r},\mathbf{R}) &= W_i(\mathbf{R})\psi_i(\mathbf{r},\mathbf{R}), \\ H_{\mathrm{el}} &= T_{\mathrm{el}} + V_{\mathrm{nn}} + V_{\mathrm{ee}} + V_{\mathrm{ne}}, \end{aligned} \tag{2.3}$$

for a fixed nuclear geometry. The $\psi_i(\mathbf{r},\mathbf{R})$ are called the electronic WFs and represent the solutions of the electronic Schrödinger equation. The eigenfunctions $\psi_i(\mathbf{r},\mathbf{R})$ depend only *parametrically* on the nuclear positions and there exists an independent eigenvalue equation for every value of $\mathbf{R}$. The eigenvalues in ascending order, which are functions of the nuclear coordinates, represent the adiabatic PE surfaces. This is the only unambiguously defined representation of multi-sheeted PE surfaces.

Solutions of the Schrödinger equation (2.1) can be expressed in terms of the electronic WFs $\psi_j(\mathbf{r},\mathbf{R})$:

$$\Psi(\mathbf{r},\mathbf{R}) \approx \sum_{i=1}^{N} \chi_i(\mathbf{R})\psi_i(\mathbf{r},\mathbf{R}) = \langle \boldsymbol{\chi} \mid \boldsymbol{\psi} \rangle \,. \tag{2.4}$$

The expansion coefficients $\chi_i(\mathbf{R})$ depend on the nuclear coordinates and are also referred to as nuclear WFs [39]. This is the key step of the BO approximation and in the limit of a complete set of eigenstates ($N \to \infty$), Eq. (2.4) is exact. For practical applications of vibronic coupling theory, N is usually restricted to a small number of strongly coupled electronic states, neglecting the influence of other electronic states. In the basis defined by (2.4), the following expression is obtained for the nuclear Schrödinger equation.

$$[T_{\mathrm{nu}} + H_{\mathrm{el}}] \sum_{i=1}^{N} \chi_i(\mathbf{R})\psi_i(\mathbf{r},\mathbf{R}) = \mathbf{E} \sum_{i=1}^{N} \chi_i(\mathbf{R})\psi_i(\mathbf{r},\mathbf{R}) \tag{2.5a}$$

$$[T_{\mathrm{nu}}\mathbf{I} + \mathbf{W} - \mathbf{\Lambda}]\, \chi = \mathbf{E}\chi. \tag{2.5b}$$

Here, $\mathbf{I}$ denotes the $N \times N$ identity matrix and $\mathbf{E}$ is the (diagonal) matrix of adiabatic energies of the electronic Schrödinger equation (2.1). The matrix $\mathbf{\Lambda}$ arises from the action of the nuclear kinetic-energy operator on the electronic WFs and is defined as the *nonadiabatic coupling term* (NACT).

The latter conventionally is split into a sum of two contributions

$$\Lambda_{ij} = \frac{1}{2M} \left(2F_{ij}\nabla + G_{ij}\right) \tag{2.6}$$

where M is the mass in atomic units, $F_{ij} = \langle \psi_i | \nabla | \psi_j \rangle$ is the *derivative coupling vector* and $G_{ij} = \langle \psi_i | \nabla^2 | \psi_j \rangle$ is called the *scalar coupling* matrix. In the *adiabatic* BO approximation, all NACTs are neglected. It is well known that in the vicinity of CIs, NACTs become important in the nuclear Schrödinger equation. Namely, the *derivative coupling vector*, originating from the nuclear kinetic-energy operator, contributes significantly to the molecular energy, invalidating the adiabatic BO approximation.

The form of the nuclear Schrödinger equation given above, i. e. an expansion in the eigenfunctions of the electronic Schrödinger equation, is defined as the adiabatic representation. There exist, however, a number of common approximations and variations of the nuclear Schrödinger equation (2.5). For $\mathbf{\Lambda} = 0$, Eq. (2.5) simplifies to the adiabatic approximation. If only the diagonal elements G_{ii} are retained in the expression of Λ_{ij}, Eq. (2.5) is called the Born-Huang approximation [2]. A particularly convenient form is obtained when Eq. (2.5) is transformed into a basis in which $\mathbf{\Lambda}$ is zero or negligibly small. The underlying principle is the invariance of

the expanded WF $\Psi(\mathbf{r}, \mathbf{R})$ in Eq. (2.4) under affine transformations

$$\sum_{i=1}^{N} \chi_i(\mathbf{R})\psi_i(\mathbf{r}, \mathbf{R}) = \langle \mathbf{U}\boldsymbol{\chi} \,|\, \mathbf{U}\boldsymbol{\psi} \rangle = \langle \mathbf{c} \,|\, \boldsymbol{\phi} \rangle \,. \tag{2.7}$$

In order to keep the electronic WFs orthonormal, we assume the transformation $\mathbf{U}$ to be unitary. The transformed electronic (ϕ_i) and nuclear (c_i) basis functions are the WFs of a *diabatic* representation. With a suitable choice of $\mathbf{U}$, the nuclear Schrödinger equation can be recast into

$$\begin{aligned} [T_{\mathrm{nu}}\mathbf{I} + \mathbf{V}]\,\mathbf{c} &= \mathbf{E}\mathbf{c} \\ \mathbf{V} &= \mathbf{U}\mathbf{W}\mathbf{U}^{\dagger}. \end{aligned} \tag{2.8}$$

Loosely speaking, in an adiabatic representation of the nuclear Schrödinger equation, the PE surfaces are coupled by the nuclear kinetic-energy operator, whereas in the diabatic picture, the PE operator couples different electronic states. A set of diabatic PE surfaces is then described as a matrix with eigenvalues corresponding to the adiabatic electronic energies of the considered electronic states.

Although it was shown by Truhlar and coworkers [40, 41] that strictly diabatic PE surfaces, where all NACTs are exactly zero, do not exist in polyatomic molecules, the diabatic representation offers many advantages over an adiabatic treatment. Most importantly, the diabatic PE matrix can be chosen to be a continuously differentiable function of the nuclear coordinates, even in the vicinity of conical intersections. Moreover, in the diabatic representation the nuclear WFs do not carry a geometric phase [42, 43] which is a substantial simplification for propagations of the nuclear WF. In vibronic coupling theory, diabatic potentials are often constructed from the adiabatic PE energies which are fitted to an analytic model potential.

2.2 Symmetry and invariant theory

The most powerful theory to exploit symmetry in quantum mechanics is provided by group theory. Traditionally, molecular systems are described by 32 molecular point groups which were discussed exhaustively in the literature (see [44] and references therein). Many of the molecular point groups are isomorphic with one of the abstract groups. From the algebraic point of view, there exist only 17 different molecular symmetry groups. Considering the matrix groups of irreducible representations, the

number of different groups further reduces to 14 [45, 46]. Since the treatment of molecular symmetry can always be based on matrix representations with respect to a vector space of electronic or nuclear basis functions, the development of symmetry-adapted approximations to PE surfaces based on abstract group theory is a general and versatile approach.

The electronic energy of an isolated molecule depends on its geometry—the shape of the molecule. The first task in the construction of any PE surface is thus to select a suitable basis for the representation of the nuclear geometry, which is closed under the symmetry group and allows an unambiguous (possibly non-linear) mapping of the molecular shape to the value of a function. Due to symmetry, identical molecular shapes must result in the same function value. In the language of algebra, the PE surface is invariant with respect to the Euclidean group of isometries $E(3)$, the semi-direct product group of the translation and orthogonal group in the three spatial dimensions $T(3) \rtimes O(3)$ ($\rtimes$ denotes the semi-direct product of two groups). [1]

Additionally, polyatomic systems that include identical atoms are subject to permutation symmetry of like nuclei. The symmetry properties of n identical nuclei are described by the symmetric group S_n. In case of several sets of identical nuclei, the resulting group is the direct product group of the symmetric groups of the different sets (the permutations of like nuclei within different sets commute) [47]. The full symmetry group of a molecular system is thus given by

$$G = T(3) \rtimes O(3) \times S_{n_1} \times S_{n_2} \times \ldots = E(3) \times S_{n_1} \times S_{n_2} \times \ldots \tag{2.9}$$

The construction of an analytic PE surface is closely related to finding a set of invariant functions which are suitable to reproduce the function of interest. Ideally, these functions provide an approximation space that is complete (for the type of functions used), efficiently evaluated and can be improved systematically. In the present work, the theory of invariant polynomials was employed to achieve these goals. The construction of arbitrary invariant functions based on invariant polynomials is straightforward and invariant polynomials may thus be considered as the fundamental building blocks of any construction of symmetry-adapted functions.

[1] The orthogonal group $O(3)$ exhibits a direct product structure of the special orthogonal group $SO(3)$ of proper rotations and the group of order 2 which is sometimes denoted as inversion group in the chemical literature [47].

A polynomial p is invariant with respect to a group G if the equation

$$\sigma \circ p = p \tag{2.10}$$

holds for all $\sigma \in G$. The action of a group G on a polynomial p is defined by the inverse action on the function arguments $\mathbf{v}$

$$\sigma \circ p(\mathbf{v}) \equiv p(\sigma^{-1}\mathbf{v}) \qquad \sigma \in G. \tag{2.11}$$

Evaluating the group action on a polynomial thus requires the definition of a basis and the corresponding representation of the group elements as matrices. Due to the very different properties of the translation and rotation group (both are infinite continuous groups) and the finite permutation groups, it is helpful to separate the problem of permutational invariance from the rotation-translation symmetry. In fact, the $E(3)$ symmetry can be easily included into permutation-invariant functions by choosing suitable primitive basis functions for the representation of the permutation group. Changing the basis, however, does not change the invariant polynomials. As the permutation symmetry can be treated independently of the rotation and translation symmetry, the following discussion is entirely devoted to the permutation problem. In some cases it is even advantageous to work with a basis that is not rotationally invariant, e. g. to simplify the expression for the quantum mechanical kinetic-energy operator of a molecule. The objective of constructing a symmetry-adapted analytic PE surface model is thus converted into the algebraic problem of finding a set of functions that is invariant under the permutation of identical nuclei.

Invariant polynomials under the action of a discrete linear group $G \subset GL(n)$ are most easily computed by means of the *Reynolds operator* [48]

$$R(p) = \frac{1}{\mid G \mid} \sum_{\sigma \in G} \sigma \circ p \tag{2.12}$$

where p is an arbitrary monomial. The Reynolds operator, by definition, acts linearly on the coordinates of the monomial p and averages its images over the entire group orbit. Due to its idempotent property, the Reynolds operator is also known as projection operator in the chemical literature [44]. In principle, an arbitrary number of (homogeneous) invariant polynomials can be obtained by successive application of the Reynolds operator to a series of monomials. However the success and efficiency

strongly depends on the choice of the coordinates and monomials. In general, all monomials up to the desired degree must be considered to ensure that all invariant polynomials are found. Such a calculation in most cases yields many linearly dependent (i. e. redundant) invariants which have to be eliminated subsequently. From the definition (2.12) it is obvious that the procedure is limited to groups of rather low order. The computational cost for the symmetric group S_n scales with the factorial of the number of identical nuclei n and the number of monomials that have to be included for an expansion of degree d in m coordinates is given by the rising factorial

$$\binom{d+m}{d} = \frac{1}{d!}(m+1)^{d-1} \tag{2.13}$$

and indicates additional exponential scaling in the degree of the expansion.

For invariants of high degree, the construction of permutationally invariant polynomials in the $E(3)$ invariant functions can be substantially simplified by a well-known theorem of classical invariant theory due to Noether, which states that the G-invariant subalgebra $\mathbb{R}[V^\Gamma]^G$ over a vector space V^Γ is finitely generated by polynomials of maximum degree $|G|$ [49, 50]. Here, Γ indicates the particular group representation associated with the coordinates of the underlying vector space and $|G|$ is the number of elements in the matrix group Γ. Many groups which are relevant in physics and chemistry, however, have considerably lower degree bounds and the term "generating" or "fundamental" set of polynomials refers to a complete set of polynomials that generates all invariant polynomials.

According to a theorem of Hochster and Roberts, it is known that any linearly reductive group G over the field of real numbers is Cohen-Macaulay and $\mathbb{R}[V^\Gamma]^G$ is generated as a module over a set of invariant and homogeneous polynomials $\mathbb{R}[f_1, \ldots, f_n]$ [48].

$$\mathbb{R}[V^\Gamma]^G = \bigoplus_{k=1}^{m} \mathbb{R}[f_1, \ldots, f_n] g_k \tag{2.14}$$

This is often called the Hironaka decomposition and the polynomials f_i are known as the primary invariant and the g_k as secondary invariants. The invariant algebra $\mathbb{R}[V^\Gamma]^G$ may thus be considered as a vector space (a module) over the secondary invariants with coefficients from the polynomial ring $\mathbb{R}[f_1, \ldots, f_n]$ or, roughly speaking, the secondary invariants can appear at most once in each term, whereas arbitrary products of primary invariants may appear as coefficients.

The number and degree of the g_k are given by the Hilbert (or Poincare) series which can be determined by Molien's formula (I is the identity element) [51]

$$\begin{aligned} H(\mathbb{R}[V^\Gamma]^G, t) &= \frac{1}{|G|} \sum_{\sigma \in G} \frac{1}{\det(I - \sigma t)} \\ &= \frac{\sum_j m_j t^{s_j}}{(1 + t^{p_1})^{n_1} (1 + t^{p_2})^{n_2} \dots (1 + t^{p_i})^{n_i}}. \end{aligned} \tag{2.15}$$

The numbers and degrees of the primary invariants are given by n_i and p_i, the numbers and degrees of the g_k by m_j and s_j, respectively. Note that there is no unique definition of primary or secondary invariants. They can be chosen in different ways and generally the result depends on the used algorithm. However, not every generating set that satisfies Eq. (2.15) is necessarily optimal in the sense of simplicity and computational efficiency. Also there appear different names for primary and secondary invariants in the chemical literature, for instance free and transient [52], basic and auxiliary [53] or denominator and numerator [54] invariants, respectively. Recent applications of invariant theory to PE surfaces typically rely on the computation of Molien's series, mainly as a consistency check for the polynomial basis [55–57].

A particularly simple situation arises if the considered representation is generated by reflections (known as Chevalley-Shephard-Todd theorem in the mathematical literature [58]). Specifically in JT problems, the relevant irreducible representations correspond to matrix groups that are reflection groups and the expansion given by Eq. (2.14) simplifies to a polynomial ring, i. e., there are no secondary invariants g_k. In practice, computer algebra systems are well-suited for the computation of a generating set of polynomials and the open-source software packages `GAP` and `Singular` have been used throughout this work [59–61].

2.3 Symmetry-adapted coordinates

Symmetry-adapted coordinates are coordinates which are associated with a set of symmetry-adapted basis functions. Symmetry properties of molecules are usually defined for the basis functions, while PE surfaces are constructed in the set of corresponding coordinates. To clarify the distinction between coordinates and basis functions, the transformation properties of linear forms are briefly explained. More rigorous and comprehensive treatments can be found in the literature [62].

Coordinates in general are linear functions in a given basis. An arbitrary point in the vector space spanned by the basis functions can be defined as the inner product of the coordinate and basis vector. In an analogous manner to a point in Cartesian coordinates, $\mathbf{x}$, defined as a linear form w. r. t. the standard basis e_1, e_2, e_3,

$$L(\mathbf{x}, \mathbf{e}) = \langle \mathbf{x} \,|\, \mathbf{e} \rangle = \mathbf{x}^\mathsf{T}\mathbf{e} = \sum_i^3 x_i e_i, \tag{2.16}$$

a point in curvilinear coordinates in a basis $S_i,\ i = 1, 2, \cdots$ is defined by

$$L(\mathbf{s}, \mathbf{S}) = \langle \mathbf{s} \,|\, \mathbf{S} \rangle = \sum_i^N s_i S_i. \tag{2.17}$$

From the algebraic point of view, the two equations (2.16) and (2.17) are just linear forms. Another important example of a linear form is the expansion of the WF in the BO approximation (cf. (2.4)). Here, the coefficients χ_i or c_i (the nuclear WFs) serve as the coordinates of a vector space spanned by the electronic WFs.

A (bijective) linear map $\mathbf{A}:\ \mathbf{S} \mapsto \mathbf{S}'$ changes the basis functions S_i to an equivalent set $\mathbf{S}'_i$. The same transformation is achieved by transforming the coordinates (or coefficients) with the inverse matrix $\mathbf{A}^{-1}$ and the vector space spanned by the coordinates is denoted the vector space V^* which is dual to the vector space V of the basis. This is summarized by the relations

$$L(\mathbf{s}', \mathbf{S}') = \mathbf{s}^\mathsf{T}\mathbf{A}^{-1}\mathbf{A}\mathbf{S} = \left\langle \mathbf{A}^{-\mathsf{T}}\mathbf{s} \,\middle|\, \mathbf{A}\mathbf{S} \right\rangle = L(\mathbf{s}, \mathbf{S}). \tag{2.18}$$

Therefore it is important to distinguish between "coordinates" or the synonym "coefficients" and "basis functions" in order to apply the correct linear transformation. The adiabatic-to-diabatic transformation in Eq. (2.7) is based in the same idea.

Somewhat arbitrarily, two different approaches to develop analytic expansions of PE surfaces can be distinguished: Either basis functions are employed that depend on a space-fixed reference geometry, or functions which only depend on the relative positions of the nuclei can be used. Expansions based on the $3N-6$ Cartesian nuclear displacements (in non-linear molecules) or symmetry-adapted linear combinations (SALCs) that are defined as displacements from a reference geometry are well-known examples for the first type. They are translation invariant, but not rotation-inversion invariant. Rotational invariance, on the other hand, requires non-linear functions of the Cartesian coordinates. Internuclear distances (or functions thereof) are examples of the second kind.

In a molecule that contains three (or less) identical nuclei, the internuclear distances determine the molecular shape unambiguously and provide the obvious choice for the computation and construction of PE surfaces. For molecules with four identical atoms, like tetrahedral molecules, the situation is more complicated. As discussed in the literature by several authors [57, 63, 64], the internuclear distances do not uniquely determine the shape of a molecule with four (or more) indistinguishable atoms. The computation of solutions to the electronic Schrödinger equation, however, requires a unique specification of the molecular geometry and hence a set of coordinates with an injective map to Cartesian coordinates.

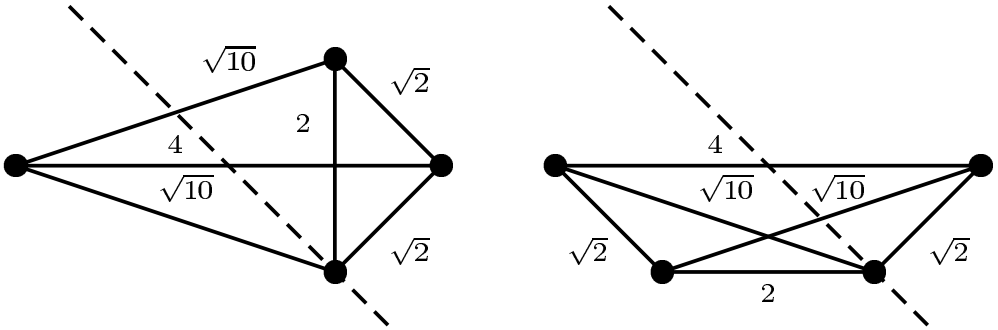

Figure 2.1: Two different geometries of four identical nuclei with the same distance distribution. Inserting additional atoms at the dashed line still results in identical distances (reproduced from [64]).

Figure 2.1 illustrates the problem for an instructive example [64]. Clearly, a linear function of the internuclear distances cannot resolve the differences between the two nuclear alignments. Although the generating set of invariant polynomials distinguishes molecular shapes unambiguously, the polynomials do not qualify as coordinates for *ab initio* calculations, since they are non-linear and there is no analytic transformation to Cartesian coordinates. As a consequence, *ab initio* electronic energies cannot be computed in rotationally invariant coordinates that exploit the permutation symmetry of more than three identical atoms. Moreover, it is impossible to derive a kinetic-energy operator w. r. t. internuclear distances in such cases—an important aspect for quantum dynamics [63].

Taking into account the shortcomings and deficiencies of the different coordinate sets discussed herein, clearly the most general method is to use both: nuclear displacement coordinates based on a fixed reference geometry which exploit the permutation symmetry of identical atoms in the *ab initio* calculations, and internuclear distances or their SALCs to construct the PE surface. Nevertheless, for

certain problems space-fixed basis functions provide the easiest route to a solution of acceptable accuracy. Cartesian normal modes for small-amplitude motions in molecular vibrations are the most important example.

2.4 Multi-dimensional Jahn-Teller potential-energy surfaces

The approximation of multi-sheeted PE surfaces represents a generalization of the previously described invariant expansion of a scalar function (Sec. 2.2). A single PE surface is defined as $\langle \phi \left| H_{\mathrm{el}} \right| \phi \rangle$, where the electronic WF ϕ is invariant under symmetry operations. For a single electronic state, there is no distinction between the adiabatic and a diabatic representation. Clearly, the Hamiltonian H_{el}, which typically is expanded in invariant polynomials, must be a totally symmetric function of the nuclear coordinates. Multi-sheeted adiabatic PE surfaces of N electronic states, on the other hand, are described by the eigenvalues of an $N \times N$ PE matrix.

In a diabatic representation, the electronic wave function can be approximated as the superposition of a number of basis functions ϕ_i, corresponding to the chosen subspace of electronic states (cf. Eqs. (2.7) and (2.18))

$$\Psi = \langle \mathbf{c} \mid \boldsymbol{\phi} \rangle = \sum_{i=1}^{N} c_i \phi_i. \tag{2.19}$$

Again, the expectation value of an operator corresponding to an observable (now a superposition of contributions from the different electronic states) must be invariant under symmetry operations. In what follows, a real-valued set of basis functions is assumed.

The electronic Hamiltonian H_{el} and its matrix representation in a finite basis depend on the nuclear coordinates and the corresponding basis functions. Diagonalization of the Hamiltonian matrix yields an equivalent canonical form in terms of the adiabatic energies (eigenvalues). In terms of equations, this reads

$$\sigma \circ \langle \Psi \left| H_{\mathrm{el}} \right| \Psi \rangle = \langle \Psi \left| H_{\mathrm{el}} \right| \Psi \rangle \qquad \forall\ \sigma \in G \tag{2.20}$$

$$\langle \Psi \left| H_{\mathrm{el}} \right| \Psi \rangle = \sum_{i,j=1}^{n} V_{ij} c_i c_j = \sum_{i=1}^{n} E_i \chi_i^2 \qquad i = 1, 2 \ldots \tag{2.21}$$

$$V_{ij} = \langle \phi_i \left| H_{\mathrm{el}} \right| \phi_j \rangle .$$

Both H_{el} and $|\Psi\rangle$ depend parametrically on the nuclear coordinates. Also, the expressions "electronic energy" and "potential energy" are used synonymously unless further specified.

The energies E_i are the adiabatic energies and are usually obtained from *ab initio* calculations for each state. Both the Hamiltonian matrix elements V_{ij} in the diabatic representation and the adiabatic energies E_i depend on the molecular geometry, but are subject to different symmetry constraints. While the adiabatic energies E_i are uniquely defined as the eigenvalues of the PE matrix and are invariant under all symmetry operations, the matrix elements V_{ij} are defined up to unitary transformations. Although the E_i can in principle be fitted with a set of invariant polynomials as demonstrated by Braams and Bowman [56], the smooth polynomial approximations cannot reproduce cusps that appear at intersections of PE surfaces. If conical intersections are present, it is therefore mandatory to determine an approximation to the PE matrix $\mathbf{V}$ in a diabatic basis where the elements V_{ij} are smooth functions of the nuclear coordinates. Apart from the advantages for a polynomial approximation, the diabatic representation of the Hamiltonian takes into account the geometric phase of the electronic wave functions, which is essential for applications to quantum dynamics. The crucial step for the approximation of multi-sheeted PE surfaces is thus the mapping from invariant polynomials to the diabatic PE matrix $\mathbf{V}$. A fundamental assumption of this method is that the total electronic wave function can be described by a finite (in practice, small) set of electronic basis functions (2.19) at all molecular geometries of interest. This assumption is fulfilled for electronic states that are separated by a large energy gap from all other electronic states.

We can expand the matrix elements V_{ij} in a suitable basis of nuclear displacements under the symmetry constraint that the expectation value is preserved.

$$\sigma \circ \langle \mathbf{c} \left| \mathbf{V}(\mathbf{r}) \right| \mathbf{c} \rangle = \left\langle \sigma^{-1}\mathbf{c} \left| \mathbf{V}(\sigma^{-1}\mathbf{r}) \right| \sigma^{-1}\mathbf{c} \right\rangle = \langle \mathbf{c} \left| \mathbf{V}(\mathbf{r}) \right| \mathbf{c} \rangle \tag{2.22}$$

The first step in the construction of multi-sheeted PE surfaces is the definition of a group representation $\Gamma^{\mathrm{el}} : G \to GL(N)$ for the chosen electronic space. The only restriction is that the vector space spanned by the electronic coordinates $c_1, \ldots, c_N$ must be closed under the action of the matrix representation Γ^{el}. Conventionally, the action of a molecular symmetry operation is defined w. r. t. the basis functions, in this case the electronic states $\phi_i, \ldots, \phi_N$. Since the basis functions are by definition fixed and normalized, all practical calculations are carried out with a representation

in the basis of coordinates $c_1, \ldots, c_N$ which form the dual vector space to the electronic basis. The representation matrices for the dual space are easily obtained by transposition of the original representation (2.3) and in what follows, it is assumed that all group representations act in the electronic coordinate space. For the nuclear coordinates, the same procedure defines a group representation over a closed set of nuclear coordinates. An obvious choice for the nuclear basis are all $n(n-1)/2$ internuclear distances. Despite of the deficiencies discussed in the previous section, which become relevant in practical applications, the set of internuclear distances is very useful for the formal derivation of the PE expansion. Furthermore, it is possible at any stage of the calculation to substitute the basis functions and coordinates with better suited functions that transform identically under the group actions.

Eq. (2.4) shows that the expectation value is essentially a 2-form in the electronic coordinates, with coefficients V_{ij} depending on the nuclear coordinates. The objective is therefore to determine the V_{ij} as polynomials in the nuclear coordinates that combine with binary products of the electronic coordinates to polynomials which are invariant under the action of the group on both, the electronic and nuclear coordinates. Since the coefficients V_{ij} are the matrix elements of the PE matrix in a diabatic representation, all invariant polynomials which are exactly of degree two in the electronic coordinates have to be found. Finding the symmetry-adapted matrices for the expansion of the PE operator is thus closely related to the algebraic problem of finding the invariant polynomials of the group representation in the vector space $V^{\mathrm{el}} \oplus V^{\mathrm{nu}}$, that is, the direct sum of the vector spaces spanned by the electronic and nuclear coordinates.

From the generating set of polynomials ($\mathbb{R}[V^{\mathrm{el}} \oplus V^{\mathrm{nu}}]^{\Gamma^{\mathrm{el}} \oplus \Gamma^{\mathrm{nu}}} = \mathbb{R}[f_1, f_2, \ldots]$), it is straightforward to select all polynomials of degree two in the electronic space and thus to determine the corresponding matrix elements. Higher-order terms are easily obtained by multiplying the matrices resulting from the generating set of polynomials with an element of $\mathbb{R}[V^{\mathrm{nu}}]^{\Gamma^{\mathrm{nu}}}$, the ring of invariant polynomials in the nuclear coordinates only. The generators of this ring are a subset of the invariant ring $\mathbb{R}[V^{\mathrm{el}} \oplus V^{\mathrm{nu}}]^{\Gamma^{\mathrm{el}} \oplus \Gamma^{\mathrm{nu}}}$ and thus are already known from the previous calculation. This provides the most general matrix expansion of a quantum-mechanical operator under consideration of the full molecular symmetry. Due to the exponential scaling of the cost of the computation of the generating set of invariant polynomials, however, the approach is limited to rather small systems.

A particularly simple situation arises if the electronic and nuclear basis functions

exhibit the same symmetry properties. For this purpose, the nuclear and electronic coordinates are expressed as SALCs of the same irreducible representation. This allows, for example, to consider specific subproblems of a full-dimensional JT PE surface in a reduced number of nuclear degrees of freedom. The specific structure of the resulting Hamiltonian matrices are the origin of the well-known JT Hamiltonians in such highly symmetric systems [5–9]. This applies to all JT PE surfaces (the JT theorem essentially is a qualitative statement about the consequences of this situation).

The construction of a symmetry-invariant expansion of multi-sheeted JT PE surfaces is tremendously simplified when it is taken into account that the electronic and nuclear coordinates form identical vector spaces. The computationally most expensive step in the derivation of expansion terms for the PE surface is the computation of the set of generating polynomials. In such JT systems, the matrix representations of the molecular symmetry group are identical in the electronic and nuclear coordinate space ($\Gamma^{\mathrm{el}} = \Gamma^{\mathrm{nu}}$). By means of *polarization* [45, 46, 50], all generating polynomials of the invariant ring of an arbitrary number of identical vector spaces can be determined from the generators of the invariant ring of a single copy of these vector spaces (see also Appendix 2). Weyl's polarization theorem [50] is particularly useful for the $E \times e$ and $T_2 \times t_2$ JT effects. In fact, it can be shown [20] that the matrices can be constructed as the Hessian matrices of the invariant polynomial expansion. Additionally, the product structure of the ring of invariant polynomials can be exploited systematically and permits complete arbitrary-order expansions using simple combinatorial rules. In Chapter 3, explicit examples are provided for the $T_2 \times (t_2 + t_2)$ and $T_2 \times e$ JT problems.

2.5 Spin-orbit coupling in Jahn-Teller systems

The relativistic theory of one- and two-electron atoms was initially developed by Heisenberg and Pauli [65, 66]. Breit later has added the retardation correction, resulting in the well-known Breit-Pauli (BP) spin-orbit (SO) operator [67, 68] which can be derived from the four-component Dirac-Coulomb Hamiltonian by a Foldy-Wouthuysen transformation [69, 70]. Accordingly, Hamiltonians employed in electronic-structure calculations evolved from empirical expressions based on atomic constants [71] to the BP form [72]. Among the relativistic effects in electronic structure, the main contribution is the spin-orbit part of the BP operator [68]. In a molecular

system or crystal with a single electron, there exist two possible alignments of the spin—parallel or anti-parallel to the orbital angular momentum. Depending on the molecular symmetry, additional symmetry properties originate from the two possible orientations of the electronic spin, leading to splittings of the electronic energy levels due to SO coupling.

The well-known JT selection rules [3] and the JT Hamiltonians [5] have originally been derived for the nonrelativistic (spin-less) Hamiltonian. Beginning with a paper by Jahn [4], the effect of SO coupling on the JT effect has been discussed by many authors. When the SO coupling effects are comparatively weak (which usually is the case for first- and second-row atoms), it is sufficient to include the zero-order contribution (in the normal-mode Taylor expansion) of the SO-coupling operator. Since the SO coupling increases strongly with the nuclear charge Z, a more systematic treatment of the SO interaction may be necessary for JT systems containing heavy elements. For the axial symmetry groups (C_{nv}, D_{nv}) the situation is simplified: since the SALCs of coordinates, electronic basis functions and angular momentum operators form bases of the same irreducible vector space, the SO operator is of the same symmetry as the electrostatic Hamiltonian [31, 73, 74]. Thus, the following discussion of SO coupling in JT systems is limited to tetrahedral and cubic systems. The Hamiltonian matrix, as usual, is expressed in a direct product basis of electronic states and spin functions. A well-known result from group theory is the decomposition of the Hamiltonian matrix into a block structure according to the Clebsch-Gordan decomposition of the direct-product basis into irreducible representations. At a tetrahedral reference geometry, the block structure of the Hamiltonian is preserved, compared to an isolated atom in an electronic state of the same symmetry. For JT active ${}^2E$ and ${}^2T_2$ electronic states in tetrahedral systems, the four- and six-dimensional space of electronic basis functions, respectively, split as [33]

$$E \otimes E_{1/2} = E_{1/2} \oplus E_{3/2} \tag{2.23a}$$

$$T_2 \otimes E_{1/2} = G_{3/2} \oplus E_{5/2}, \tag{2.23b}$$

where the energetic splitting between the different irreducible spaces is known as zero-order splitting and occurs, for instance, also in atoms with an unpaired electron in a $p-$orbital.

The BP SO operator for a single unpaired electron in the field of four identical nuclei reads [68]

$$H_{\mathrm{SO}} = -ig_e\beta_e^2 q\mathbf{S}\cdot\sum_{k=1}^{4}\frac{1}{r_k}\left(\mathbf{r}_k\times\nabla\right) = g_e\beta_e^2 q\mathbf{S}\cdot\mathbf{L} \tag{2.24a}$$

with

$$\mathbf{S} = \frac{1}{2}\left(\mathbf{i}\sigma_x + \mathbf{j}\sigma_y + \mathbf{k}\sigma_z\right) \tag{2.24b}$$

$$\mathbf{L} = -i\sum_{k=1}^{4}\frac{1}{r_k}\left(\mathbf{r}_k\times\nabla\right). \tag{2.24c}$$

Here $g_e = 2.0023$ is the g-factor of the electron, $\beta_e = e\hbar/(2m_e c)$ is the Bohr magneton, q is the effective charge of the equivalent atoms, $\sigma_x, \sigma_y, \sigma_z$ are the Pauli spin-matrices, $\mathbf{i}, \mathbf{j}, \mathbf{k}$ are the Cartesian unit vectors and $r_k = |\mathbf{r} - \mathbf{R}_k|$, where $\mathbf{r}$ is the radius vector of the single unpaired electron and $\mathbf{R}_k, k = 1\ldots4$, are the radius vectors to the four corners of the tetrahedron. In Eq. (2.24), the curl operator represents an angular momentum vector operator, which is mapped from a Cartesian basis into the vector space of traceless Pauli spin-matrices by means of the dot product $\mathbf{S}\cdot\mathbf{L}$. The complete BP SO operator is given as a 2×2 matrix over the field of complex numbers where the components of the angular momentum operator can be considered as the parameters of the vector space defined by the Pauli spin-matrices (see Eq. (2.25) below).

The simple one-electron Hamiltonian (2.24) has been used for the analysis of the symmetry properties of the SO coupling operator which remains unchanged in the presence of a central atom (i. e. the same symmetry considerations apply to molecules of X_4 and YX_4 type). Clearly, the BP operator for an atom must be invariant under rotations. In the presence of ligands, however, the symmetry is reduced to invariance under permutations of like nuclei (r_k). With a description of symmetry based on a molecular point group, the components of the curl operator $\mathbf{L}$ transform according to the irreducible representation of rotations, indicated as R_x, R_y and R_z in the character tables of the chemical literature [44]. The sum in Eq. (2.24) forms a basis of the T_1 irreducible representation of the molecular point group T_d which is generated by proper rotations.

In order to evaluate the group action on the BP SO operator, the homomorphism

$\phi : SO(3) \mapsto SU(2)$ between the special orthogonal group of 3×3 and the special unitary group of 2×2 matrices can be used. As shown by Wigner [75], the action of a proper rotation in a three dimensional vector space under the homomorphism ϕ is given by conjugation with the image of ϕ:

$$\pm\phi(\mathbf{C})\left[x\sigma_x + y\sigma_y + z\sigma_z\right]\left(\pm\phi(\mathbf{C})^\dagger\right) = \mathbf{S}\begin{pmatrix} x' \\ y' \\ z' \end{pmatrix} = \mathbf{SC}\begin{pmatrix} x \\ y \\ z \end{pmatrix} \qquad \mathbf{C} \in SO(3) \quad (2.25)$$

The undefined sign of the mapped matrices indicates that ϕ is a (injective) 2-to-1 mapping. Consequently, there must be twice as many valid symmetry operations in the $SU(2)$ image than in the $SO(3)$ group. Even more important, there exist pairs of eigenfunctions with identical eigenvalues arising from the $(+)$ and $(-)$ transformations. The resulting two-fold degeneracy of the PE surfaces is known as Kramers' theorem [76].

Molecular point groups with representations in terms of proper rotations (i. e. subgroups of $SO(3)$) can be mapped to a subgroup of $SU(2)$ in exactly the same manner. This naturally leads to the concept of double groups which describe the symmetry of electronic states of systems with an odd number of electrons. The matrix group of the T_1 irreducible representation can be obtained, for example, from the three matrices

$$\mathbf{g_1} = \begin{pmatrix} 0 & 0 & 1 \\ 1 & 0 & 0 \\ 0 & 1 & 0 \end{pmatrix} \quad \mathbf{g_2} = \begin{pmatrix} 1 & 0 & 0 \\ 0 & -1 & 0 \\ 0 & 0 & -1 \end{pmatrix} \quad \mathbf{g_3} = \begin{pmatrix} 0 & -1 & 0 \\ -1 & 0 & 0 \\ 0 & 0 & -1 \end{pmatrix}. \qquad (2.26)$$

It is straight forward to obtain a set of corresponding matrices in the $SU(2)$ matrix group under the map ϕ (up to the sign).

$$\mathbf{g}'_1 = \frac{1}{2}\begin{pmatrix} -1-i & -1+i \\ 1+i & -1+i \end{pmatrix} \quad \mathbf{g}'_2 = \begin{pmatrix} 0 & i \\ i & 0 \end{pmatrix} \quad \mathbf{g}'_3 = \frac{1}{\sqrt{2}}\begin{pmatrix} 0 & -1-i \\ 1-i & 0 \end{pmatrix} \qquad (2.27)$$

Taking the closure over the group elements, the entire double group can be obtained and equivalent sets of generating matrices have been published by several authors [33, 77]. The resulting double group for tetrahedral systems contains the group T_d as a subgroup including all of its irreducible representations. Faithful irreducible representations of the T'_d double group, however, comprise only proper rotation matrices ($\det(\mathbf{g}_i) = 1$).

Following Domcke and Poluyanov [33], the Hamiltonian can be expanded in a polynomial series around a reference point of the highest (typically the minimum-energy geometry of a non-degenerate reference state):

$$H_{\mathrm{SO}} = \sum_{i=0}^{N} \lambda_i {H_{\mathrm{SO}}}^{(i)} \tag{2.28}$$

where (i) defines the degree of the homogeneous polynomials in the expansion. The expanded Hamiltonian must have the same symmetry as the BP SO operator and, therefore, must be invariant under the action of the molecular point group. With respect to the homomorphism ϕ in Eq. (2.25) and the matrix representation defined by (2.27), the symmetry of the Hamiltonian operator can be expressed as

$$\mathbf{g}_i' H_{\mathrm{SO}}(\mathbf{g}_i')^\dagger = H_{\mathrm{SO}} = \mathbf{S} \circ \left((x\ y\ z)\mathbf{g}_i^\dagger \right) \qquad \forall\ \mathbf{g}_i' \in T_d' \ \wedge\ \mathbf{g}_i \in T_d. \tag{2.29}$$

Based on these relations, the Reynolds operator (see Eq. (2.12)) can be used to determine a set of invariant polynomials which is an easy task with modern computer algebra systems. To obtain the final model Hamiltonian, two additional mappings are required: First, the Hamiltonian has to be expressed in a set of coordinates that span a vector space of the T_1 irreducible representation (cf. the dihedral point groups, where rotation vectors transform as the degenerate symmetry-adapted coordinates). It is convenient to express the T_1 basis functions in terms of the nuclear displacements of T_2 symmetry for consistency with the conventional nonrelativistic JT theory. The second required mapping transforms the invariant 2×2 Hamiltonian matrix in spin space into a representation of spin-polarized molecular orbitals. Results of such calculations up to first order have been given by Poluyanov and Domcke for a number of different groups in a series of articles [32, 33, 73, 78]. Explicit expressions for the relevant SO Hamiltonians of tetrahedral molecules are provided in Chapter 5 with an application to photoelectron spectroscopy.

2.6 Quantum dynamics: The Chebyshev wave-packet propagation method

The simulation of vibrational spectra in molecules can be performed by two methodically different, but effectively equivalent approaches: Either by the time-independent

method where the vibronic matrix is explicitly diagonalized (e. g. the multi-mode approach [11]) or by the time-dependent wave-packet propagation of an initial wave function [79]. Both approaches rely on a representation of the nuclear wave function in a finite basis. Algorithms which compute the elements of the Hamiltonian matrix analytically are used in spectral methods. Pseudo-spectral or interpolating approaches interpolate the wave-packet on discrete grid points and determine the integrals over the interpolating functions [80]. Although in principle independent, there are serious drawbacks for certain combinations of the wave-packet representation (spectral or pseudo-spectral) and the algorithm (time-dependent or time-independent) for the solution of the Schrödinger equation. A particularly efficient and numerically stable algorithm on the basis of a grid representation of the nuclear wave-packet is the Chebyshev propagator [81, 82], which was used in the present work. The motivation for the use of a pseudo-spectral method mainly comes from the high-order expansion of the PE surface, which tremendously increases the number of non-vanishing matrix elements in the vibronic basis set (actually, this affects all spectral methods), but does not introduce additional difficulties in a pseudo-spectral time-dependent approach, where the PE values are evaluated on a discrete grid.

The well-known time-dependent Schrödinger equation is given by ($\hbar = 1$)

$$i\frac{\partial}{\partial t}\Psi(x,t) = H\Psi(x,t). \tag{2.30}$$

For time-independent Hamiltonians, the time-evolution of the wave function $\Psi(x,t)$ is determined by the analytic solution

$$\Psi(x,t) = \mathrm{e}^{-iHt}\Psi(x,0) \tag{2.31}$$

which represents an initial value problem. Numerical approaches to solve Eq. (2.30) by propagating an initial wave function according to Eq. (2.31) rely on a suitable discretization of the time-evolution operator ($U(t) \mapsto U(n\Delta t)$). Repeated application of the discretized time-evolution operator $U(\Delta t)$ allows the stepwise computation of a time-ordered series of wave function vectors in a finite basis. Time-independent observables, however, are completely determined by the solutions of the time-independent Schrödinger equation

$$H\psi_i(x) = E_i\psi_i(x) \qquad i = 1, 2, \ldots \tag{2.32}$$

and thus by the stationary states $\psi_i(x)$ with corresponding eigenvalues E_i. The stationary states $\psi_i(x)$ of Eq. (2.32) are also solutions of the generalized eigenvalue problem

$$f(H)\psi_i(x) = f(E_i)\psi_i(x) \tag{2.33}$$

where $f(x)$ is an arbitrary invertible function. This leads to a modified time-dependent Schrödinger equation

$$i\frac{\partial}{\partial t}\Psi_f(x,t) = f(H)\Psi_f(x,t) \tag{2.34a}$$

$$\Psi_f(x,t) = \mathrm{e}^{-if(H)t}\Psi_f(x,0) \tag{2.34b}$$

which contains the same information as Eq. (2.30), since the stationary states and thus observables are the same. With a suitable mapping f, the computational efficiency of the wave-packet propagation can be optimized.

The target function of a wave-packet calculation of electronic spectra is the autocorrelation function. The Fourier transformed autocorrelation function defines the spectrum in the energy domain. It is defined as

$$C(t) = \langle \Psi(x,T) \,|\, \Psi(x,t+T)\rangle = C(-t) \quad T \in \mathbb{R} \tag{2.35}$$

and obeys translational and Hermitian symmetry. Accordingly, starting from a real wave function ($T = 0$) and taking into account the Hermitian symmetry, the entire propagation can be performed over the field of real numbers (given that the Hamiltonian is real and symmetric):

$$\begin{aligned} C(t) &= \frac{1}{2}\left(\langle \Psi(x,0) \,|\, \Psi(x,t)\rangle + \langle \Psi(x,0) \,|\, \Psi(x,-t)\rangle\right) \\ &= \frac{1}{2}\left(\left\langle \Psi(x,0)\right| \left(\mathrm{e}^{-iHt} + \mathrm{e}^{iHt}\right) \left|\, \Psi(x,0)\right\rangle\right) \\ &= \langle \Psi(x,0) \,|\, \cos(Ht) |\, \Psi(x,0)\rangle \,. \end{aligned} \tag{2.36}$$

Simultaneous forward and backward propagation in time, therefore, is identical to the action of the cosine operator on an initial wave function. The autocorrelation function is preserved up to a scaling factor of two. Since the cosine operator is just the real part of the exponential time-evolution operator and permits the propagation of an initially real wave-packet using only real arithmetic, the propagation scheme is known as the real wave-packet method [83, 84].

Under the map

$$f(H) = -\frac{1}{\Delta t}\arccos(H) \tag{2.37}$$

the discretized cosine operator $\cos(Hk\Delta t),\ t \mapsto k\Delta t$, is equivalent to the definition of the series of Chebyshev polynomials

$$T_k(x) = \cos(k\arccos(x)) \tag{2.38}$$

and Eq. (2.34b) simplifies to

$$\Psi_k = T_k(H)\Psi_0 \qquad k = 0, 1, \ldots \tag{2.39}$$

In Eq. (2.39), the integer k denotes the degree of the respective Chebyshev polynomial. The mapping f in Eq. (2.37), however, requires the evaluation of the arctan function of the Hamiltonian operator, which is defined only in an interval between -1 and 1. In order to evaluate the Chebyshev polynomials in Eq. (2.39), the spectral range of the Hamiltonian must be scaled and shifted to a scaled Hamiltonian H_{sc} with eigenvalues in the range [-1:1]. If the function f is uniquely invertible, the resulting energy levels in the spectrum can be easily transformed back to their actual values.

The Hamiltonian employed in all propagations was defined in terms of mass-weighted Cartesian coordinates

$$H = T + V = -\frac{1}{2}\sum_{i=1}^{n}\frac{\partial^2}{\partial q_i^2} + \mathbf{V}(q_1, \ldots, q_n) \tag{2.40}$$

where the sum over the nuclear degrees of freedom is typically limited to approximately $n \leq 5$. The matrix $\mathbf{V}(q_1, \ldots, q_n)$ is a function of the n nuclear coordinates and represents the (Hermitian) PE operator.

The Hamiltonian matrix was constructed on a discrete variable representation (DVR) grid [85]. As interpolating primitive basis functions we used Whittaker's cardinal ($\mathrm{sinc}(x)$) functions [86] on an equidistant grid. The grid was constructed as a tensor grid of all considered degrees of freedom. In this representation, the kinetic-energy operator has a particularly simple and sparse structure [80]. For each degree of freedom, a $m \times m$ matrix is obtained where m denotes the number of grid points along the respective coordinate q_i in the interval Δq_i. The matrix elements

are given as

$$\mathbf{T}^{(i)}_{j,j+k} = \begin{cases} -\frac{1}{6}\left(\frac{\pi}{\Delta q_i}\right)^2 & k = 0 \\ -\frac{(-1)^k}{(k\Delta q_i)^2} & k \neq 0 \end{cases}. \tag{2.41}$$

The grid has been optimized by the Harris, Engerholm and Gwinn (HEG) methodology [87, 88] along each dimension. This contraction scheme is based on the diagonalization of a one-dimensional Hamiltonian (for each $\mathbf{T}^{(i)}$) along a path on the PE surface. For each dimension a subset of the resulting collocation points has been selected from which the final tensor grid was created. We reduced the grid representation to either a given number of eigenfunctions (beginning with the lowest eigenvalue) of all eigenfunctions of the one-dimensional Hamiltonians or all eigenfunctions within a certain energy domain, determined by the energy range of the simulated spectrum.

The full kinetic-energy operator of dimension $(\prod_{i=1}^{n} m_i) \times (\prod_{i=1}^{n} m_i)$ is given by

$$\mathbf{T} = \sum_{i=1}^{n} \mathbf{I}_{m_1} \otimes \cdots \otimes \mathbf{I}_{m_{i-1}} \otimes \mathbf{T}^{(i)} \otimes \mathbf{I}_{m_{i+1}} \otimes \cdots \otimes \mathbf{I}_{m_n} \tag{2.42}$$

where $\mathbf{I}_{m_i}$ is the identity matrix of dimension m_i (the number of grid points of the contracted grid) and $\otimes$ refers to the Kronecker product. Due to its special structure, the matrix $\mathbf{T}$ is constructed on the fly during the Chebyshev iteration, referencing only the non-zero elements. The PE operator was constructed as an $(\prod_{i=1}^{n} m_i) \times N\,(N+1)$ matrix using the standard LAPACK [89] packed storage format (N is the number of electronic states, i. e. the dimension of the JT Hamiltonian).

The mapping of the Hamiltonian matrix $\mathbf{H} \mapsto \mathbf{H}_{\mathrm{sc}}$ is given as

$$\begin{aligned} \mathbf{H} &\mapsto \frac{\mathbf{H} - \bar{\mathbf{H}}}{\Delta H} \\ \bar{\mathbf{H}} &= \frac{1}{2}(\lambda_{\max} + \lambda_{\min})\mathbf{I} \\ \Delta H &= \frac{1}{2}(\lambda_{\max} - \lambda_{\min}) \end{aligned} \tag{2.43}$$

where $\mathbf{I}$ is the identity matrix of the same dimension as $\mathbf{H}$ and $\lambda_{\max}/\lambda_{\min}$ denote the largest/smallest eigenvalue of the Hamiltonian matrix, respectively. In the present work $\lambda_{\max}$ was computed numerically by

$$\lambda_{\max} = \lim_{k\to\infty} \frac{\left\langle \Psi_0 \left| \mathbf{H}^{k+1} \right| \Psi_0 \right\rangle}{\left\langle \Psi_0 \left| \mathbf{H}^{k} \right| \Psi_0 \right\rangle} \tag{2.44}$$

and as the smallest eigenvalue $\lambda_{\min}$ the grid point with the lowest adiabatic potential energy was chosen.

The propagation of an initial wave function follows the recursion relation of the Chebyshev polynomials

$$T_k(\mathbf{H}_{\mathrm{sc}}) = 2\mathbf{H}_{\mathrm{sc}}T_{k-1}(\mathbf{H}_{\mathrm{sc}}) - T_{k-2}(\mathbf{H}_{\mathrm{sc}}) \qquad k \in \mathbb{N}|k > 1 \tag{2.45}$$

which, according to Eq. (2.39), becomes

$$\Psi_k = 2\mathbf{H}_{\mathrm{sc}}\Psi_{k-1} - \Psi_{k-2}. \tag{2.46}$$

Therefore, the iterative propagation of the wave function involves only matrix-vector multiplications of the Hamiltonian matrix $\mathbf{H}_{\mathrm{sc}}$ with the vector Ψ_k.

The method described so far was directly applied for all electrostatic (real-valued) Hamiltonians. The computation of relativistic JT spectra requires an extension of the wave-packet propagation code for Hamiltonians containing complex-valued matrix elements. To achieve this extension, we use the mapping

$$x + iy \mapsto \begin{pmatrix} x & -y \\ y & x \end{pmatrix} \qquad x, y \in \mathbb{R} \tag{2.47}$$

between complex numbers and real 2×2 matrices. Relation (2.47) is an isomorphism. More generally, any complex $N \times N$ matrix can be mapped to an isomorphic real $2N \times 2N$ matrix. This remains true for functions of matrices, provided that

$$f(\lambda_i^*) = f^*(\lambda_i) \tag{2.48}$$

where the λ_i are the eigenvalues of the matrix [90]. Any real function of a Hermitian operator fulfills Eq. (2.48). The Hermitian Hamiltonians in the recursive propagation scheme of Eq. (2.46) are thus mapped to real symmetric matrices. Analogously, a vector $\mathbf{v} \in \mathbb{C}^N$ can be mapped to a real representation $\mathbf{v}' \in \mathbb{R}^{2N}$ by

$$v_i \mapsto \begin{pmatrix} \mathrm{Re}[v_i] \\ \mathrm{Im}[v_i] \end{pmatrix}. \tag{2.49}$$

The mappings (2.47) and (2.49) preserve the matrix-vector product. In particular, the 2-form $\langle \Psi_0 \, | T_{2k}(\mathbf{H}_{\mathrm{sc}}) | \, \Psi_0 \rangle$, which defines the autocorrelation function of a wave

function vector Ψ is invariant under the mappings (2.47, 2.49) and the spectral distribution is preserved. Since the propagation scheme (2.46) involves only matrix-vector multiplications, the complex arithmetic required for the computation of relativistic JT spectra can be carried out over the field of real numbers. The numerical cost for matrix-vector multiplication scales quadratically with the dimension. The propagation of a complex-valued wave-packet with a complex-valued PE operator therefore requires approximately four times of CPU time and twice the amount of memory of the propagation of a real-valued wave-packet with a real-valued Hamiltonian.

In every iteration step, the autocorrelation function of the wave-packet was calculated using the relations

$$\begin{aligned} C_{2k} &= \langle \Psi_0 \left| T_{2k}(\mathbf{H}_{\mathrm{sc}}) \right| \Psi_0 \rangle = \langle \Psi_k \left| \Psi_k \right. \rangle - C_0 \\ C_{2k+1} &= 2 \left\langle \Psi_{k+1} \left| \Psi_k \right. \right\rangle - C_1 \end{aligned}, \tag{2.50}$$

i. e. propagating k steps yields $2k$ points of the Chebyshev autocorrelation function.

From the C_k, the expansion coefficients and the time-dependent autocorrelation function are given by

$$C(t) = \mathrm{e}^{-i\frac{\bar{\mathbf{H}}}{2}t} \sum_{k=0}^{N} (2 - \delta_{0k})(-i)^k J_k \left(\frac{\bar{\mathbf{H}}t}{2} \right) C_k \tag{2.51}$$

where $J_k(t)$ is the k th Bessel function of the first kind [81]. From the time-dependent autocorrelation function $C(t)$ the spectrum is easily obtained by Fourier transform. A direct and numerically favorable conversion of the Chebyshev autocorrelation function to the spectral distribution function is given by

$$\begin{aligned} \sigma(E) &\propto \sum_{k=1}^{N} (2 - \delta_{0k}) \frac{\cos(k\phi)}{\sin(\phi)} C_k \\ \phi &= \arccos\left(\frac{E - \bar{H}}{\Delta H} \right) \end{aligned} \tag{2.52}$$

and has been used to compute all spectra in this work.

3 High-order expansions of electrostatic Jahn-Teller PE surfaces

The symmetry of four- and five-atomic molecules with four identical nuclei is described by the tetrahedral molecular point group T_d. The point group T_d, however, is isomorphic to the permutation group S_4. Considering T_d symmetry in the expansion of the PE surface therefore accounts for the full permutation symmetry of four identical nuclei. Open-shell systems of this symmetry are subject to $T_2 \times t_2$ and $T_2 \times e$ JT effects [5–9].

In many cases, the JT couplings are fairly strong and the standard JT approximation up to second order in normal coordinates [5–9] is insufficient. This applies in particular to situations where large amplitude motions become relevant, or an exchange of identical nuclei is feasible. Presumably the first complete set of symmetry-adapted polynomials for four indistinguishable points was determined by Aslaksen et al. [91], motivated by its potential application to orientation-independent shape-recognition algorithms. Recently, Cassam-Chenai and Patras published an expansion for five-atomic YX_4 molecules comprising 151 generating polynomials [55]. Taking into account that the number of terms in a JT matrix expansion increases considerably compared to the scalar expansion, renders an application of their generating set of polynomials to JT PE surfaces impracticable. In what follows it is demonstrated that the number of generating polynomials can be reduced to 9 for X_4 systems and 31 for YX_4 systems. A compact expansion based on a rather small number of generating polynomials is developed for the PE matrix expansion, using simple combinatorics. Additionally, the complete set of invariant polynomials is well-suited to identify symmetry-equivalent molecular geometries. If all generating polynomials of two sets of molecular coordinates yield the same value, the molecular structures are energetically degenerate. This is very useful to avoid the computation of redundant *ab initio* points.

Regarding the permutation symmetry of identical nuclei, the number of symmetry-equivalent points is determined by the number of points in the group orbit. The T_d group entails $|T_d| = 24$ different symmetry operations. Any displacement which destroys the symmetry completely has 24 equivalent images in the group orbit. This is, however, not true for displacements that preserve a certain amount of symmetry. In cases where the nuclear displacements do not completely destroy the symmetry, the number of equivalent points is given by the ratio $|G|/|H|$ of the group order of the molecular symmetry group and a subgroup $H \leq G$. Subgroups of a molecular point group which describe the molecular symmetry under displacements of one or several symmetry-adapted coordinates are known as *epikernel* groups [92]. In tetrahedral systems, there exist the epikernel groups $C_{2v}, C_s, C_{3v}, D_{2d}, D_2$ [92]. The numbers of equivalent points in the corresponding group orbits are $6, 12, 4, 3, 6$, respectively and define the borders of the group's fundamental domains. It should be noted that this refers only to the permutation symmetry. Considering also spatial inversion, for instance, effectively doubles the group order of T_d and thus the numbers of degenerate points in the group orbit. Geometries that exhibit a specific epikernel symmetry generally correspond to critical points on the PE surface and thus are naturally of great importance for the nuclear motion within a molecule, including, e. g. chemical reaction barriers or tunneling splittings in vibrational spectra.

3.1 The $T_2 \times t_2$ and $T_2 \times (t_2 + t_2)$ cases

For a discussion of the $T_2 \times (t_2 + t_2)$ JT effect in tetrahedral YX_4 systems it is instructive to begin with the discussion of the $T_2 \times t_2$ JT effect. Using Weyl's polarization theorem [50], it is straightforward to extend a polynomial expansion to an arbitrary number of t_2 modes. The pure $T_2 \times t_2$ JT effect occurs in four-atomic tetrahedral open-shell systems consisting of identical nuclei. Tetrahedral X_4 systems possess six internal nuclear degrees of freedom ($3N - 6 = 6$) which can be defined on a basis of SALCs of symmetry a_1, e and t_2.

In a first approximation, the analysis of the $T_2 \times t_2$ problem is based on a three-sheeted PE surface in three coordinates of t_2 symmetry, conventionally denoted as x, y, z. It should be noted that the coordinates x, y, z are only defined by their symmetry properties, i. e. by the action of the T_d group operations on the coordinate vector. The underlying primitive basis remains undefined and can be chosen specifically adapted to the considered problem. Any nuclear geometry in the three-

dimensional subspace of t_2 coordinates is described by a superposition (a linear form) of SALCs S_x, S_y, S_z multiplied with the associated coordinates. In a similar manner, the electronic states are described as a superposition of three electronic basis functions, the three components of the electronic T_2 state $|x\rangle, |y\rangle, |z\rangle$. The nuclear geometry and the electronic states can be defined as linear forms in a set of coordinates w. r. t. a set of basis functions:

$$\begin{aligned} \langle \mathbf{c} \mid \boldsymbol{\phi} \rangle &= c_x |x\rangle + c_y |y\rangle + c_z |z\rangle \\ \langle \mathbf{s} \mid \mathbf{S} \rangle &= x S_x + y S_y + z S_z. \end{aligned} \tag{3.1}$$

Eq. (3.1) is just a special case of (2.18).

With a fixed basis of (normalized) SALCs and assuming real coefficients, the PE in the subspace of the degenerate electronic state can be considered as a function of the nuclear coordinates x, y, z and the coefficients c_x, c_y, c_z of the electronic basis functions. The general $T_2 \times t_2$ PE operator in the coordinates defined by Eq. (2.18) reads

$$V(c_x, c_y, c_z, x, y, z) = \mathbf{c}^{\mathsf{T}} \mathbf{V} \mathbf{c} = \begin{pmatrix} c_x \\ c_y \\ c_z \end{pmatrix}^T \begin{pmatrix} V_{xx}(x,y,z) & V_{xy}(x,y,z) & V_{xz}(x,y,z) \\ V_{xy}(x,y,z) & V_{yy}(x,y,z) & V_{yz}(x,y,z) \\ V_{xz}(x,y,z) & V_{yz}(x,y,z) & V_{zz}(x,y,z) \end{pmatrix} \begin{pmatrix} c_x \\ c_y \\ c_z \end{pmatrix} \tag{3.2a}$$

$$\begin{aligned} &= c_x V_{xx}(x,y,z) c_x + c_y V_{yy}(x,y,z) c_y + c_z V_{zz}(x,y,z) c_z \\ &+ 2 \left[c_x V_{xy}(x,y,z) c_y + c_x V_{xz}(x,y,z) c_z + c_y V_{yz}(x,y,z) c_z \right]. \end{aligned} \tag{3.2b}$$

The eigenvalues of the vibronic matrix $\mathbf{V}$ are the adiabatic PE surfaces of the JT system.

The matrix elements $V_{ij}(x, y, z)$ are expanded as polynomials in the symmetry-adapted nuclear displacement coordinates. It should be noted that the expansion in powers of displacements from a reference geometry excludes the description of dissociative processes. Our analysis is appropriate for large-amplitude motions in strongly JT-coupled systems, provided the energy levels of interest are sufficiently below the dissociation threshold of the system.

Equation (3.2) reveals that the expansion of a PE surface of coupled electronic states is equivalent to the construction of T_d-invariant polynomials in the vector space $[V^{t_2} \oplus V^{t_2}]$ of both electronic and nuclear coordinates, i. e., the invariants in the coordinates of two identical vector spaces. In fact, the decomposition of

the quadratic form (3.2b) into as many (linearly independent) invariant terms as possible yields the most flexible parameter space for the fitting of *ab initio* points that preserves the molecular symmetry. The advantage of an orthogonal basis (i. e., a basis in which the T_2 representation matrices are orthogonal) is evident: The invariants in the dual space of nuclear coordinates are just the invariants of T_2, since they are invariants with respect to the transposed T_2 representation of T_d. Knowing the mapping of the Hamiltonian matrix to invariant polynomials, we can employ computer-algebra systems to find the complete set of invariant polynomials up to high order in the expansion.

The invariant ring of the T_2 representation in T_d is generated by three polynomials of degree 2, 3 and 4. This follows from the fact that the T_2 representation is just the complement of the totally-symmetric irreducible A_1 representation of the permutation representation of the symmetric group of four elements (S_4). In practice, these calculations are well-suited for computer algebra systems and many results in this work have been obtained or verified with the `Singular` software [60, 61]. The generating set in the coordinates x, y, z is given by

$$\begin{aligned} f_1 &= x^2 + y^2 + z^2 \\ f_2 &= xyz \\ f_3 &= x^4 + y^4 + z^4. \end{aligned} \tag{3.3}$$

Any polynomial of the invariant ring $\mathbb{R}[x, y, z]^{T_d}$ can be expressed in terms of these generators:

$$\mathbb{R}[x, y, z]^{T_d} = \mathbb{R}[f_1, f_2, f_3]. \tag{3.4}$$

A subset of the elements of $\mathbb{R}[f_1, f_2, f_3]$ forms a vector space and the adiabatic PE surface may be approximated by restricting the expansion to all possible linearly independent terms up to a certain order. It turns out that an expansion up to 8 th order in the three coordinates x, y, z, for instance, consists of 14 terms compared to $\sum_{d=1}^{8} \binom{3+d-1}{d} = 164$ terms without invoking symmetry. If the expansion involves several t_2 coordinate sets, the benefit is even larger.

In order to determine the expansion of the potential $V(c_x, c_y, c_z, x, y, z)$ we make use of Weyl's polarization method [46, 50]. Polarization according to Weyl is a formal procedure of substituting variables of a vector space V in invariant polynomials by another set of variables from another copy of an identical vector space. Weyl's theorem states that if some polynomials $\{p_1, \ldots, p_n\}$ are a generating set for an

S_n-invariant ring $\mathbb{R}[V]^{S_n}$, then their polarized forms generate the ring $\mathbb{R}[V+V]^{S_n}$, where S_n denotes the symmetric group of n elements. According to Eq. (3.2), the potential energy (assuming that the $V_{ij}(x,y,z)$ are expanded as polynomials) is given by a doubly polarized invariant polynomial in the combined vector spaces of nuclear coordinates $\mathbf{s}$ and coefficients $\mathbf{c}$, since both transform identical under the group $T_d \simeq S_4$. The potential matrix is obtained from the decomposition of the polynomial into vectors $\mathbf{c}^\mathsf{T}, \mathbf{c}$ and the symmetric matrix $\mathbf{V}$. The invariant polynomial is recovered by the usual tensor contraction.

Once all doubly polarized generating invariants have been determined, it is easy to set up the symmetry-adapted expansion of the JT matrix by rearrangement of Eq. (3.2). From the definition of the polarization process and Eq. (3.2) it follows that any term in the expansion of the Hamiltonian matrix is just the Hessian of an invariant polynomial of the ring $\mathbb{R}\left[x,y,z\right]^{T_d}$, up to multiplication with a constant factor. As an example, the $T_2 \times t_2$ JT matrices of first and second order [5] follow immediately from the generators of degree three and four in Eq. (3.3)

$$\mathbf{V}^{(1)} = \kappa^{(1)} \begin{pmatrix} 0 & z & y \\ z & 0 & x \\ y & x & 0 \end{pmatrix}, \qquad \mathbf{V}^{(2)} = \kappa^{(2)} \begin{pmatrix} x^2 & 0 & 0 \\ 0 & y^2 & 0 \\ 0 & 0 & z^2 \end{pmatrix}, \qquad \kappa^{(1)}, \kappa^{(2)} \in \mathbb{R}. \quad (3.5)$$

Moreover, it can be shown that all JT matrices (i. e., all Hessians of the elements of $\mathbb{R}\left[f_1, f_2, f_3\right]^{T_d}$) are also finitely generated (see Appendix 2).

Using the procedure described above, we determined the generating polynomials for the $T_2 \times t_2$ JT Hamiltonian. The invariants can be reduced to only three sets which generate the complete expansion up to arbitrary degree under element-wise multiplication:

$$\mathbf{t}^n \in \begin{pmatrix} x \\ y \\ z \end{pmatrix}^n, \begin{pmatrix} yz \\ xz \\ xy \end{pmatrix}^n, \ \mathbf{a}^l = \begin{pmatrix} y^2 \\ x^2 \\ x^2 \end{pmatrix}^l + \begin{pmatrix} z^2 \\ z^2 \\ y^2 \end{pmatrix}^l, \qquad n, l = 1, 2, \ldots \quad (3.6)$$

The letters t and a indicate the symmetry of the respective generator (actually t_2 and a_1). The terms of the polynomial expansion are determined from the elements t_i, a_i $(i = 1, 2, 3)$ up to multiplication with a constant factor by the following rules:

1. Diagonal elements V_{ii} of the potential-energy matrix are products of $t_i t_i$ and a_i.

2. Off-diagonal matrix elements $V_{ij} = V_{ji}$ are given by the symmetric product $t_i t'_j + t_j t'_i$ or t_k, $i, j, k = 1, 2, 3$, where $i \neq j \neq k$.

3. Products of V_{ij} with diagonal matrix elements (a_k or $t_k t_k$) preserve the position.

4. Even powers of off-diagonal elements are symmetric, since V_{ij} transforms as t_k and t_k^2 is a diagonal element.

The general elements of the potential matrix may thus be written as

$$
\begin{aligned}
V_{11} &= t_1^{2n} \left(t_2 t_3\right)^{2m} a_1^l \\
V_{22} &= t_2^{2n} \left(t_1 t_3\right)^{2m} a_2^l \\
V_{33} &= t_3^{2n} \left(t_1 t_2\right)^{2m} a_3^l, \qquad l, m, n \in 0, 1, 2, \ldots \\
V_{12} &= t_3^{2n'} \left(t_1 t_2\right)^{2m'+1} a_3^{l'}, \quad \text{or} \quad V_{12} = t_3^{2m'+1} \left(t_1 t_2\right)^{2n'} a_3^{l'} \\
V_{13} &= t_2^{2n'} \left(t_1 t_3\right)^{2m'+1} a_2^{l'}, \quad \text{or} \quad V_{13} = t_2^{2m'+1} \left(t_1 t_3\right)^{2n'} a_2^{l'} \\
V_{23} &= t_1^{2n'} \left(t_2 t_3\right)^{2m'+1} a_1^{l'}, \quad \text{or} \quad V_{23} = t_1^{2m'+1} \left(t_2 t_3\right)^{2n'} a_1^{l'}, \qquad l', m', n' \in 0, 1, 2, \ldots
\end{aligned}
\tag{3.7}
$$

This expansion is already optimized in the sense that the overlap of the polynomials is minimized. This reduces the interdependence of the expansion parameters and improves the convergence in a non-linear parameter-optimization procedure. The determination of the expansion up to arbitrary order is now reduced to a simple combinatorial problem. Matrix elements up to 8 th order are given explicitly in Eq. (3.9) to illustrate the application of the multiplication rules. In general, we find a potential-energy matrix with a highly symmetric structure

$$
\mathbf{V}(x, y, z) = \begin{pmatrix} W(x, y, z) & Z(z, x, y) & Z(y, x, z) \\ Z(z, x, y) & W(y, x, z) & Z(x, y, z) \\ Z(y, x, z) & Z(x, y, z) & W(z, x, y) \end{pmatrix} \tag{3.8}
$$

where W and Z are sums of the respective diagonal (off-diagonal) elements $W^{(n)}$ ($Z^{(n)}$) of order n in Eq. (3.9) and $Z(z, x, y) = Z(z, y, x)$, $W(z, x, y) = W(z, y, x)$.

The $a_i^{(n)}$, $b_i^{(n)}$ are fitting parameters:

$$
\begin{aligned}
W^{(1)}(x,y,z) &= 0 \\
W^{(2)}(x,y,z) &= a_1^{(2)}x^2 + a_2^{(2)}(z^2+y^2) \\
W^{(3)}(x,y,z) &= a_1^{(3)}xyz \\
W^{(4)}(x,y,z) &= a_1^{(4)}x^4 + a_2^{(4)}(y^4+z^4) + a_3^{(4)}x^2(y^2+z^2) + a_3^{(4)}y^2z^2 \\
W^{(5)}(x,y,z) &= a_1^{(5)}x^3yz + a_2^{(5)}xyz(y^2+z^2) \\
W^{(6)}(x,y,z) &= a_1^{(6)}(y^6+z^6) + a_2^{(6)}x^6 + a_3^{(6)}x^4(y^2+z^2) + a_4^{(6)}x^2(y^4+z^4) + a_5^{(6)}(yz)^2(y^2+z^2) \\
&\quad + a_6^{(6)}x^2y^2z^2 \\
W^{(7)}(x,y,z) &= a_1^{(7)}xyz(y^4+z^4) + a_2^{(7)}x^3yz(y^2+z^2) + a_3^{(7)}xy^3z^3 + a_4^{(7)}x^5yz \\
W^{(8)}(x,y,z) &= a_1^{(8)}(y^8+z^8) + a_2^{(8)}x^8 + a_3^{(8)}(yz)^4 + a_4^{(8)}(yz)^2(y^4+z^4) + a_5^{(8)}x^6(y^2+z^2) \\
&\quad + a_6^{(8)}x^4(y^4+z^4) + b_7^{(8)}x^2(y^6+z^6) + a_8^{(8)}x^4y^2z^2 + a_9^{(8)}x^2y^2z^2(y^2+z^2) \\
Z^{(1)}(x,y,z) &= b_1^{(1)}x \\
Z^{(2)}(x,y,z) &= b_1^{(2)}yz \\
Z^{(3)}(x,y,z) &= b_1^{(3)}x^3 + b_2^{(3)}x(y^2+z^2) \\
Z^{(4)}(x,y,z) &= b_1^{(4)}x^2yz + b_2^{(4)}yz(y^2+z^2) \\
Z^{(5)}(x,y,z) &= b_1^{(5)}x^5 + b_2^{(5)}(y^2+z^2)x^3 + b_3^{(5)}x(y^4+z^4) + b_4^{(5)}xy^2z^2 \\
Z^{(6)}(x,y,z) &= b_1^{(6)}(yz)^3 + b_2^{(6)}yz(y^2+z^2) + b_3^{(6)}x^4yz + b_4^{(6)}x^2yz(y^2+z^2) \\
Z^{(7)}(x,y,z) &= b_1^{(7)}x^7 + b_2^{(7)}x^5(y^2+z^2) + b_3^{(7)}x^3(y^4+z^4) + b_4^{(7)}x(y^6+z^6) + b_5^{(7)}x^3y^2z^2 \\
&\quad + b_6^{(7)}xy^2z^2(y^2+z^2) \\
Z^{(8)}(x,y,z) &= b_1^{(8)}yz(y^6+z^6) + b_2^{(8)}(yz)^3(y^2+z^2) + b_3^{(8)}x^2yz(y^2+z^2) + b_4^{(8)}x^4yz(y^2+z^2) \\
&\quad + b_5^{(8)}x^6yz + b_6^{(8)}x^2y^3z^3.
\end{aligned}
\tag{3.9}
$$

The expansion terms up to 12 th order in powers of generators are tabulated in Appendix 5. Thus the JT matrix elements consist of two different kinds of functions whose position (and symmetry) in the matrix is determined by the first argument. Expressing the matrix elements as sums of products of the generating polynomials and taking into account the symmetry of $\mathbf{V}$ (i. e. the symmetry of $W(x,y,z)$ and $Z(x,y,z)$ under permutation of the arguments) allows an efficient and transparent implementation via a programming language.

Molecules such as YX_4 systems include additional nuclear degrees of freedom which transform as t_2. For these molecules, one t_2 coordinate vector corresponds

to bond stretching and a second set of t_2 coordinates to bending displacements. In order to distinguish the two t_2 coordinate tuples we use the identifiers x_1, y_1, z_1 and x_2, y_2, z_2. Again, the first step is the determination of the generating set of totally-symmetric invariant polynomials in the six-dimensional nuclear coordinate space. If the generating set of one t_2 mode is already known, Weyl's polarization method provides a convenient scheme to obtain the generators for several t_2 coordinate vectors. Obviously, the generators of Eq. (3.3) apply for any t_2 coordinate vector and the displacements along a second t_2 coordinate are given by the same expansion with different parameters. In addition, there are a number of mixed generators, which can be obtained by partial polarization. There are 12 generators in total:

$$\begin{aligned}
f_1 &= x_1^2 + y_1^2 + z_1^2 \\
f_2 &= x_1 y_1 z_1 \\
f_3 &= x_1^4 + y_1^4 + z_1^4 \\
f_4 &= x_2^2 + y_2^2 + z_2^2 \\
f_5 &= x_2 y_2 z_2 \\
f_6 &= x_2^4 + y_2^4 + z_2^4 \\
f_7 &= x_1 x_2 + y_1 y_2 + z_1 z_2 \\
f_8 &= z_1 x_2 y_2 + y_1 x_2 z_2 + x_1 y_2 z_2 \\
f_9 &= y_1 z_1 x_2 + x_1 z_1 y_2 + x_1 y_1 z_2 \\
f_{10} &= x_1 x_2^3 + y_1 y_2^3 + z_1 z_2^3 \\
f_{11} &= x_1^2 x_2^2 + y_1^2 y_2^2 + z_1^2 z_2^2 \\
f_{12} &= x_1^3 x_2 + y_1^3 y_2 + z_1^3 z_2
\end{aligned} \tag{3.10}$$

The same result can be obtained by the application of the Reynolds operator in Eq. (2.12), using the six-dimensional direct sum-representation $\sigma \in T_2 \oplus T_2$. Recently, an equivalent generating set of polynomials has been obtained by Cassam-Chenai et al. using a Hironaka-decomposition [55]. For the purpose of a compact Jahn-Teller expansion, however, the generators in Eq. (3.10) are better suited.

In principle, the generating set for the $T_2 \times (t_2 + t_2)$ matrix expansion can be determined by the same procedure as for the $T_2 \times t_2$ matrix (i. e., by mapping polarized invariants to the potential matrix). Alternatively, we can apply the polarization operators to the polynomials in Eq. (3.6). After eliminating redundant terms, we directly obtain the generating elements for the $T_2 \times (t_2 + t_2)$ JT-matrix and the

resulting terms comply with the multiplication rules given for the $T_2 \times t_2$ expansion before. The expansion up to fourth order is

$$
\begin{aligned}
W^{(1)}(x_1,x_2,y_1,y_2,z_1,z_2) &= 0\\
W^{(2)}(x_1,x_2,y_1,y_2,z_1,z_2) &= c_1^{(2)}x_1x_2 + c_2^{(2)}(z_1z_2+y_1y_2)\\
W^{(3)}(x_1,x_2,y_1,y_2,z_1,z_2) &= c_1^{(3)}x_1y_2z_2 + c_2^{(3)}x_2y_1z_1 + c_3^{(3)}x_1(y_1z_2+y_2z_1) + c_4^{(3)}x_2(y_1z_2+y_2z_1)\\
W^{(4)}(x_1,x_2,y_1,y_2,z_1,z_2) &= c_1^{(4)}x_1^3x_2 + c_2^{(4)}x_1^2x_2^2 + c_3^{(4)}x_1x_2^3 + c_4^{(4)}x_1^2(y_2^2+z_2^2)\\
&\quad + c_5^{(4)}x_2^2(y_1^2+z_1^2) + c_6^{(4)}x_1^2(y_1y_2+z_1z_2) + c_7^{(4)}x_2^2(y_1y_2+z_1z_2)\\
&\quad + c_8^{(4)}x_1x_2(y_2^2+z_2^2) + c_9^{(4)}x_1x_2(y_1^2+z_1^2) + c_{10}^{(4)}x_1x_2(y_1y_2+z_1z_2)\\
&\quad + c_{11}^{(4)}y_1y_2z_1z_2 + c_{12}^{(4)}y_1z_1(y_1z_2+y_2z_1) + c_{13}^{(4)}y_2z_2(y_1z_2+y_2z_1)\\
&\quad + c_{14}^{(4)}(y_1^2y_2^2+z_1^2z_2^2) + c_{15}^{(4)}(y_1^2z_2^2+y_2^2z_1^2) + c_{16}^{(4)}(y_1^3y_2+z_1^3z_2)\\
&\quad + c_{17}^{(4)}(y_2^3y_1+z_2^3z_1)\\
Z^{(1)}(x_1,x_2,y_1,y_2,z_1,z_2) &= 0\\
Z^{(2)}(x_1,x_2,y_1,y_2,z_1,z_2) &= d_1^{(2)}(y_1z_2+y_2z_1)\\
Z^{(3)}(x_1,x_2,y_1,y_2,z_1,z_2) &= d_1^{(3)}x_1^2x_2 + d_2^{(3)}x_2^2x_1 + d_3^{(3)}x_1(y_2^2+z_2^2) + d_4^{(3)}x_2(y_1^2+z_1^2)\\
&\quad + d_5^{(3)}x_1(y_1z_2+y_2z_1) + d_6^{(3)}x_2(y_1z_2+y_2z_1)\\
Z^{(4)}(x_1,x_2,y_1,y_2,z_1,z_2) &= d_1^{(4)}x_1^2y_2z_2 + d_2^{(4)}x_2^2y_1z_1 + d_3^{(4)}x_1x_2y_1z_1 + d_4^{(4)}x_1x_2y_2z_2\\
&\quad + d_5^{(4)}x_1^2(y_1z_2+y_2z_1) + d_6^{(4)}x_2^2(y_1z_2+y_2z_1) + d_7^{(4)}x_1x_2(y_1z_2+y_2z_1)\\
&\quad + d_8^{(4)}y_1z_1(y_2^2+z_2^2) + d_9^{(4)}y_2z_2(y_1^2+z_1^2) + d_{10}^{(4)}y_1z_1(y_1y_2+z_1z_2)\\
&\quad + d_{11}^{(4)}y_2z_2(y_1y_2+z_1z_2) + d_{12}^{(4)}(y_1^3z_2+z_1^3y_2) + d_{13}^{(4)}(y_2^3z_1+z_2^3y_1).
\end{aligned}
\tag{3.11}
$$

For brevity, the expansion is given for one diagonal element ($W(x_1,x_2,y_1,y_2,z_1,z_2)$) and one off-diagonal element ($Z(x_1,x_2,y_1,y_2,z_1,z_2)$). According to Eq. (3.8), the other matrix elements are obtained by permuting variables. The second diagonal element $W(y_1,y_2,x_1,x_2,z_1,z_2)$, for instance, is obtained by permuting (x_1,x_2) with (y_1,y_2) in the expansion (3.11). For displacements $(x_1,x_2,0,0,0,0)$, the system has C_{2v} symmetry; for displacements $(x_1,x_2,y_1,y_2,0,0)$, it has C_s symmetry. Equal displacements along all six coordinates result in C_{3v} structures with a doubly-degenerate (E) electronic state.

3.2 The $T_2 \times e$ case

The $T_2 \times e$ JT PE surface describes the three-sheeted electronic PE surface of an T_2 electronic state in a two-dimensional subspace of nuclear coordinates of e symmetry. Nuclear coordinates of e symmetry are present in all molecules of tetrahedral symmetry. The E irreducible representation forms a matrix group which is isomorphic to the symmetric group of three identical elements S_3, a subgroup of S_4 and T_d. Accordingly, there are six different representation matrices in a basis of SALCs of nuclear coordinates and displacements along coordinates of E symmetry cannot completely destroy the molecular symmetry. The nuclear geometry and molecular electronic state are defined as superpositions of SALCs:

$$\begin{aligned} \langle \mathbf{c} \,|\, \boldsymbol{\phi} \rangle &= c_x \,|x\rangle + c_y \,|y\rangle + c_z \,|z\rangle \\ \langle \mathbf{s} \,|\, \mathbf{S} \rangle &= a S_a + b S_b \end{aligned} \tag{3.12}$$

The curvilinear displacements along a and b are illustrated in Fig. 1 in Appendix 4.2. In order to construct the $T_2 \times e$ diabatic PE matrix, the five-dimensional $E \oplus T_2$ representation must be considered, coupling the electronic WF and the nuclear displacements.

Using SALCs as defined in section 2.3, the $E \oplus T_2$ representation is generated by the direct sum of the generating matrices of the E and T_2 representations where

$$\mathbf{G}_i = \mathbf{E}_i \oplus \mathbf{T}_i \qquad i = 1, 2 \tag{3.13}$$

$$\mathbf{E}_1 = \begin{pmatrix} 0 & 1 \\ -1 & -1 \end{pmatrix}, \; \mathbf{E}_2 = \begin{pmatrix} 0 & 1 \\ 1 & 0 \end{pmatrix}, \; \mathbf{T}_1 = \begin{pmatrix} 0 & -1 & 0 \\ 0 & 0 & 1 \\ -1 & 0 & 0 \end{pmatrix}, \; \mathbf{T}_2 = \begin{pmatrix} 0 & 0 & 1 \\ 0 & 1 & 0 \\ 1 & 0 & 0 \end{pmatrix}. \tag{3.14}$$

The representation matrices are defined by the symmetry properties of the SALCs and in the present $T_2 \times e$ JT problem, the T_2 representation matrices act on the electronic basis functions, whereas the E representation matrices act on the space of nuclear SALCs. The coordinates (or coefficients) associated with the SALCs transform as the transposed representations in Eq. (3.14) according to the transformation properties of linear forms. In what follows, the electronic coefficients of T_2 symmetry are denoted as x, y, z instead of c_x, c_y, c_z in Eq. (3.12). On the one hand, this keeps the notation of invariant polynomials consistent among the different parts of this

work. On the other hand, this emphasizes the generality of the formulation: the invariant expansion is only determined by the transformation properties of the basis function under the group action and is independent of the physical meaning, i. e. whether the group acts on the electronic or the nuclear vector space. The vibrational modes are represented by the displacement coordinates a, b which transform as e in T_d.

In contrast to the standard definition, we have chosen a basis in which the C_3 operators of the E representation are not orthogonal. The matrices $\mathbf{E}_1, \mathbf{E}_2$ are related to the conventional orthogonal rotations and reflections by a similarity transformation. As will become apparent later, the JT Hamiltonian has a more compact expansion in this basis (in particular, there appear no square roots in the elements of the JT PE matrix). Nuclear displacements parameterized by the coordinate vectors $(u, 0)$, $(0, u)$ or $(-u, -u)$ $(u \in \mathbb{R})$ with respect to a SALC basis correspond to identical distortions in different spatial directions or, equivalently, act on different nuclei. These displacements distort the tetrahedral system along the three principal axes of the reference geometry.

The derivation of the $T_2 \times e$ Hamiltonian up to high orders is based on the formalism described in Chapter 2. The expansion of the $T_2 \times e$ JT PE matrix is determined by the first and second derivatives of the totally symmetric invariant polynomials with respect to the coordinates that transform as the coefficients of the electronic T_2 state. In a first step, a generating set of polynomials was determined which generates all invariant polynomials with respect to the five-dimensional $E \oplus T_2$ representation. Since the coordinates transform covariantly with respect to the basis functions of the representation defined by the $\mathbf{G}_i$ in Eq. (3.14), the invariant polynomials in these coordinates are determined by the transposed representation generated by $\mathbf{G}_1^\mathsf{T}$ and $\mathbf{G}_2^\mathsf{T}$. Again, we used the software package `Singular` [60, 61] to find a minimal generating set of the invariant algebra in the symmetry coordinates. The set of

polynomials generating the invariant ring $\mathbb{R}[a,b,x,y,z]^{E\oplus T_2}$ is given by

$$\begin{aligned}
f_1 &= x^2+y^2+z^2 \\
f_2 &= xyz \\
f_3 &= x^4+y^4+z^4 \\
f_{13} &= a^2-ab+b^2 \\
f_{14} &= a^3-\frac{3}{2}\left(a^2b+ab^2\right)+b^3 \\
f_{15} &= (a-2b)\,x^2+(a+b)\,y^2+(b-2a)\,z^2 \\
f_{16} &= a^2x^2+(a-b)^2\,y^2+b^2z^2 \\
f_{17} &= (a-2b)\,x^4+(a+b)\,y^4+(b-2a)\,z^4
\end{aligned} \quad . \tag{3.15}$$

and represents, together with the totally symmetric breathing coordinate, a complete generating set of polynomials for X_4 molecules. The polynomials in Eq. (3.15) may be used to derive any $X \times Y$, $(X, Y \in T_2, E)$ JT expansion up to arbitrary order, following the same procedure. The polynomials f_{13} and f_{14}, which are required for the $E \times e$ JT problem, are just the totally symmetric second and third order terms of Viel and Eisfeld [18] in a non-orthogonal basis. The polynomials f_1, f_2, f_3 are the well known generating invariants of the T_2 representation and define the expansion of the $T_2 \times t_2$ JT matrix. The $T_2 \times e$ JT matrix expansion is determined by the polynomials f_{15}, f_{16} and f_{17} which couple coordinates of E and T_2 symmetry.

We obtained the two non-redundant generating matrices

$$\mathbf{A} = \begin{pmatrix} a-2b & 0 & 0 \\ 0 & a+b & 0 \\ 0 & 0 & b-2a \end{pmatrix} \qquad \mathbf{B} = \begin{pmatrix} a^2 & 0 & 0 \\ 0 & (a-b)^2 & 0 \\ 0 & 0 & b^2 \end{pmatrix} \tag{3.16}$$

for the $T_2 \times e$ potential matrix from the Hessian matrix of the generating polynomials f_{15} and f_{16} in Eq. (3.15) with respect to the coordinates of T_2 symmetry. Since we consider here only the $T_2 \times e$ problem, all x, y or z were put to zero after the matrices have been constructed and all first derivatives vanish. It turns out that the structure of the JT expansion can be simplified if a third (redundant) generating matrix is defined:

$$\mathbf{C} = \frac{1}{4}\left(\mathbf{A}^2-\mathbf{B}\right) = \begin{pmatrix} b^2-ab & 0 & 0 \\ 0 & ab & 0 \\ 0 & 0 & a^2-ab \end{pmatrix}. \tag{3.17}$$

It is clear from the definition of $\mathbf{C}$ that all powers of $\mathbf{A}$ higher than one can be omitted since

$$\mathbf{A}^2 = 4\mathbf{C} - \mathbf{B}. \tag{3.18}$$

Furthermore, the totally symmetric polynomials f_{13} and f_{14} are already included by

$$\begin{aligned} f_{13}\mathbf{I} &= \mathbf{B} + \mathbf{C} \\ f_{14}\mathbf{I} &= \mathbf{A}(\mathbf{B} - \frac{1}{2}\mathbf{C}), \end{aligned} \tag{3.19}$$

where $\mathbf{I}$ is the unit matrix of dimension 3.

From these matrices follows an expansion which is similar to a binomial expansion in $\mathbf{B}$ and $\mathbf{C}$. All terms of an even order $(2n)$ are given by the terms in the expansion of $(\mathbf{B} + \mathbf{C})^n$:

$$\mathbf{V}^{(2n)}(a, b) = \sum_{k=0}^{n} \lambda_k^{(2n)} \mathbf{B}^{n-k} \mathbf{C}^k, \tag{3.20}$$

where the λ_k are arbitrary fitting parameters. Terms of odd degree $(2n + 1)$ are obtained by multiplication of the term of order $2n$ with $\mathbf{A}$:

$$\mathbf{V}^{(2n+1)}(a, b) = \sum_{k=0}^{n} \lambda_k^{(2n+1)} \mathbf{A}\mathbf{B}^{n-k} \mathbf{C}^k. \tag{3.21}$$

In Table (3.1) the powers of $\mathbf{B}$ and $\mathbf{C}$ are explicitly listed which have been used in the expansion of the $T_2 \times e$ JT matrix up to tenth order in the nuclear coordinates. The expansion problem is thus reduced to elementary combinatorics of binomials in the matrices of $\mathbf{B}$ and $\mathbf{C}$. The resulting $T_2 \times e$ potential is a diagonal matrix (since $\mathbf{A}, \mathbf{B}, \mathbf{C}$ are diagonal) which is the sum of the expressions in Eqs. (3.20) and (3.21)

$$\mathbf{V}(a, b) = \sum_{n=1}^{N} \mathbf{V}^n(a, b). \tag{3.22}$$

tot. deg.	2		4			6				8					10					
B	1	0	2	1	0	3	2	1	0	4	3	2	1	0	5	4	3	2	1	0
C	0	1	0	1	2	0	1	2	3	0	1	2	3	4	0	1	2	3	4	5

Table 3.1: Even-order generating polynomials defined by Eq. (3.15) and (3.17) in the $T_2 \times e$ expansion up to 10 th order. The first and second order terms are $\mathbf{A}$, $\mathbf{B}$ and $\mathbf{C}$. The odd-order terms of degree $2n + 1$ are obtained by multiplying the $2n$-order term with $\mathbf{A}$ and thus have been omitted.

The expansion can be divided into two partitions. The first partition consists of all terms $\mathbf{A}^k\mathbf{B}^l$ and $\mathbf{A}^k\mathbf{C}^l$, $\quad k = 0, 1, \quad l \in \mathbb{N}$. Any other term of the $T_2 \times e$ expansion vanishes if either a or b is zero. Inspection of the expansion terms shows that 19 terms contribute to the potential in this one-dimensional subspace. Moreover, for displacements along one coordinate the terms arising from the products $\mathbf{A}^k\mathbf{B}^l$ and $\mathbf{A}^k\mathbf{C}^l$, $(k = 0, 1)$, $l \in \mathbb{N}$ can be assigned to a non-degenerate electronic state of A and a degenerate electronic state of E symmetry, respectively. The first-order matrix in the Jahn-Teller expansion is an exception of the (otherwise complete) separation of E and A electronic states in a one-dimensional cut and determines the gradients of the diabatic states at the reference geometry, which are related by

$$-2\frac{\partial V^E(a,b)}{\partial a}\Big|_{a,b=0} = \frac{\partial V^A(a,b)}{\partial a}\Big|_{a,b=0}. \tag{3.23}$$

The remaining terms of the type $\mathbf{A}^k\mathbf{B}^l\mathbf{C}^m$, $m \in \mathbb{N}$, describe the coupling between the two coordinates of E symmetry. Depending on the choice of SALCs for the nuclear coordinates there is a considerable benefit of this rearrangement which becomes obvious during the fitting of *ab initio* data, where the parameters of the first partition can be fitted as a one-dimensional function to the *ab initio* electronic energies for displacements of a single coordinate.

3.3 Full-dimensional expansion in internuclear distances

The PE surfaces developed so far are very efficient if the coordinates allow the separate treatment of the individual degrees of freedom. Unfortunately, there are disadvantages with regard to practical applications. One aspect is related to the coordinates: Only if the symmetry coordinates can be mapped to a unique molecular shape, it is possible to compute *ab initio* data along a defined pathway on the PE surface. Thus the method is limited to SALCs that are based on a space-fixed reference geometry and the development of rotation-invariant PE surfaces is impossible in general. Another important point related to the inverse transformation, from Cartesian (or any other equivalent coordinate system) to symmetry coordinates. Since displacements in one or a few other coordinates naturally correspond to displacements in possibly all degrees of freedom in the SALC-coordinates, a full-dimensional PE surface is mandatory in order to use the PE surface with existing

simulation software. In rotation-invariant SALCs based on internuclear distances (and in the remainder of this section only such SALCs and coordinates are considered) the sum of all $X - X$ distances (s_0) forms an invariant polynomial of degree one, which is essential for a unique correspondence between function values (of the polynomial expansion) and energetically non-degenerate geometries. With two generating invariants of degree one, the number of terms in a high-order expansion tremendously increases and a manual analysis of the expansion terms (there are already 500 totally symmetric terms up to sixth order) is not feasible. Therefore, a different approach is applied which separates the expansion into totally symmetric and JT splitting terms. Any $N \times N$ matrix can be written as the sum of a multiple of the identity matrix and a traceless matrix:

$$\begin{aligned} \mathbf{V} &= \frac{1}{N}\mathrm{Tr}(\mathbf{V})\mathbf{I} + \mathbf{V}^{\mathrm{JT}} \\ \mathrm{Tr}(\mathbf{V}^{\mathrm{JT}}) &= 0. \end{aligned} \tag{3.24}$$

The trace of a matrix is an invariant under similarity transformation, i. e.

$$\mathrm{Tr}(\mathbf{V}) = \mathrm{Tr}(\mathbf{A}\mathbf{V}\mathbf{A}^{-1}) = \sum_i \lambda_i \qquad \forall\ \mathbf{A} \in GL(N), \tag{3.25}$$

where λ_i are the eigenvalues of the matrix $\mathbf{V}$. Clearly, the trace of the PE operator must be an invariant polynomial since the adiabatic PE surfaces λ_i are totally symmetric. A similar relation applies to the determinant (it is the product of the eigenvalues and thus invariant as well) but the trace has the important property of being additive.

$$\mathrm{Tr}(\mathbf{V}_1 + \mathbf{V}_2) = \mathrm{Tr}(\mathbf{V}_1) + \mathrm{Tr}(\mathbf{V}_2). \tag{3.26}$$

The approximation of the trace of a PE surface is rather simple: the sum of all relevant electronic energies can be added and fitted to a scalar expansion in invariant polynomials. Due to the additivity of the traces of individual terms, the problem is simplified to a linear least-squares problem. Note that the PE surface along all totally symmetric coordinates is also included into the fitted trace function and, in a good approximation, the splitting terms $\mathbf{V}^{\mathrm{JT}}$ can be limited to polynomials in the JT active coordinates.

The remaining traceless terms $\mathbf{V}^{\mathrm{JT}}$ which lead to the Jahn-Teller splitting of the PE surfaces are—as in the expansions before—determined by the first and second partial derivatives of the generating polynomials. The restriction to traceless ma-

trices, however, reduces the number of terms with non-zero diagonal. A complete list of the traceless generating matrices ($\mathbf{g}_i$) is provided in Appendix 3. These were initially determined for one t_2 mode and the e mode and subsequently extended by polarization for the $t_2 \times t_2$ coordinate space. Again, each traceless matrix appears only once in the final expansion and is just multiplied with an invariant polynomial (the trace remains zero). The matrix expansion, in terms of the generators $\mathbf{g}_i$ and f_i is given by

$$\mathbf{V} = \mathbf{I} \circ \mathbb{R}[f_1, \ldots, f_n] + \bigoplus_{i=1}^{n} \mathbf{g}_i \circ \mathbb{R}[f_1, \ldots, f_n]. \tag{3.27}$$

If both s_0 and s_1 are set to zero, the expansion in (3.27) is equivalent (though not identical) to the previous $T_2 \times (t_2 + t_2)$ and $T_2 \times e$ expansion of Sections 3.1 and 3.2. Most conveniently, high-order expansion are generated by computer programs, avoiding the cumbersome implementation of an expansion of several hundreds of terms and error-prone manual implementations. For this purpose, a program was implemented in the Python programming language to create all expansion terms in Eq. (3.27) up to a given order as a Fortran subroutine.

4 Application to CH_4^+

The methane cation is presumably the most fundamental cation in organic chemistry. In its triply degenerate ground state of T_2 symmetry, it is subject to a variety of JT effects, including strong $T_2 \times t_2$ and $T_2 \times e$ JT effects. Two normal modes of the same (t_2) symmetry and one normal mode of E symmetry are JT active, resulting in the $T_2 \times (t_2 + t_2 + e)$ JT effect. Displacements of the nuclei from the highly symmetric reference geometry, which lower the symmetry, lift the degeneracy of the electronic energy level, resulting in adiabatic potential-energy (PE) surfaces exhibiting considerable topographical complexity [93–95].

The PE surface of the methane cation has a long history in the chemical literature. The He I photoelectron spectrum of CH_4 exhibits an extended and highly irregular vibrational structure which is the signature of very strong multi-mode JT coupling [22, 23]. Early explorations of the lowest adiabatic PE surface revealed a very complex topography with numerous local minima and saddle points of different symmetries [96–98]. Several of them have been suggested as minimum geometry [19, 96] until Meyer et al. predicted the correct C_{2v} symmetry [99] based on *ab initio* calculations. The first experimental evidence for a PE minimum geometry of C_{2v} symmetry was obtained by Knight et al. using electron spin resonance (ESR) measurements [100]. The currently best resolved photoelectron spectrum of the methane cation was determined experimentally using VUV pulsed-field ionization zero-kinetic-energy (PFI-ZEKE) spectroscopy and is described in a series of articles by Merkt and coworkers [24, 25, 101, 102]. The assignment of these highly complex and dense spectra represents a challenge for theory. An accurate three-sheeted nine-dimensional *ab initio* PE surface of the T_2 state of CH_4^+ is needed as the basis for theoretical investigations of the nuclear dynamics and the interpretation of the photoelectron spectrum.

4.1 *Ab initio* electronic-structure calculations

In order to solve the *ab initio* electronic-structure problem, a set of coordinates based on a space-fixed reference geometry was used to define a number of relevant geometries. The three adiabatic PE surfaces of the T_2 ground state of CH_4^+ have been determined by *ab initio* calculations at the multi-reference configuration-interaction (MRCI) level of theory using the correlation-consistent polarized valence triple-zeta (cc-pVTZ) basis set [103]. For each nuclear geometry, the reference wave functions have been obtained from a state-averaged complete-active-space self-consistent-field (CASSCF) calculation including the three components of the T_2 electronic state. All valence orbitals have been included in the active space of the CASSCF calculations. The 1s core orbital of the C-atom was optimized in the CASSCF calculation, but excluded from the active space. In the subsequent MRCI calculations, the core orbital was frozen, while all other orbitals were included in the CI expansion. The energy minimum of tetrahedral CH_4^+ was found at a CH distance of 1.14 Å. Data points at several thousands of nuclear geometries were acquired, mostly along cuts involving up to four different symmetry coordinates. Energies up to 6 eV above the energy of the reference geometry of T_d symmetry have been considered for the PE surface of CH_4^+. In consideration of the computation of photoelectron spectra, also the geometry of the uncharged methane molecule has been optimized. The CH bond length at the PE minimum in a tetrahedral nuclear arrangement was found at 1.09 Å with the CCSD(T) electronic structure method and the cc-pVTZ basis set. The vertical ionization potential was determined by a RCCSD(T) calculation and amounts to 14.35 eV, in excellent agreement with previously published experimental results [23]. Harmonic vibrational frequencies of the methane molecule also have been calculated at the CCSD(T)/cc-pVTZ level of theory. The calculation yields 0.376 eV, 0.195 eV, 0.391 eV and 0.167 eV for the modes of a_1, e, t_2 (stretch) and t_2 (bend) symmetry.

4.2 Fitting strategy

Fitting multi-sheeted JT PE surface in general poses a non-linear optimization problem unless the *ab initio* data are explicitly obtained in a diabatic representation. Quantum chemistry software usually provides solutions of the electronic structure problem for a particular geometry as adiabatic energies. In order to work in the

same basis, the analytic expansion of the PE matrix was diagonalized for every data point to obtain the adiabatic eigenvalues. The eigenvalues of the 3×3 Hamiltonian matrix have been fitted to the adiabatic *ab initio* energies. Since the eigenvalues in general do not linearly depend on the fitting parameters, we employed a Marquardt-Levenberg algorithm for the non-linear optimization. It should be emphasized that there is no analytical solution to the non-linear least-squares minimization problem. In particular, there is no guarantee that the algorithm converges to the global error minimum. Due to the large number of parameters , it is indispensable to follow a systematic strategy to solve the non-linear optimization problem. However, the fitting strategy strongly depends on the chosen SALCs. Symmetry-adapted coordinates which are based on a space-fixed reference geometry, allow a very efficient separation of the nine degrees of freedom. Expressing the PE expansion in a set of SALCs that does not depend on a (space-fixed) reference geometry, on the other hand, is hampered by the coupling of many degrees of freedom which requires the simultaneous fitting of a large number of parameters.

In a set of coordinates based on the tetrahedral reference geometry, the diabatic 3×3 matrix of the $T_2 \times (t_2 + t_2)$ JT PE surface has been expanded in invariant polynomials up to 8 th and 12 th order in the stretching and bending coordinates, respectively. The stretch-bend coupling terms were expanded up to fourth order. There are 54/139 parameters in the pure stretching/bending expansions and 43 in the stretch-bend coupling terms. The choice of symmetry-adapted coordinates and the expansion in invariant polynomials result in important simplifications. Many terms vanish if one or a few coordinates are equal to zero. Step-wise increase of the number of coordinates, while the parameters of previous fits are frozen, considerably reduces the number of parameters that have to be fitted simultaneously.

In the first step, the parameters of the individual t_2 modes have been determined by splitting the parameter space into three subspaces, corresponding to displacements in either one, two or three coordinates of t_2 symmetry. The parameter determination for displacements in a single coordinate can be solved analytically and the optimal parameters can be found by linear regression. For displacements in one out of the three equivalent t_2 coordinates, the molecular symmetry is reduced to C_{2v}, resulting in the lifting of the electronic degeneracy. Our expansions of the one-dimensional stretching (bending) potential contain 8 (12) parameters for the first and third JT-coupled surfaces (B_1 and B_2 symmetry) and 4 (6) parameters for the potential of A_1 symmetry which is only subject to quadratic JT coupling.

In the second step, the parameters determined in the one-dimensional cuts were fixed, and the set of 22 (51) stretching (bending) parameters describing the PE for displacements in two t_2 coordinates have been fitted to the adiabatic *ab initio* energies. In this case, the symmetry is reduced to C_s, and the electronic T_2 state splits into two A' and one A'' state.

In the third step, the remaining parameters were fitted to *ab initio* energies for displacements in all coordinates in the three dimensional t_2 space, again fixing all previously fitted parameters. The molecular symmetry group is reduced to the kernel group of the T_2 representation which is the (trivial) C_1 group, except for equal displacements of all three t_2 coordinates ($x = y = z$). For the latter displacements, the molecular symmetry group is C_{3v}, and the electronic T_2 state splits into states of E and A symmetry. Since $T_2 \times t_2$ JT systems typically have potential minima in this symmetry, we explicitly considered cuts of this symmetry.

The fitting strategy for the simultaneous displacements in two t_2 coordinates followed a similar strategy as for the $T_2 \times t_2$ cases. All parameters of the two previously fitted three-dimensional T_2-surfaces have been frozen and the potential was expressed as a sum of the two previous expansions and the coupling terms. The additional 43 parameters have been fitted step by step, using cuts of an increasing number of mixed stretching and bending displacements. Since the expansion was terminated at fourth order, only cuts involving at most four different t_2 displacements have been included.

For the expansion of the T_2 electronic state up to 10 th order in the coordinates of e symmetry, 35 parameters have be adjusted to reproduce the *ab initio* data as accurately as possible. Energies up to 5 eV have been taken into account in the parameter optimization. Intersections of components of the T_2 electronic state with states of different electronic character at energies below 5 eV were observed for calculations along cuts across the PE surface in the two-dimensional subspace of the e coordinates. Data points that belong to different electronic states have been removed by assigning a weight factor of zero in the fitting procedure. Although the PE matrix is diagonal, a linear fitting procedure would require a previous diabatization of the *ab initio* data due to several intersections between the diabatic PE surfaces. We rather employed the Marquardt-Levenberg algorithm to perform an iterative optimization of the parameters. For the cut along a single nuclear coordinate, we chose the coordinate s_{2a}, which allowed us to exploit C_{2v} symmetry in the *ab initio* calculations (the molecule has D_{2d} symmetry along this cut).

If one of the two coordinates in the subspace of e symmetry is zero, the parameter space in our model Hamiltonian comprises 19 parameters. Since the distortion along one of the coordinates preserves D_{2d} symmetry, the T_2 electronic state splits into a degenerate state of E and another state of A symmetry. Sixteen terms of the JT expansion vanish at geometries of D_{2d} symmetry. These have been fitted to five different cuts across the $T_2 \times e$ PE surface involving both e coordinates. The parameter optimization benefits from the previously fitted parameters of the potential along a single coordinate, which already provides a reasonable approximation for the PE surface for combined displacements in a and b.

For the construction of the full-dimensional PE surface, the internuclear distances in the SALCs have been substituted by

$$r \mapsto \mathrm{e}^{-\alpha r} \tag{4.1}$$

where the parameter α has been chosen as 0.5 for the CH bond lengths and 1.0 for the HH distances. In order to determine the fitting parameters for the full-dimensional $E(3)$-invariant PE surface (see Sec. 3.3), we first fitted the sum of the adiabatic *ab initio* energies to a completely invariant scalar expansion in invariant polynomials using a standard linear least-squares procedure. Since the number of terms tremendously increases with the order, the expansion was terminated at sixth order for both the trace and the JT matrix expansion. The reason of the strongly increasing number is the additional totally symmetric polynomial of first order (denoted s_0 in App. 4.2) which is essential for a unique mapping between molecular geometry and the energies, but cancels for reference-geometry based expansions. The parameters in the matrix expansion of the trace-less splitting terms were optimized employing the mentioned Marquardt-Levenberg algorithm, excluding polynomials in the coordinates of the totally symmetric SALCs, s_0 and s_1. For SALCs of internuclear distances (or function thereof), the different coordinates can not be separated as described before. The fitting of the traceless JT splitting terms was rather performed in three steps, fitting the irreducible subspaces in the order e, t_2 bend, t_2 stretch.

4.3 The potential-energy surface of the T_2 ground state of CH_4^+

The accuracy of the fitted PE surfaces in important regions can be assessed from cuts along epikernel symmetries. These cuts represent lines connecting critical points of the PE surface which typically correspond to transition states or saddle points.

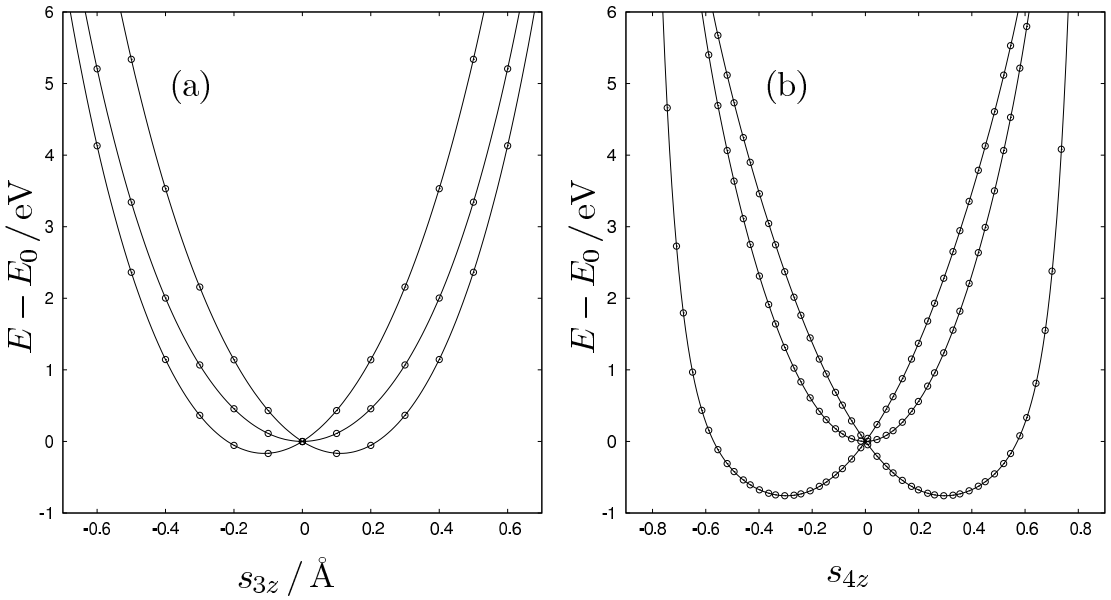

Figure 4.1: Adiabatic PE surfaces for displacements in a single stretching (s_{3z}) and bending (s_{4z}) coordinate, fitted with a 8 th and 12 th order expansion, respectively. The symmetry is C_{2v}, resulting in the splitting of the T_2 state in A_1, B_1 and B_2 electronic states. The dots are the *ab initio* data; the lines represent the fit.

Fig. (4.1) shows the fitted PE curves for displacements in one of the stretching (a) and bending (b) coordinates of t_2 symmetry. It is seen that the JT stabilization energy of the bending mode ($\approx 0.76\,\text{eV}$) is much larger than the JT stabilization energy of the stretching mode ($\approx 0.17\,\text{eV}$). The pronounced anharmonicity of the bending PE function renders a high-order expansion indispensable. The expansion of the stretching potentials up to 8 th order and the bending potentials up to 12 th order results in a balanced accuracy of the fit. A significant fraction of the total JT stabilization energy at the global minimum of C_{2v} symmetry can be attributed to the displacements shown in Fig. (4.1). To every point of the PE curves in Fig. 4.1 there exist five images which are equivalent due to symmetry (there are $|T_d|/|C_{2v}| = 6$

different points in the C_{2v} group orbit). The minima of the lowest PE curves shown in Fig. 4.1 are also referred to as orthorhombic minima [104, 105].

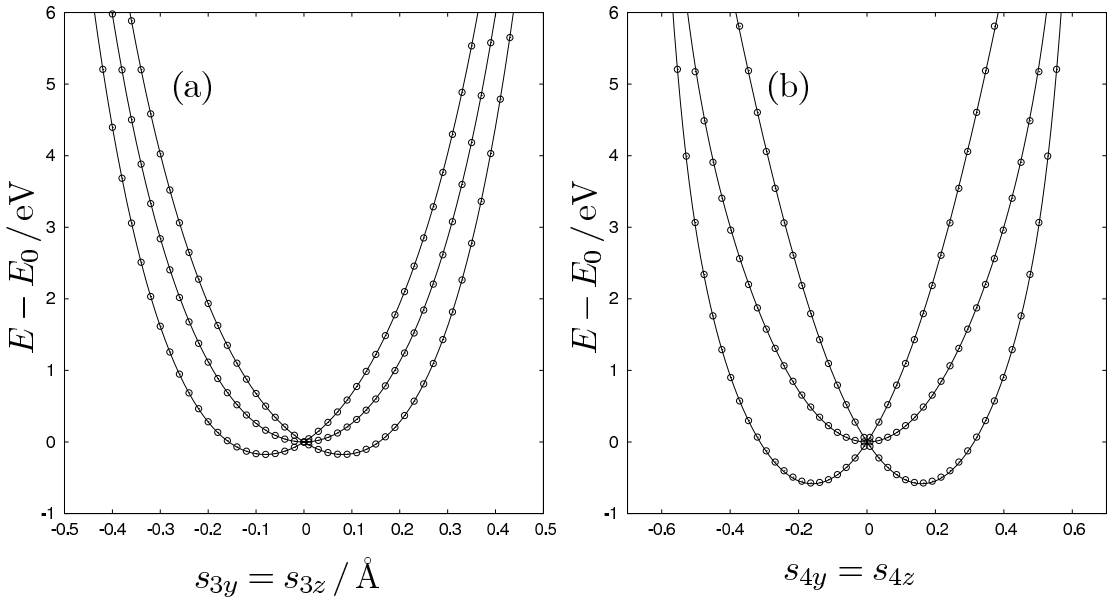

Figure 4.2: Diagonal cuts along two stretching (a) and two bending (b) coordinates. The symmetry is reduced to C_s and the T_2 electronic state splits into $2A' + A''$. The dots are the *ab initio* data; the lines represent the fit.

Fig. (4.2) shows the *ab initio* data and the fit for diagonal cuts in two components of a t_2 coordinate vector. The symmetry of the molecule along these displacements is C_s and each molecular geometry of C_s symmetry represents one of 12 equivalent images. The energy minima of the lowest surfaces in Fig. 4.2 correspond to saddle points between the six equivalent minima of C_{2v} symmetry.

In Fig. 4.3, we have plotted the PE surface for equal displacements of the three stretching (a) and bending (b) coordinates of T_2 symmetry. These preserve the epikernel symmetry C_{3v} and one of the surfaces is doubly degenerate. From the order of the epikernel group ($|C_{3v}| = 6$), the number of images is four. The minima in the PE curves are the trigonal minima and show a remarkable JT stabilization energy [104, 105].

We have determined the 43 parameters of the stretch-bend coupling terms by fitting *ab initio* points along 21 parameterized curves with more than 3000 energy points. It turns out that the single $T_2 \times t_2$ expansions already give a reasonable approximation of the six-dimensional $T_2 \times (t_2 + t_2)$ potential. The expansion of the stretch-bend coupling terms was therefore terminated at 4 th order. To illustrate

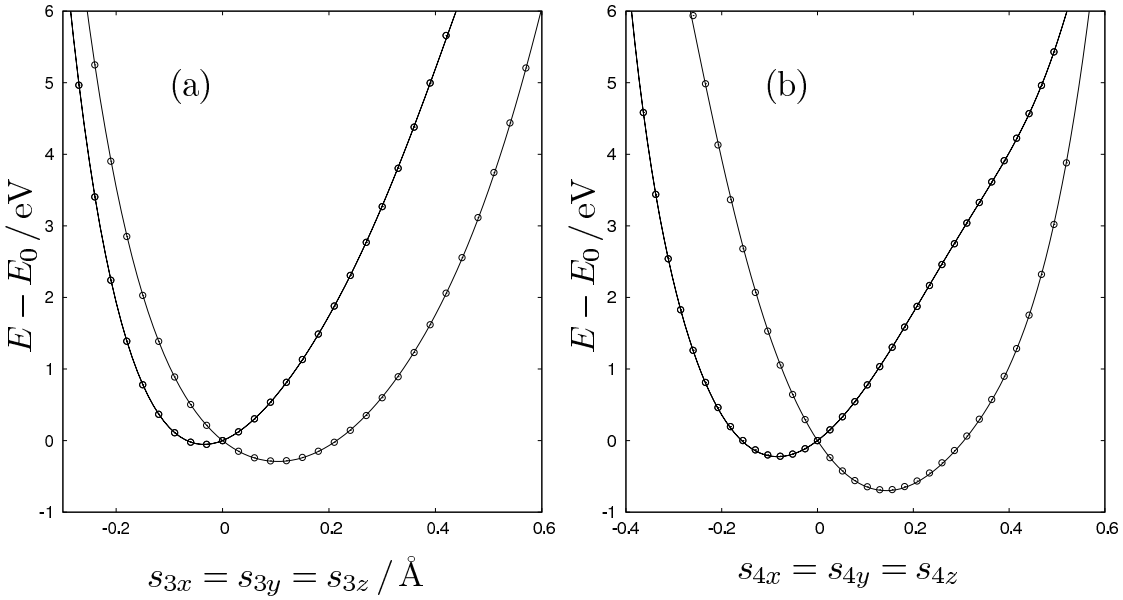

Figure 4.3: PE cuts for equal displacements of three stretching (a) and bending (b) coordinates. The nuclear displacements preserve C_{3v} symmetry. The T_2 electronic state splits into A and E electronic states.

the accuracy of the analytical potential, we have plotted in Fig. 4.4 the potentials along four different resulting cuts in the six-dimensional $t_2 + t_2$ space. The abscissa corresponds to a parameter u and the six-dimensional coordinate vectors are chosen as linear functions of this parameter,

$$\begin{aligned}
\mathbf{f}_a &= (0, \frac{1}{3}u + \frac{4}{15}, 0, 0, 0, -\frac{\sqrt{3}}{2}u)^\mathsf{T} \\
\mathbf{f}_b &= (0, u, 0, 0, -\frac{5\sqrt{3}}{9}u, -\frac{5\sqrt{3}}{8}u)^\mathsf{T} \\
\mathbf{f}_c &= (0, 0, u, 0, -\frac{\sqrt{3}}{2}u, 0)^\mathsf{T} \\
\mathbf{f}_d &= (u, 0, \frac{10}{3}u, -\sqrt{3}u, -\frac{5\sqrt{3}}{4}u, 0)^\mathsf{T},
\end{aligned} \tag{4.2}$$

where the stretching coordinates (the first three elements of the coordinate vectors) are given in Ångstrom.

An estimate of the accuracy of the analytical PE surface can be obtained from the residuals of the function values with respect to the *ab initio* data. Figure 4.5 relates the absolute values of the residuals to the energies of all calculated *ab initio* points. The lower parts of the PE surfaces (up to $\approx 2\,\mathrm{eV}$) exhibit mostly residuals less than

0.02 eV. The critical points of the surfaces are located at epikernel symmetries which correspond to the cuts shown in Figs (4.1–4.3) and are in very good agreement with the *ab initio* data.

Figure 4.6 shows the absolute values of the residuals for the 3179 data points of the six-dimensional $T_2 \times (t_2 + t_2)$ surface. It is obvious from Fig. 4.6 that the accuracy of the six-dimensional surface is lower than the accuracy of the two three-dimensional surfaces. However, in the low-energy region (which is the most important in many applications) the approximation is still fairly accurate.

The PE surfaces in the coordinate space of e symmetry are notably more complex compared to the topography in the t_2 modes. Perhaps most importantly, the spatial inversion of the methane cation occurs via a planar transition state involving at least one of the e coordinates. Particularly in this region, excited doublet electronic states of different symmetry intersect with a (doublet) T_2 electronic state below 5 eV. Additionally, there exist a vast number of intersection between the components of the T_2 electronic ground state and, mostly at energies above 5 eV, also with higher electronic states.

Figure 4.7a displays the data points of the electronic potential along with the fitted analytic PE surfaces for displacements of a single coordinate of e symmetry. All molecular geometries exhibit D_{2d} symmetry in this case and there exist three equivalent geometries to every point shown in Fig. 4.7a. The local maximum of the lowest graph in the center corresponds to a geometry of D_{4h} symmetry, with a planar quadratic arrangement of the hydrogen atoms. However, the epikernel subgroup is still D_{2d} (D_{4h} is not a subgroup of T_d) and it follows that there are three such planar structures. As mentioned previously, spatial inversion through a planar structure is not a symmetry operation of the molecular point group and cannot be achieved by permutations of identical nuclei. Thus in our coordinates, which depend on a space-fixed reference geometry, all coordinates that belong to geometries beyond the inversion threshold have been mapped to values that describe an energetically identical structure that is close to the reference orientation. The mapping was implemented numerically as a transformation from e-type symmetry coordinates to Cartesian coordinates, appropriate reflections in the planes defined by the three planar D_{4h} geometries of the molecule and subsequent back-transformation to symmetry coordinates.

Figure 4.7b shows two cuts of the fitted PE surface. Even though they are of considerable complexity, the fitted polynomial expansion (solid lines) reproduce the data

points (circles) with high accuracy. Displacements in the e coordinates in tetrahedral systems do not completely destroy the symmetry. For arbitrary displacements, the molecule still exhibits D_2 symmetry. Therefore, there exist $T_d/D_2 = 6$ identical energy points which considerably simplifies the acquisition of the *ab initio* points. The parameter optimization by the Marquardt-Levenberg algorithm was found to be straightforward.

Despite the large JT stabilization energy of the e mode ($\approx 1.3\,\mathrm{eV}$) and the extreme anharmonicity of the $T_2 \times e$ PE surface, an accurate analytic representation of the *ab initio* data points could be obtained over a wide range of the displacement coordinates of e symmetry. The results demonstrate that high-order polynomial expansions are very useful for accurate representations of PE surfaces in cases of strong JT coupling.

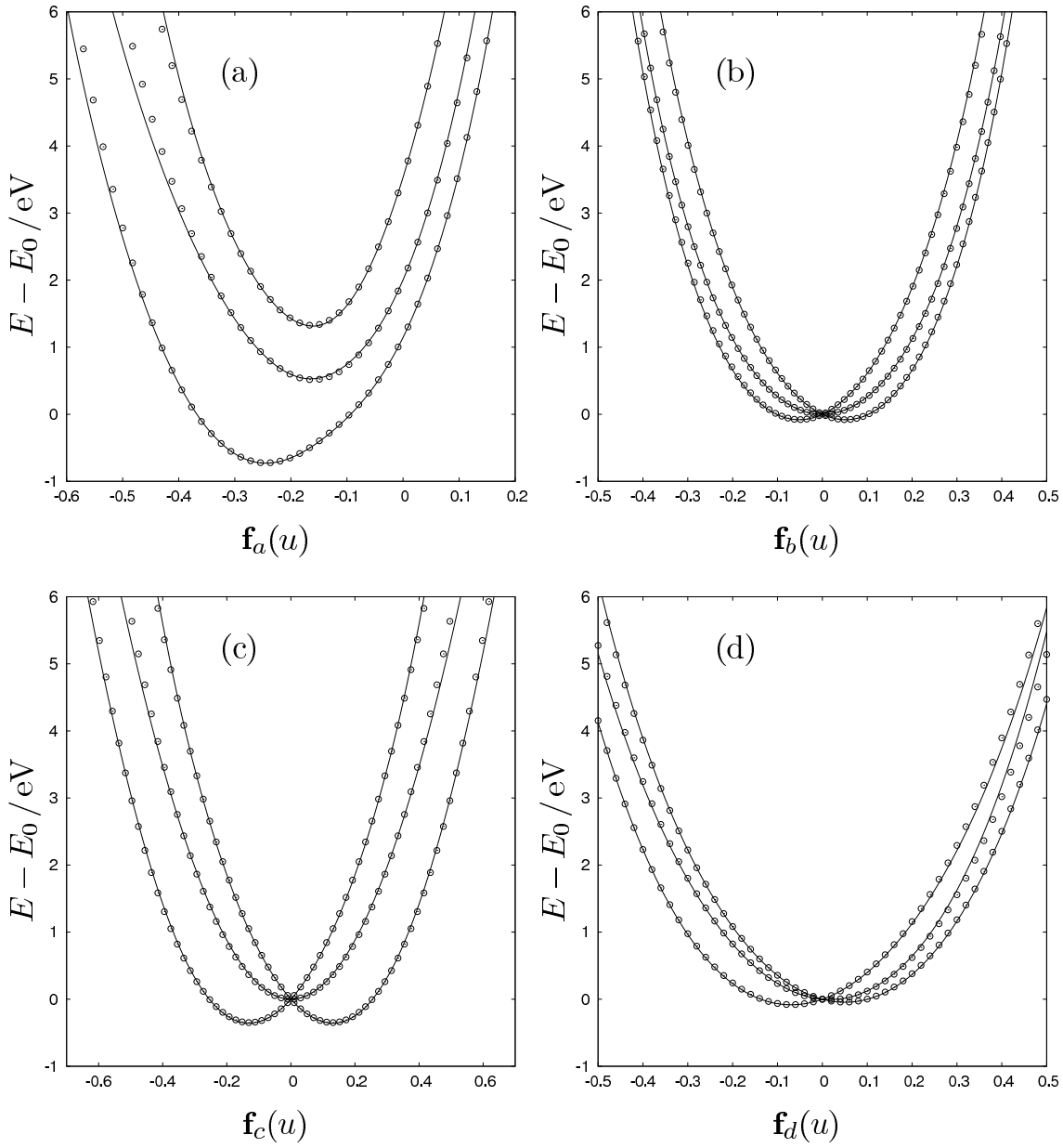

Figure 4.4: *Ab initio* (dots) and fitted (solid lines) potentials along four cuts of the $T_2 \times (t_2 + t_2)$ PE surfaces (see text for details).

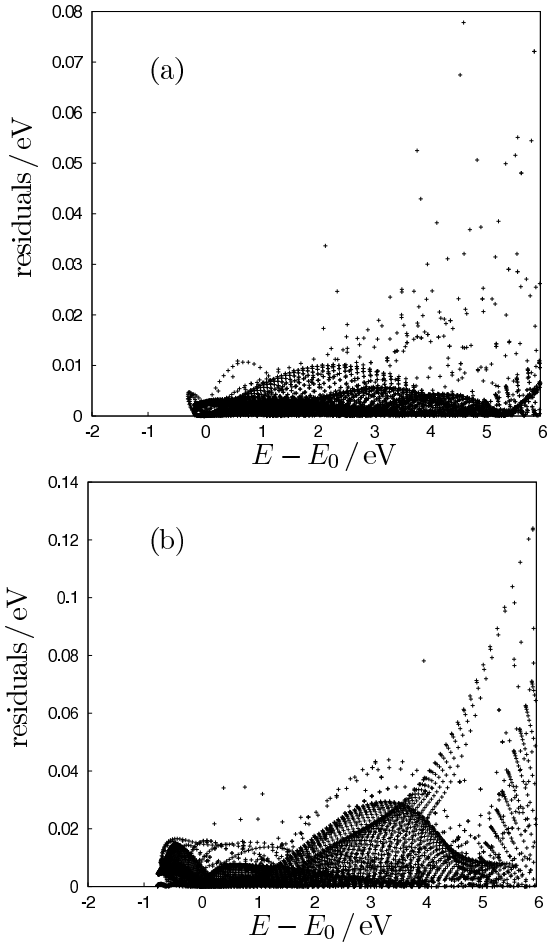

Figure 4.5: Residuals (absolute values) of the fitted PE surfaces. (a): stretching mode (7651 energies). (b): bending mode (7161 energies).

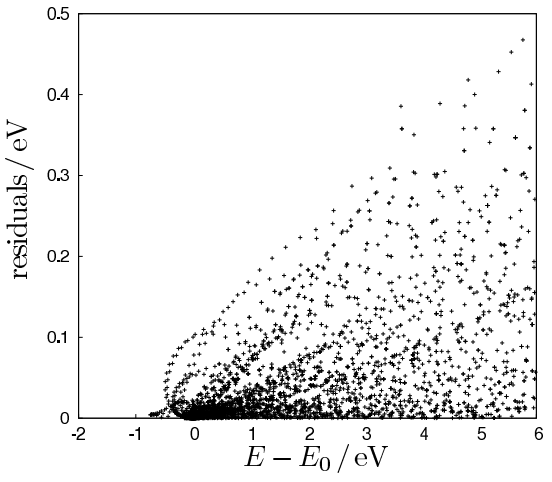

Figure 4.6: Absolute values of the 3179 residuals of the $T_2 \times (t_2 + t_2)$ surface.

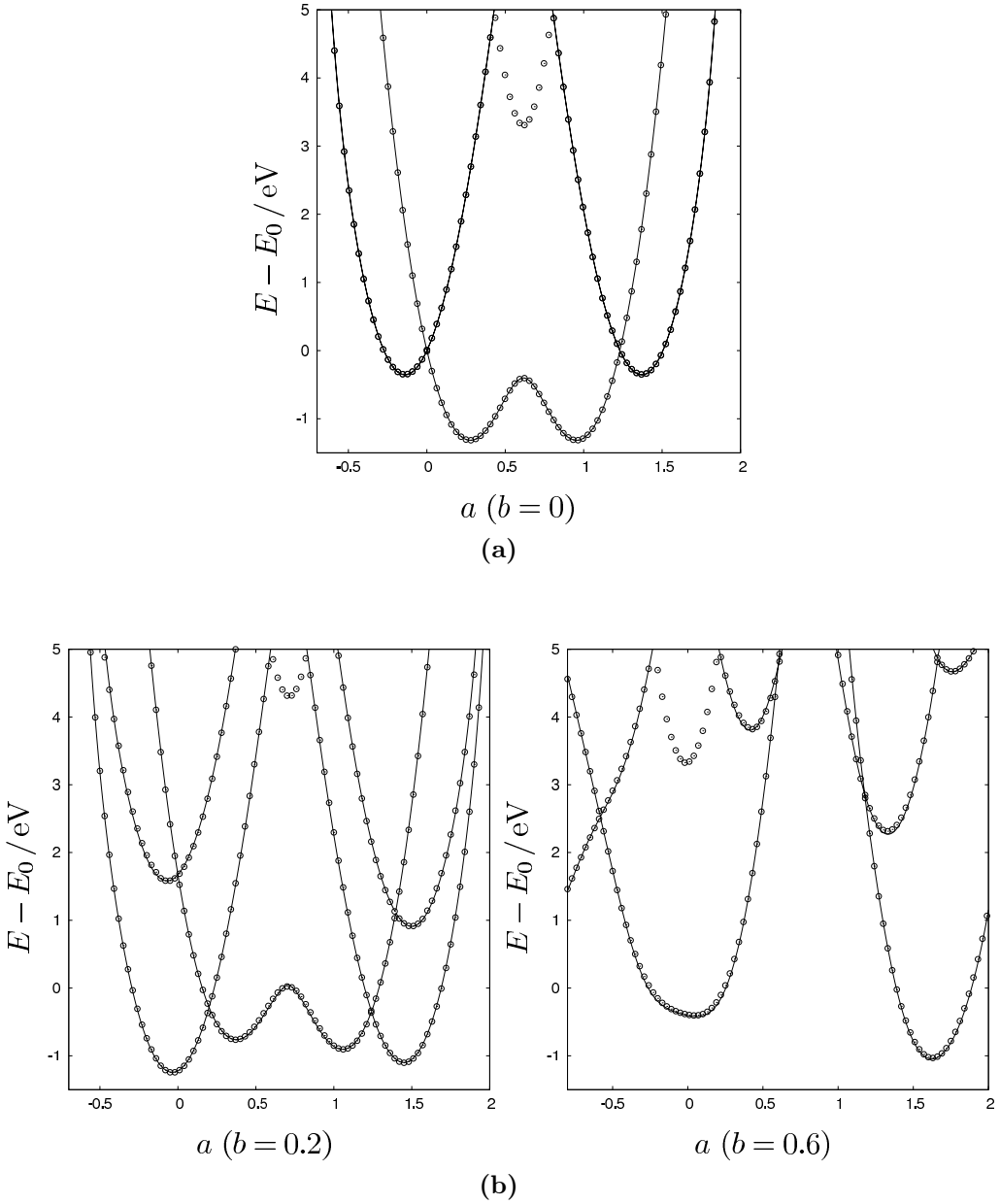

Figure 4.7: PE curves along symmetry coordinates of e symmetry (a, b). The circles represent energies obtained by *ab initio* calculations. The solid lines are the values of the fitted analytic potentials of the JT Hamiltonian, expanded up to 10 th order. Circles which are not connected by solid lines belong to additional electronic states (i. e., electronic states which are not components of the triply degenerate ground state at the reference geometry).

4.4 Jahn-Teller spectra of CH_4^+

The influence of different JT effects in the methane cation has been examined by simulations of photoelectron spectra of methane. All simulations were based on a full-dimensional analytic PE surface expansion up to sixth order, where couplings between modes of different symmetry have been neglected for the JT splitting terms (see Sec. 3.3). The analytic form of the trace of the PE matrix, however, includes all invariant terms up to sixth order to achieve a unique mapping between different molecular geometries and potential-energy values.

Wave-packet propagations were performed for 20000 steps using the Chebyshev propagation method as described in Sec. 2.6, using the harmonic ground state of the methane molecule as initial state. The nuclear wave function was represented on a DVR grid in mass-weighted Cartesian normal coordinates q_1, q_{2a}, q_{2b}, q_{3x}, q_{3y}, q_{3z}, q_{4x}, q_{4y}, q_{4z}. The photoelectron spectra have been convoluted with a Gaussian function of full-width at half-maximum (FWHM) of 0.05 eV (low-resolution) or 0.0017 eV (high-resolution). The computed vertical ionization energy of 14.35 eV has been used for the definition of the energy scale, since the PE minima w. r. t. specific combinations of Cartesian normal modes (and thus the zero-point energies of the cation) are not known.

The experimental UV photoelectron spectra indicate three broad intensity maxima at 13.6, 14.4 and 15.0 eV which have been attributed to the three sheets of the T_2 electronic state [22, 106]. The appearance of three widely spaced maxima clearly indicates a strong JT effect which induces various progressions within the three maxima. The extremely high line density prevented a reliable assignment of the progressions so far. In order to obtain more insight into the different overlapping progressions of the experimental spectrum, we consider the two- and three-dimensional $T_2 \times e$ and $T_2 \times t_2$ JT problems separately.

Figure 4.8a shows the $T_2 \times e$ photoelectron spectrum, simulated on a contracted direct-product grid of 41 points in each dimension. The spectrum consists of a superposition of three bands, arising from the JT splitting of the three sheets of the T_2 electronic state. The three progressions, which are not resolved in the low-resolution spectrum, are illustrated in Fig. 4.8a by Gaussian functions enveloping the progressions of the high-resolution spectrum. The average line spacing amounts to approximately 0.16 eV which is in good agreement with the theoretical prediction of Dixon [19]. All three progressions show identical line spacings, the typical charac-

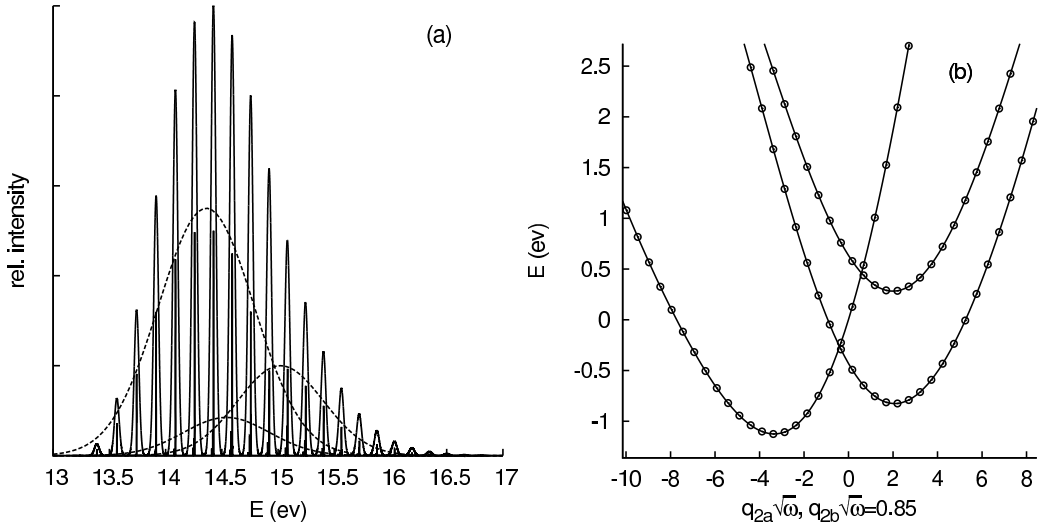

Figure 4.8: Left: $T_2 \times e$ JT spectrum of CH_4^+. Right: Analytic PE curves along the dimensionless normal coordinate $q_{2a}\sqrt{\omega}$ with a constant displacement in the second e coordinate.

teristic of harmonic potentials with very similar frequencies. Figure 4.8b shows a cut through the analytic $T_2 \times e$ PE surface along the dimensionless normal coordinate $q_{2a}\sqrt{\omega}$ with a small displacement in the second (dimensionless) e coordinate. It is seen that the three diabatic electronic states exhibit a nearly harmonic shape with very similar frequencies. Since the $T_2 \times e$ Hamiltonian matrix (see Sec. 3.2) is diagonal, the three sheets of the $T_2 \times e$ PE surfaces are uncoupled and three independent progressions can be expected. In fact, no vibronic coupling is observed in the $T_2 \times e$ JT spectrum in Fig. 4.8a.

The $T_2 \times t_2$ spectrum in the bending coordinates (q_{4x}, q_{4y}, q_{4z}) has been computed on a grid with 31 points in each dimension. A rather large basis of DVR points was required due to the high spectral density. The spectrum is shown in Fig. 4.9a and shows the highest line density compared to the JT spectra of the e mode and the t_2 stretching mode. Fig. 4.9b shows the onset of the photoelectron band in Fig. 4.9a. The effective vibrational spacing in the simulated spectrum was determined as approximately 0.12 eV between the centers of the first four multiplets in Fig. 4.9b. Most interestingly, the first three members of the progression show the same pattern as found in the experimental spectrum [22, 23] which was assigned, however, to the vibrational mode of e symmetry. It should be mentioned, that for the previous assignments a D_{2d} equilibrium structure was assumed, which corresponds to a displacement along a coordinate of e symmetry (see Fig. 1 for an illustration of the

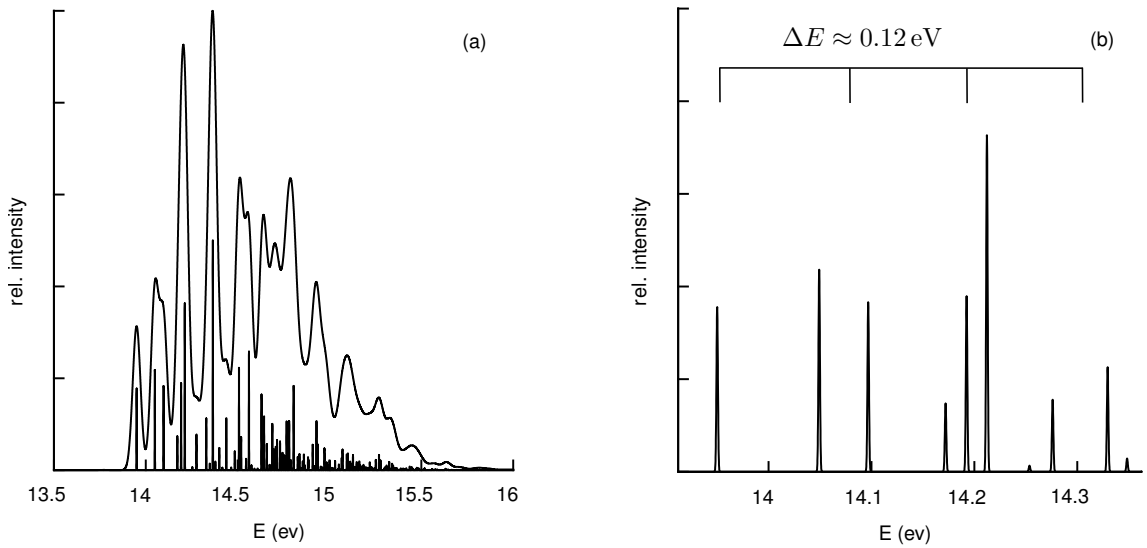

Figure 4.9: Left: $T_2 \times t_2$ JT spectrum of CH_4^+, taking the t_2 bending normal mode into account. Right: onset of the $T_2 \times t_2$ JT spectrum shown in the left figure.

symmetry adapted displacements). The latest theoretical and experimental results [25, 99, 100], however, indicate an equilibrium geometry of C_{2v} symmetry which requires a displacement along one of the t_2 coordinates. These results support the interpretation of the simulated spectra, which indicate that the t_2 (bending) mode is involved in the lowest vibrational progression of the photoelectron spectrum.

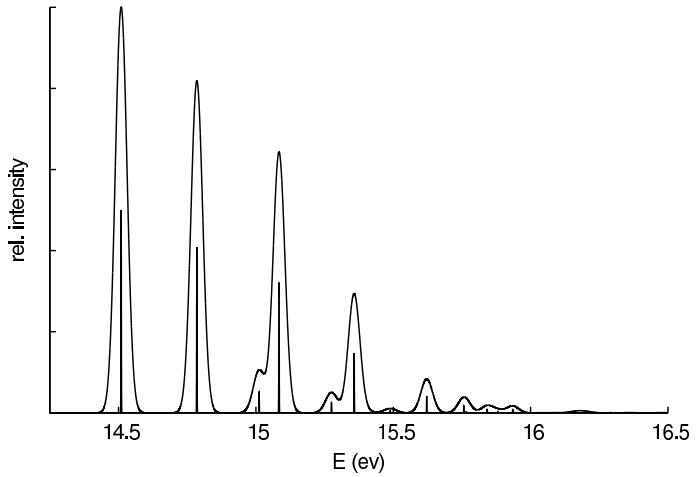

Figure 4.10: $T_2 \times t_2$ JT spectrum of CH_4^+ taking the CH bond-stretching coordinates of t_2 symmetry into account.

Fig. 4.10 shows the photoelectron spectrum calculated in the three-dimensional subspace of the t_2 stretching coordinate, describing the elongation and contraction

of the CH bond lengths. 11 grid points have been included along every degree of freedom. The spectrum consists of a superposition of three regular progressions which can be assigned to the three sheets of the electronic T_2 PE surface. Compared to the t_2 bending mode, an entirely different pattern is observed. Most notably, the photoelectron spectrum lacks the characteristic multiplets that originate from the energetic splittings of different combinations of vibrational excitations (Fig. 4.9). The highest progression, beginning at 15.75 eV, is of very low intensity. The progression associated with this adiabatic electronic state may be considered as the $T_2 \times t_2$ counterpart of Slonczewski resonances in the $E \times e$ JT effect. The vibrational energy levels appear at equal distances within an electronic band and, in contrast to the $T_2 \times e$ spectrum, with different spacings for different electronic transitions. The spectrum in Fig. 4.10 is representative of a rather weak JT effect with very low barriers between identical minima. Each spectral line is $\binom{3+v-1}{v}$ times degenerate (cf. 3D harmonic oscillator), where $v = v_x + v_y + v_z$ is the total vibrational quantum number. The comparison of the PE surfaces of the two t_2 modes in the methane cation reveals the origin of the very different photoelectron spectra. Figure 4.11 shows two-dimensional plots of the lowest T_2 PE surface in two of the three t_2 symmetry coordinates. While the t_2 bending surface exhibits well-defined minima of four-fold symmetry, the t_2 stretching PE surface is reminiscent of a Mexican hat in $x,\ y$ space (see Fig. 4.11). The orthorhombic PE minima in the t_2 stretching mode (-0.17 eV) are significantly higher in energy than the t_2 bending minima (-0.76 eV). Similar considerations apply to the trigonal minima (Fig. 4.3), explaining the "harmonic" structure of the progression in the t_2 stretching mode.

Approximate $T_2 \times (e + t_2)$ (bending) and $T_2 \times (e + t_2 + t_2)$ spectra have been obtained by convolution of the single-mode spectra, but do not allow for a reliable interpretation due to the very high line density and the neglected mode coupling. More powerful quantum wave-packet propagation methods such as the multi-layer multi-configuration time-dependent Hartree (ML-MCTDH) method [107, 108] are required for an analysis of the couplings between different modes. The convoluted spectra are illustrated in Appendix 6.

The general qualitative picture of the photoelectron spectrum of CH_4^+ emerging from the JT spectra Figs. 4.8–4.10 indicates that the extremely high line density in the experimental spectrum is largely induced by large-amplitude vibrations in the t_2 bending mode of the hydrogen atoms. The e vibration does not show a complex vibronic coupling pattern within our resolution, although the spectrum indicates

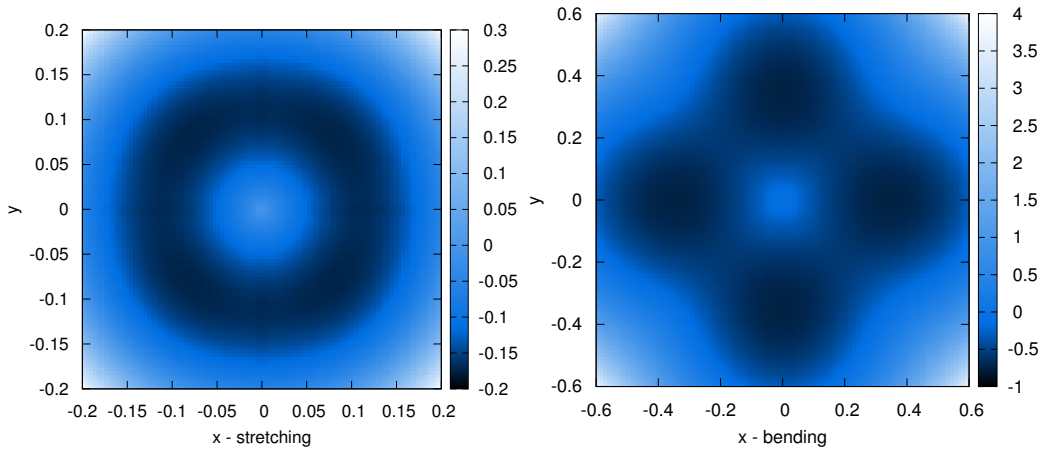

Figure 4.11: Two-dimensional PE surfaces as functions of the t_2 stretching (left) and t_2 bending (right) symmetry coordinates.

a very strong static JT effect in accordance with the structure of the PE surface. Unfortunately, converged simulations to compute the full-dimensional photoelectron spectrum are not feasible with the approach applied in this work. The agreement of the calculated multiplets of the $T_2 \times t_2$ bending mode spectrum with features of the experimental spectra, however, suggests that the vibrational line pattern in the low energy range of the photoelectron spectrum arises from the t_2 bending mode, in disagreement with earlier assignments of the structure of the UV photoelectron spectrum of CH_4^+ [22, 23].

5 The relativistic Jahn-Teller effect in tetrahedral systems

Tetrahedral systems exhibit a variety of Jahn-Teller (JT) effects of electrostatic and relativistic origin. At the electrostatic level [3], the doubly degenerate vibrational mode (e) is JT active (in first order) in doubly degenerate states (E) of tetrahedral systems. In triply degenerate states (T_1, T_2), both the e mode and the triply degenerate vibrational mode (t_2) are JT active [3, 5, 7]. At the relativistic level, when the spin of the electron and spin-orbit (SO) coupling are included, on the other hand, the t_2 mode is JT active (in first order) in ^2E states, while both e and t_2 modes are JT active in $^2T_2$ states [32, 33]. The relativistic JT forces are thus complementary to the electrostatic JT forces in ^2E states, whereas the electrostatic and relativistic JT forces act additively in $^2T_2$ states. In the latter case, the relativistic JT forces can either enhance or weaken the electrostatic JT forces [32, 33]. While the electrostatic JT couplings are expected to be weakly dependent on the nuclear charge of the constituting atoms, the relativistic JT couplings increase strongly with the nuclear charge. It should therefore be insightful to analyze the potential-energy (PE) surfaces and the vibronic spectra of an isoelectronic series of JT-active systems with increasing nuclear charges.

The tetramers of the atoms of the fifth main group, X_4^+ (X = P, As, Sb, Bi), represent such a series. Experimental photoelectron spectra of P_4, As_4 and Sb_4 have been reported by several groups more than 20 years ago [34–38]. It has been found that the ionized clusters exhibit very strong JT effects, involving the e mode in the ^2E ground state and the e and t_2 modes in the $^2T_2$ first excited state of the radical cations. In addition, effects of (zero-order) SO splittings were identified in the spectra of As_4^+ and Sb_4^+ [34–38]. This series of tetrahedral radical cations is well suited for a systematic investigation of the interplay of electrostatic and relativistic JT couplings in electronic spectra.

Recent *ab initio* calculations of the matrix elements of the Breit-Pauli operator

with nonrelativistic complete-active-space self-consistent-field (CASSCF) wave functions have confirmed the existence of substantial linear relativistic JT couplings in the heavier of the group-V tetramers [109]. In this chapter, we report a systematic analysis of the impact of genuinely relativistic JT couplings on the photoelectron spectra of the group-V tetramers.

An *ab initio* based analysis of the vibronic structure of the photoelectron spectrum of P_4 without the inclusion of SO coupling has been reported much earlier by Meiswinkel and Köppel [110], abbreviated as MK in the following. Beyond the linear-plus-quadratic ${}^2E \times e$ and ${}^2T_2 \times (t_2 + e)$ JT effects, MK considered also the pseudo-JT (PJT) coupling of the ${}^2E$ and ${}^2T_2$ states via the vibrational mode of t_2 symmetry. They found that the PJT coupling has a significant impact on the vibronic fine structure of the photoelectron band corresponding to the upper (${}^2T_2$) electronic state, while the low-resolution band shape is marginally affected by the PJT coupling [110]. Herein, we focus in novel phenomena arising from the SO coupling operator and neglect the additional complications arising from the electrostatic quadratic JT coupling and ${}^2E - {}^2T_2$ PJT coupling. We ignore, furthermore, the totally symmetric stretching mode which decouples from the JT active modes in first order (that is, neglecting (a_1, e) and (a_1, t_2) bilinear coupling terms).

5.1 Jahn-Teller Hamiltonians

The six vibrational normal modes of four-atomic tetrahedral systems transform according to the a_1, e and t_2 irreducible representations of T_d. The electronic ground state of the X_4^+ cations is of ${}^2E$ symmetry, the first excited state of ${}^2T_2$ symmetry [34–38]. In the two-component description of relativistic electronic-structure theory, which can be derived from the four-component Dirac-Coulomb formulation by the elimination of the small components [68, 111], the electronic Hamiltonian is written as

$$H_{\mathrm{el}} = H_{\mathrm{ES}} + H_{\mathrm{SO}} \tag{5.1}$$

where H_{ES} is the (spin-free) Hamiltonian containing the Coulombic interactions and H_{SO} is the SO-coupling operator. In the applications discussed below, H_{ES} is the generalized Fock operator of multi-configuration self-consistent-field (MCSCF) theory and H_{SO} is the full microscopic Breit-Pauli Hamiltonian containing one-electron and two-electron terms [112].

The electrostatic JT Hamiltonians of E and T_1, T_2 electronic states in tetrahedral

systems up to second order in normal-mode displacements are well known and can be found in many reviews and text books [5, 113, 114]. The effect of SO coupling in the ^2E and $^2T_{1,2}$ states at the tetrahedral reference geometry is also well known [5, 113–115]: The four-fold degeneracy of a ^2E state is retained (that is, there is no SO splitting of ^2E states in tetrahedral symmetry). The six-fold degenerate $^2T_1$ ($^2T_2$) state splits into a four-fold degenerate state transforming as $G_{3/2}$ in the spin double group T_d' [116] and a two-fold degenerate state transforming as $E_{1/2}$ ($E_{5/2}$) in T_d'. As a consequence of time-reversal symmetry [75], the two-fold degeneracy of the $E_{1/2}$ and $E_{5/2}$ levels cannot be lifted in the absence of external magnetic fields, while the levels of the $G_{3/2}$ manifold can split into two two-fold degenerate levels.

To obtain the relativistic JT Hamiltonians, the Breit-Pauli operator is expanded in a Taylor series in normal-mode displacements up to first order

$$H_{\mathrm{SO}} = h_0 + h_x Q_x + h_y Q_y + h_z Q_z + h_a q_a + h_b q_b. \tag{5.2}$$

Here Q_x, Q_y, Q_z are the normal coordinates transforming according to the t_2 irreducible representation and q_a, q_b are the normal coordinates of e symmetry. The nonvanishing matrix elements of H_{SO} in a spin-orbital basis are determined by symmetry selection rules in the spin double group T_d'. The details of the derivation can be found in Refs. [32, 33]. Expansion terms of second or higher order are neglected at the present stage of development of the theory.

For simplicity and clarity, we drop the (well-known) quadratic coupling terms of electrostatic origin and keep only the linear coupling terms of electrostatic or relativistic origin. The electrostatic coupling parameters are denoted by Latin symbols, while Greek symbols are used to denote relativistic JT couplings. With these simplifications, the JT Hamiltonians of a ^2E state are [32]

$$\mathbf{H}_{\mathrm{ES}}(^2E \times e) = \frac{1}{2}\omega_e^{(E)}\rho^2 \mathbf{I}_4 + b \begin{pmatrix} q_a & q_b & 0 & 0 \\ q_b & -q_a & 0 & 0 \\ 0 & 0 & -q_a & q_b \\ 0 & 0 & q_b & q_a \end{pmatrix} \tag{5.3}$$

$$\mathbf{H}_{\mathrm{SO}}(^2E \times t_2) = \frac{1}{2}\omega_{t_2}^{(E)} R^2 \mathbf{I}_4 + \beta \begin{pmatrix} 0 & iQ_z & iQ_- & 0 \\ -iQ_z & 0 & 0 & -iQ_- \\ -iQ_+ & 0 & 0 & iQ_z \\ 0 & iQ_+ & -iQ_z & 0 \end{pmatrix}. \tag{5.4}$$

Here, $\mathbf{I}_4$ is the 4×4 unit matrix, ρ and R are the radial coordinates in q_a, q_b and Q_x, Q_y, Q_z space, respectively

$$\rho = \left(q_a^2 + q_b^2\right)^{\frac{1}{2}} \tag{5.5a}$$

$$R = \left(Q_x^2 + Q_y^2 + Q_z^2\right)^{\frac{1}{2}} \tag{5.5b}$$

and

$$Q_\pm = Q_x \pm iQ_y. \tag{5.5c}$$

$\omega_e^{(E)}$ and $\omega_{t_2}^{(E)}$ are the harmonic vibrational frequencies of the e and t_2 normal modes, respectively, in the ^2E state. b is the linear electrostatic JT coupling constant of the e mode in the ^2E state, while β is the linear relativistic JT coupling constant of the t_2 mode in the ^2E state. As mentioned above, the linear JT couplings are complementary in ^2E states: while the e mode is JT active through electrostatic forces, the t_2 mode is JT active through relativistic forces [32].

In $^2T_{1,2}$ states, on the other hand, the e mode as well as the t_2 mode are JT active in first order through both the electrostatic and relativistic forces [33]. The zeroth-order SO coupling within a $^2T_{1,2}$ state is described by a 6×6 matrix which contains a single SO matrix element Δ. The diagonalization of this matrix defines the SO-adapted diabatic electronic basis. In this basis, the linear $^2T_2 \times e$ JT Hamiltonian takes the form [33]

$$\begin{aligned}\mathbf{H}_{\text{ES+SO}}\left({}^2T_2 \times e\right) = {} & \frac{1}{2}\omega_e^{(T_2)}\rho^2\mathbf{I}_6 \\ & + \begin{pmatrix} -\Delta + \tilde{c}_1 q_- & 0 & 0 & \tilde{c}_1 q^+ & -\tilde{c}_2 q_- & 0 \\ 0 & -\Delta - \tilde{c}_1 q_- & -\tilde{c}_1 q^+ & 0 & 0 & \tilde{c}_2 q^+ \\ 0 & -\tilde{c}_1 q^+ & -\Delta + \tilde{c}_1 q_- & 0 & 0 & \tilde{c}_2 q_- \\ \tilde{c}_1 q^+ & 0 & 0 & -\Delta - \tilde{c}_1 q_- & \tilde{c}_2 q^+ & 0 \\ -\tilde{c}_2 q_- & 0 & 0 & \tilde{c}_2 q^+ & 2\Delta & 0 \\ 0 & \tilde{c}_2 q^+ & \tilde{c}_2 q_- & 0 & 0 & 2\Delta \end{pmatrix}\end{aligned} \tag{5.6}$$

where

$$q_\pm = \frac{1}{2}\sqrt{3}q_a \pm \frac{1}{2}q_b \tag{5.7a}$$

$$q^{\pm} = \frac{1}{2} q_a \pm \frac{1}{2}\sqrt{3} q_b \tag{5.7b}$$

and

$$\tilde{c}_1 = \frac{c}{2} - \gamma \tag{5.8a}$$

$$\tilde{c}_2 = 2^{-\frac{1}{2}} (c + \gamma) . \tag{5.8b}$$

Here $\mathbf{I}_6$ is the 6×6 unit matrix and the real-valued parameters c and γ are the linear electrostatic and relativistic ${}^2T_2 \times e$ JT coupling constants, respectively. It is seen from Eqs. (5.6, 5.7, 5.8) that the electrostatic and relativistic JT couplings interfere constructively or destructively, depending on the signs of c and γ.

The relativistically generalized JT Hamiltonian for the t_2 mode reads [33]

$$\mathbf{H}_{\mathrm{ES+SO}}\left({}^2T_2 \times t_2\right) = \frac{1}{2}\omega_{t_2}^{(T_2)} R^2 \mathbf{I}_6 + \begin{pmatrix} -\Delta & -i\tilde{a}_1 Q_+ & 0 & i\tilde{a}_1 Q_z & 0 & i\tilde{a}_2 Q_- \\ i\tilde{a}_1 Q_- & -\Delta & -i\tilde{a}_1 Q_z & 0 & -\frac{i}{\sqrt{3}}\tilde{a}_2 Q_- & \frac{2i}{\sqrt{3}}\tilde{a}_2 Q_z \\ 0 & i\tilde{a}_1 Q_z & -\Delta & i\tilde{a}_1 Q_- & -i\tilde{a}_2 Q_+ & 0 \\ -i\tilde{a}_1 Q_z & 0 & -i\tilde{a}_1 Q_+ & -\Delta & -\frac{2i}{\sqrt{3}}\tilde{a}_2 Q_z & -\frac{i}{\sqrt{3}}\tilde{a}_2 Q_+ \\ 0 & \frac{i}{\sqrt{3}}\tilde{a}_2 Q_+ & i\tilde{a}_2 Q_- & \frac{2i}{\sqrt{3}}\tilde{a}_2 Q_z & 2\Delta & 0 \\ -i\tilde{a}_2 Q_+ & -\frac{2i}{\sqrt{3}}\tilde{a}_2 Q_z & 0 & \frac{i}{\sqrt{3}}\tilde{a}_2 Q_- & 0 & 2\Delta \end{pmatrix} \tag{5.9}$$

where $Q_\pm$ is defined in Eq. (5.5c) and

$$\tilde{a}_1 = 3^{-\frac{1}{2}} (a + 2\alpha) \tag{5.10a}$$

$$\tilde{a}_2 = 2^{-\frac{1}{2}} (a - \alpha) . \tag{5.10b}$$

The real-valued parameters a and α are the linear electrostatic and relativistic ${}^2T_2 \times t_2$ JT coupling constants. As for the e mode, there can be constructive or destructive interference of the electrostatic and relativistic JT couplings, depending on the signs of a and α.

If the zeroth-order SO splitting 3Δ (see Eqs. (5.6) and (5.9)) is sufficiently large, the sub-block corresponding to the $G_{3/2}$ representation (with diagonal elements $-\Delta$) and the sub-block corresponding to the $E_{5/2}$ representation (with diagonal elements 2Δ) can approximately be decoupled. This (artificial) limit, which reduces the 6×6

	P	As	Sb	Bi
ω_{a_1}	75.55	43.45	29.15	20.70
ω_e	45.39	25.29	16.46	11.65
ω_{t_2}	57.13	32.28	21.43	15.18
$r_0(\mathrm{X}_4)$	2.22	2.46	2.86	3.03
$r_0^{T_2}(\mathrm{X}_4^+)$	2.28	2.54	2.93	3.09
$r_0^{E}(\mathrm{X}_4^+)$	2.16	2.43	2.84	3.03
IP	9552.8	8786.8	7913.1	7345.3

Table 5.1: Equilibrium internuclear distances (r_0) at the tetrahedral geometry for the X_4 clusters in the A_1 electronic ground state and the X_4^+ ions in the $^2T_2$ electronic state (in Ångstrom). Harmonic frequencies of the neutral molecules and vertical ionization potentials (IP) are given in meV.

JT matrix to a 4×4 matrix, was frequently considered in the ancient literature on the JT effect in crystals [117]. Here, we treat the nonadiabatic dynamics of the full 6×6 $^2T_2 \times (t_2 + e)$ JT Hamiltonian.

Finally, the nuclear kinetic-energy operator has to be added to yield the JT Hamiltonians

$$\mathbf{H}(^2E \times (e + t_2)) = T_N \mathbf{I}_4 + \mathbf{H}_{\mathrm{ES+SO}}(^2E \times (e + t_2)) \tag{5.11a}$$

$$\mathbf{H}(^2T_2 \times (e + t_2)) = T_N \mathbf{I}_6 + \mathbf{H}_{\mathrm{ES+SO}}(^2T_2 \times (e + t_2)) \tag{5.11b}$$

T_N is written in dimensionless ground-state normal coordinates as

$$T_N = -\frac{1}{2}\omega_e \left(\frac{\partial^2}{\partial q_a^2} + \frac{\partial^2}{\partial q_b^2} \right) - \frac{1}{2}\omega_{t_2} \left(\frac{\partial^2}{\partial Q_x^2} + \frac{\partial^2}{\partial Q_y^2} + \frac{\partial^2}{\partial Q_z^2} \right), \tag{5.12}$$

ω_e and ω_{t_2} are the harmonic vibrational frequencies of the e and t_2 normal modes, respectively, in the electronic ground state of the neutral X_4 systems.

5.2 Computational methods

5.2.1 *Ab initio* electronic-structure calculations

In order to determine the magnitudes of the electrostatic and relativistic JT coupling parameters, we have performed relativistic *ab initio* electronic-structure calculations for the ^2E ground state and the $^2T_2$ first excited electronic state of the cluster cations P_4^+, As_4^+, Sb_4^+, Bi_4^+. The calculations were carried out in C_{2v} symmetry along

	P_4^+	As_4^+	Sb_4^+	Bi_4^+
$\omega_{a_1}(^2E)$	69.22	37.90	26.00	18.48
$\omega_e(^2E)$	38.79	22.60	15.00	10.65
$\omega_{t_2}(^2E)$	44.92	26.16	17.99	12.88
$\Delta(^2T_2)$	-5.18	-27.10	-71.45	-264.30
$\omega_{a_1}(^2T_2)$	63.63	36.50	25.27	18.25
$\omega_e(^2T_2)$	40.02	22.54	14.90	10.49
$\omega_{t_2}(^2T_2)$	51.10	29.59	19.97	14.21
b	197.18	129.03	85.19	63.73
β	1.60	4.58	8.57	15.16
c	-20.88	2.68	1.60	5.81
γ	-	-	3.14	5.74
a	144.26	94.55	63.86	48.45
α	-	-10.55	-10.94	-16.05

Table 5.2: Parameters used in the model Hamiltonians for the simulation of photoelectron spectra. All values are given in meV.

symmetry coordinates of e and t_2 symmetry. All symmetry-adapted coordinates are defined in Appendix 4.1.

The wave function of the electrostatic Hamiltonian has been constructed in the state-averaged CASSCF approximation, which is a full-configuration-interaction calculation in a restricted space of so-called active molecular orbitals [118]. The active space included the 12 p-orbitals of the four atoms of the cluster. The remaining occupied orbitals were restricted to double occupation. Matrix elements of the Breit-Pauli Hamiltonian have been computed with the CASSCF wave functions of the lowest five electronic states corresponding to the manifold ^2E and $^2T_2$. By diagonalizing the 10×10 SO matrix, SO-corrected adiabatic potentials have been computed.

The PE surfaces of P_4^+ were computed using Dunning's correlation-consistent triple-ζ basis set [119]. For the clusters of the heavier elements, pseudo- or effective core potentials (PPs, ECPs) developed by Metz et al. [120] were employed, which implicitly include relativistic effects of the core electrons. The core definitions correspond to [Ne], [Ar]+3d and [Kr]+4d4f for As, Sb and Bi, comprising 10, 28 and 60 electrons, respectively. Thus all (n-1) spd and n sp electrons were treated explicitly in the *ab initio* calculations, where n denotes the principal quantum number of the respective element. As basis functions for the valence electrons, we used the correlation-consistent polarized valence triple-ζ (cc-pVTZ-PP) basis with pseudo-

potentials of Peterson [121]. All *ab initio* calculations were performed with the MOLPRO quantum chemistry software [122].

Equilibrium geometries and harmonic frequencies have been computed for the neutral X_4 clusters in the electronic ground state at the coupled-cluster level including single, double and perturbative triple excitations (CCSD(T)). Vertical ionization potentials have been computed using an open-shell coupled-cluster (RCCSD(T)) method. The tetrahedral reference geometries of the ions were determined as the minima of the PE curves along the totally symmetric coordinate in the lowest electronic state of T_2 symmetry. Vibrational frequencies of the e and t_2 modes of the cations have been obtained from the second derivatives of the mean energy $(V_1 + V_2)/2$ of the ^2E manifold and the mean energy $(V_1 + V_2 + V_3)/3$ of the $^2T_2$ manifold, respectively (see Table 5.2). Table 5.1 gives the optimized geometries as well as the harmonic vibrational frequencies of the neutral and cationic clusters. Fig. 5.1 illustrates the computed PE surfaces of Sb_4^+.

5.2.2 Jahn-Teller parameters

The JT coupling parameters were determined by fitting the adiabatic PE functions of the JT Hamiltonians to *ab initio* data along cuts of C_{2v} symmetry in a suitable range close to the conical intersection at the tetrahedral reference geometry. The parameters of the PE matrices which have been used in the present work are summarized in Table 5.2. The table includes the linear electrostatic $T_2 \times t_2$, $T_2 \times e$ and $E \times e$ JT coupling parameters, as well as the corresponding zero-order and linear relativistic parameters. Despite of the reasonable trends in the JT parameters, these should be interpreted with some care since the nonlinear fitting procedure is very sensitive to the selected range of *ab initio* data. It should be mentioned that the electrostatic $E \times e$ and $T_2 \times t_2$ JT effects in the P_4^+, As_4^+ and Sb_4^+ cluster cations are among the strongest JT effects known in nature [37, 110]. An example of a parametrized PE surface for a JT system exhibiting rather small SO coupling effects is provided in Fig. 5.2.

It is helpful to consider dimensionless JT parameters for a comparison of the magnitudes of the JT effect within the series of X_4 clusters. While the magnitudes of the dimensionless electrostatic $T_2 \times t_2$ (a/ω_{t_2}) and $T_2 \times e$ (c/ω_e) JT coupling parameters are roughly constant throughout the series, the relativistic JT coupling parameters increase strongly with Z. For Bi_4^+, the relativistic $T_2 \times t_2$ JT coupling even exceeds the electrostatic JT coupling and represents a truly pronounced JT

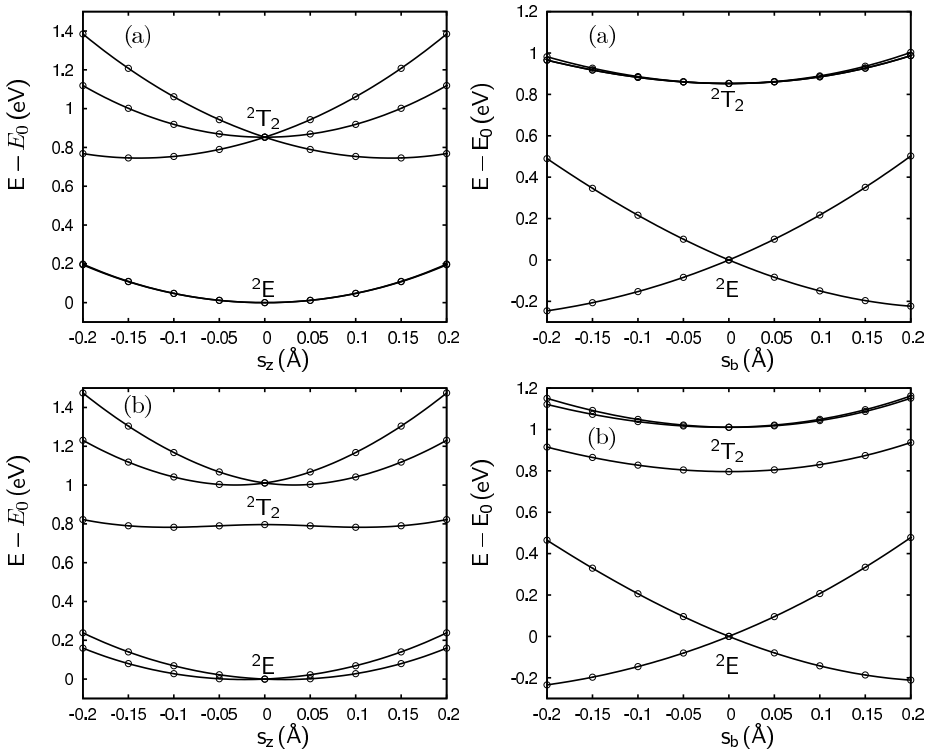

Figure 5.1: *Ab initio* PE surfaces of Sb_4^+ along a symmetry coordinate of T_2 symmetry (left) and of E symmetry (right). The upper panels (a) show the results of nonrelativistic *ab initio* calculations. The data displayed in the lower panels (b) have been computed including the microscopic Breit-Pauli spin-orbit operator.

effect ($\alpha/\omega_{t_2} \approx -2.01$). For the ^2E ground state, the electrostatic $E \times e$ JT coupling (b/ω_e) is likewise roughly constant throughout the series, while the magnitude of the relativistic $^2E \times t_2$ JT coupling (β/ω_e) increases with Z. It should be noted that the t_2 mode is not JT active in the ^2E state in the nonrelativistic approximation. A more detailed discussion of the JT effects in the context of photoelectron spectra is provided in Section 5.3.

5.2.3 Propagation of the nuclear wave function

The photoelectron spectra of P_4^+, As_4^+, Sb_4^+ and Bi_4^+ were computed by the Chebyshev method described in Sec. 2.6. Calculations have been performed with two ($^2E \times e$, $^2T_2 \times e$), three ($^2E \times t_2$, $^2T_2 \times t_2$) and five ($^2E \times (e + t_2)$) vibrational degrees of freedom. The wave-packet and the diabatic potentials were represented on a direct-product discrete variable representation (DVR) grid based on sinc(x) func-

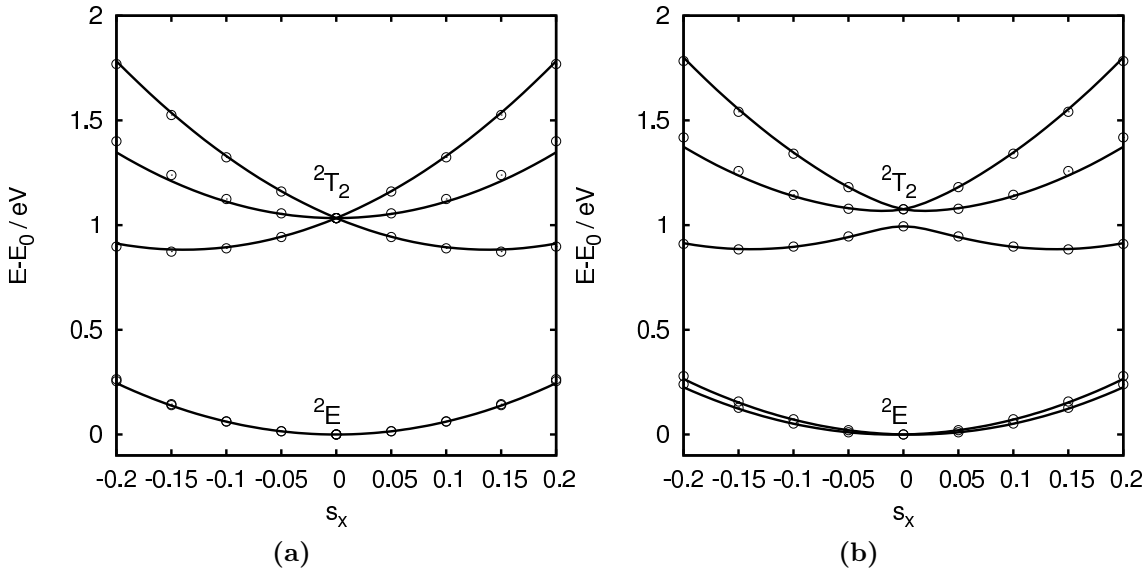

Figure 5.2: Electrostatic (left) and relativistic (right) PE surfaces of the electronic ^2E ground and first excited $^2T_2$ state for As_4^+ (dots: *ab initio* data; solid lines: fit).

tions [80]. All spectra (except the 5D $^2E \times (t_2 + e)$ spectra) have been computed several times with different grid parameters until convergence was achieved. Particularly demanding are the simulations of the relativistic $^2T_2 \times t_2$ JT spectra for the heavier clusters since the computational cost increases strongly with the spectral range of the Hamiltonian, which increases with the zero-order SO splitting. The grid parameters employed in the present work are listed in Tab. 5.3. All propagations involved 20000 iterations according to Eq. (2.46), starting from the harmonic vibrational ground state of the respective neutral cluster.

The low-resolution spectra of the electronic ^2E state have been obtained by convolution with a Gaussian of 35, 20, 15 and 10 meV full width at half maximum (FWHM) for P_4^+, As_4^+, Sb_4^+ and Bi_4^+, respectively. The spectral envelopes of the $^2T_2 \times t_2$ spectra were computed with a Gaussian convolution of 40 and 20 meV FWHM for P_4^+ and As_4^+. For the low-resolution spectra of the lowest electronic $^2T_2$ state of Sb_4^+ and Bi_4^+ a FWHM of 10 meV was used. For the high-resolution spectra, the FWHM has been reduced by a factor of 1/30 with respect to the low-resolution spectra.

	electrostatic		relativistic
	$^2E \times e$	$^2T_2 \times t_2$	$^2T_2 \times t_2$
P_4^+	-500.0/500.0 (141)	-300.0/300.0 (121)	–
As_4^+	-1000.0/1000.0 (181)	-1000.0/1000.0 (121)	-1000.0/1000.0 (161)
Sb_4^+	-1500.0/1500.0 (201)	-1000.0/1000.0 (121)	-1000.0/1000.0 (121)
Bi_4^+	-2000.0/2000.0 (201)	-2000.0/2000.0 (161)	-1500.0/1500.0 (161)

Table 5.3: Parameters of the direct-product grids employed in the computation of the JT spectra. The grid range of the respective electronic state/coordinate in mass-weighted normal coordinates is given. The numbers in parentheses are the numbers of equidistant gridpoints per degree of freedom used in the uncontracted grid. For zero- and first-order relativistic Hamiltonians the same grid parameters were used.

5.3 Photoelectron spectra and discussion

The emphasis of the present investigation is on the understanding of the effects of novel relativistic JT couplings on the photoelectron spectra of the group-V tetramers, which are known to exhibit very strong JT effects in the ^2E ground state as well as in the $^2T_2$ first excited state [34–38, 110]. For brevity and clarity, we restrict the present analysis to zeroth-order SO splittings and first-order electrostatic and relativistic JT couplings. Quadratic JT couplings of electrostatic origin and ^2E-$^2T_2$ PJT couplings are known to be relevant from the work on MK on P_4^+ [110], but are beyond the scope of the present work. We also ignore the totally symmetric breathing mode which is separable from the JT dynamics in first order. Moreover, we assume zero temperature, that is, ionization from the vibrational ground state of the clusters.

5.3.1 The ^2E state

The vibronic structures and band shapes of the photoelectron bands corresponding to the ^2E ground state of P_4^+, As_4^+, Sb_4^+ and Bi_4^+ are shown in Fig. 5.3 (from top to bottom). The vibronic dynamics in the ^2E state is characterized by an exceptionally strong electrostatic $E \times e$ JT effect, as was shown in Refs. [34–38, 110]. The t_2 mode is not JT active in first order in ^2E states at the electrostatic level, but becomes JT active (in first order) through the SO operator [32]. The relativistic $^2E \times t_2$ JT effect is, however, too weak to compete with the very pronounced $^2E \times e$ JT effect, except for the heaviest system, see below.

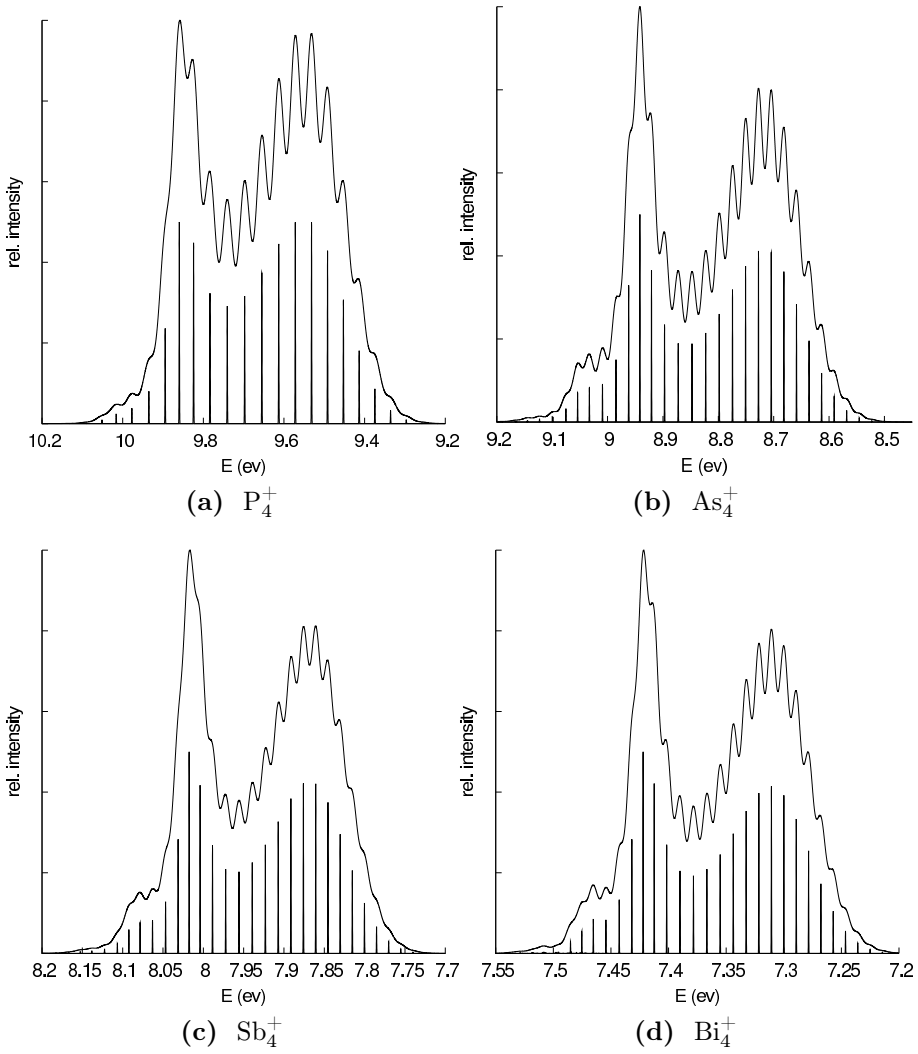

(a) P_4^+ **(b)** As_4^+

(c) Sb_4^+ **(d)** Bi_4^+

Figure 5.3: Electrostatic ${}^2E \times e$ Jahn-Teller spectra of P_4^+, As_4^+, Sb_4^+ and Bi_4^+.

The ${}^2E \times e$ JT spectra exhibit a very extended approximately equidistant progression in the e mode, as discussed previously by Wang et al. [37, 38]. The narrower second hump of the envelope represents a so-called Slonczewski resonance [123]. It is the well-known signature of a very strong $E \times e$ JT effect [37, 124]. For P_4^+, the dimensionless JT coupling parameter $\frac{b}{\omega_e}$ has been estimated as 5.3 by MK (*ab initio*, with Koopmans' theorem) and as 5.75 by Wang et al. (empirical fit), in good qualitative agreement with the present *ab initio* result (5.1). The vibronic line density is much higher in the ${}^2E \times e$ spectrum of MK, since they included quadratic JT coupling as well as ${}^2E - {}^2T_2$ PJT coupling [110]. The low-resolution envelope of the ${}^2E$ band of P_4^+ in Fig. 5.3a is, however, in good agreement with the result of MK [110].

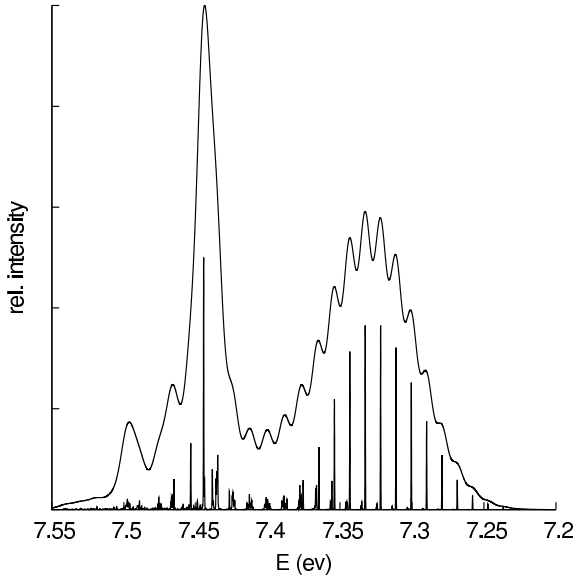

Figure 5.4: $E \times (e + t_2)$ Jahn-Teller spectrum of Bi_4^+ including SO coupling.

As far as the purely relativistic ${}^2E \times t_2$ JT coupling is concerned, the dimensionless coupling parameter $\frac{\beta}{\omega_e}$ is very small in P_4^+ (0.04), but becomes significant in Bi_4^+ (1.42), see Table 5.2. The ${}^2E$ photoelectron spectrum of Bi_4, calculated with the inclusion of both e and t_2 modes, is shown in Fig. 5.4. The first-order relativistic ${}^2E \times t_2$ coupling (recall that the zeroth-order SO splitting of the ${}^2E$ state is zero) has a minor effect on the lower sub-band, but results in a significant narrowing and irregular vibronic fine structure of the upper sub-band (compare Figs. 5.3d and 5.4). In the case of Bi_4^+, the relativistic ${}^2E \times t_2$ JT coupling thus has a measurable impact on the low-resolution band shape as well as on the detailed vibronic structure.

5.3.2 The ${}^2T_2$ state

In contrast to the ${}^2E$ state, the ${}^2T_2$ state exhibits a zero-order SO splitting 3Δ, cf. Eqs. (5.6) and (5.9). In addition, the electrostatic linear JT coupling constants are additively/destructively modified by the linear relativistic JT couplings, cf. Eqs. (5.8) and (5.10b). The calculated SO-splitting parameter Δ is given in Table 5.2. The SO splitting 3Δ increases from 15 meV in P_4^+ to 793 meV in Bi_4^+.

For the t_2 mode, we have $\tilde{a}_1 < a$ and $\tilde{a}_2 > a$ (see Eq. (5.10b) and Table 5.2), that is, the JT couplings within the $G_{3/2}$ manifold are reduced, while the coupling between the $G_{3/2}$ and $E_{5/2}$ manifolds is increased by the relativistic coupling parameter α. These effects are illustrated by the adiabatic JT PE curves shown in Fig. 5.2 for As_4^+,

for example. Figure 5.2a exhibits the very strong electrostatic ${}^2T_2 \times t_2$ JT coupling in the ${}^2T_2$ state of As_4^+. Figure 5.2b illustrates the zeroth-order SO splitting of the ${}^2T_2$ state (into the $G_{3/2}$ and $E_{5/2}$ manifolds) and the existence of a weak, but noticeable, relativistic linear ${}^2E \times t_2$ JT coupling in the ${}^2E$ state.

For the e mode, the nonrelativistic ${}^2T_2 \times e$ JT coupling is modified by the relativistic JT coupling parameter γ, see Eq. (5.8). Since c and γ are of the same sign, $\tilde{c}_1 < c$ and $\tilde{c}_2 > c$, that is, the JT effect within the $G_{3/2}$ manifold is decreased, while the $G_{3/2} - E_{5/2}$ coupling is enhanced by the relativistic JT coupling. Since c as well as γ are small compared to the coupling parameters a and α of the t_2 mode, these effects are hardly visible in the vibronic spectra. Therefore, we show and discuss the pure ${}^2T_2 \times t_2$ spectra in what follows.

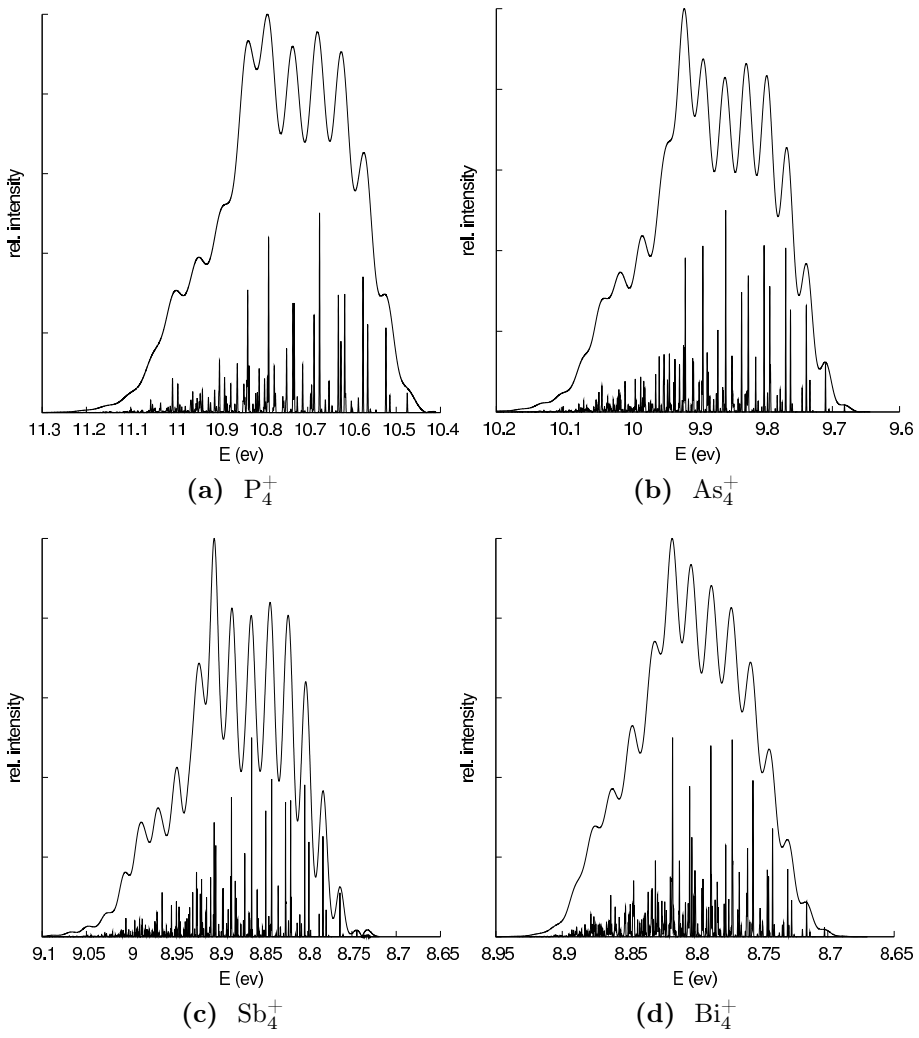

Figure 5.5: Electrostatic ${}^2T_2 \times t_2$ Jahn-Teller spectra of P_4^+, As_4^+, Sb_4^+ and Bi_4^+.

The nonrelativistic ${}^2T_2 \times t_2$ JT spectra of P_4^+, As_4^+, Sb_4^+ and Bi_4^+ are displayed in Fig. 5.5. They are representatives of a very strong ${}^2T_2 \times t_2$ JT effect. The dimensionless JT coupling parameter $\frac{a}{\omega_{t_2}}$ increases from 2.8 for P_4^+ to 3.4 for Bi_4^+. While the vibronic fine structure is highly irregular, the low-resolution envelopes exhibit a quasi-regular progression. Surprisingly, this partially resolved progression survives even for the heaviest systems, despite the strongly reduced vibrational frequency of the t_2 mode in Sb_4^+ and Bi_4^+.

The ${}^2T_2 \times t_2$ JT spectra obtained with inclusion of SO splitting and linear relativistic JT coupling are shown in Figs. 5.6–5.8 for As_4^+, Sb_4^+ and Bi_4^+ (the SO coupling effects in P_4^+ are too minor to be of interest). In these three figures, the panels (a) show the spectra obtained with inclusion of zeroth-order SO splitting 3Δ, but neglect of the linear relativistic JT coupling, determined by the parameter $\frac{\alpha}{\omega_{t_2}}$. The lower panels (b) show the spectra obtained with complete inclusion of SO-coupling effects up to first order in the t_2 mode.

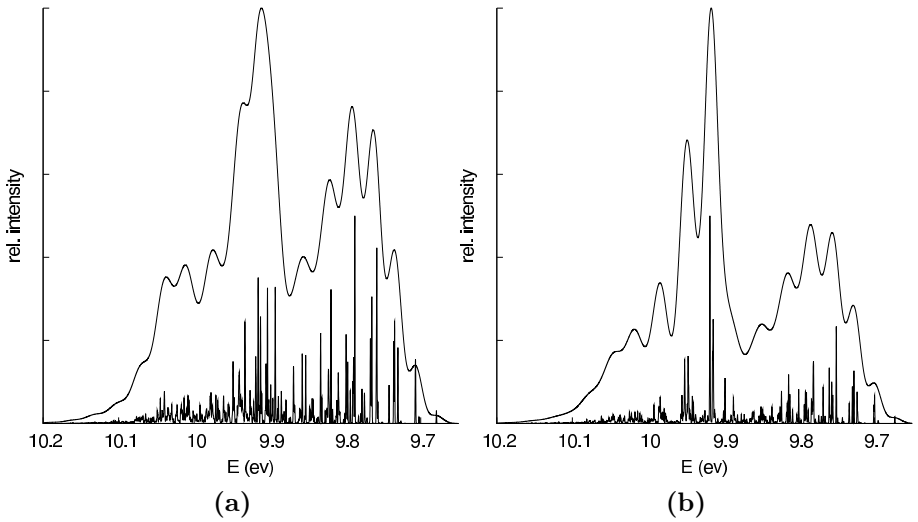

Figure 5.6: ${}^2T_2 \times t_2$ Jahn-Teller spectra of As_4^+ including zeroth-order (left) and zeroth-order plus first-order (right) spin-orbit coupling.

The comparison of the lhs frames of Figs. 5.6–5.8 with the corresponding spectra in Fig. 5.5 reveals the effect of the SO splitting 3Δ of the ${}^2T_2$ state. For Bi_4^+, due to large SO splitting of about 0.8 eV, only the upper ($G_{3/2}$) band is shown in Fig. 5.8. Already in As_4^+, the band shape exhibits a doublet structure. The apparent splitting (≈ 0.15 eV) is significantly larger than the zeroth-order SO splitting of 0.08 eV (Table 5.2). For Sb_4^+ and Bi_4^+, the apparent splitting of the ${}^2T_2$ photoelectron band approaches the value 3Δ. As expected, strong SO splitting quenches the (electrostatic) JT effect, that is, the SO-separated bands become narrower and the vibronic progressions are reduced. This phenomenon is generally known as the "Ham effect" [125].

Of particular interest in the context of the present work is the effect of linear relativistic JT coupling on the vibronic spectra, that is, the difference of the spectra in the lhs and rhs panels of Figs. 5.6–5.8. In all three cases, a reduction of the

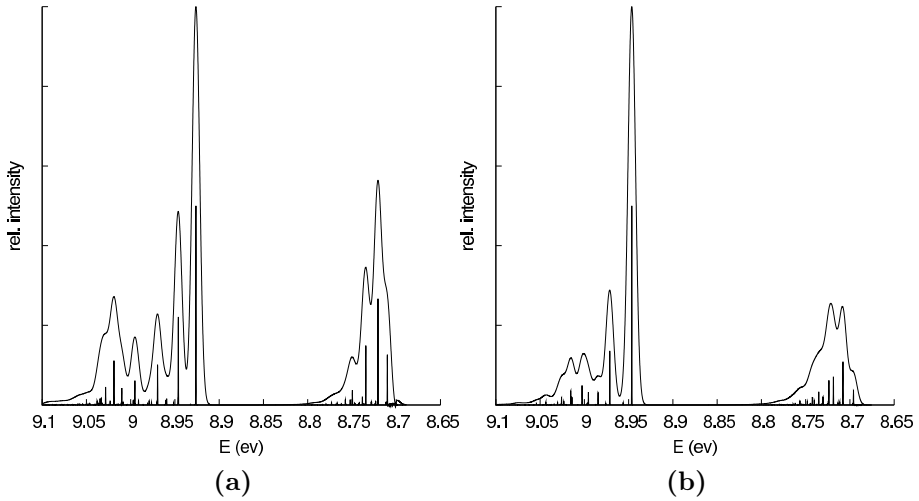

Figure 5.7: ${}^2T_2 \times t_2$ Jahn-Teller spectra of Sb_4^+ including zeroth-order (left) and zeroth-order plus first-order (right) spin-orbit coupling.

vibrational pseudo-progressions in the upper ($G_{3/2}$) sub-band is observed which is concomitant with the destructive interference of electrostatic and SO-induced JT couplings ($\tilde{a}_1 < a$). This effect is very pronounced for Bi_4^+ (Fig. 5.8): here the vibronic spectrum of the upper sub-band contracts to a double-peak envelope, as expected for a two-state JT effect (the $G_{3/2}$ manifold splits into two Kramers doublets). Very interesting is the relativistic JT spectrum of the ${}^2T_2$ state of As_4^+: here a novel quasi-regular progression develops in the upper sub-band, see Fig. 5.6b.

Unfortunately, a comparison of these pronounced JT and SO-coupling effects with experiment is currently not possible. The available experimental photoelectron spectra of P_4, As_4 and Sb_4 are strongly broadened due to the high temperature of the clusters (between 450 and 1150 K) [34–38]. The excitation of the totally symmetric breathing mode is another effect which conceals the features due to the JT effect. As a result, the existing photoelectron spectra of As_4, Sb_4 and Bi_4 are structureless [34–38].

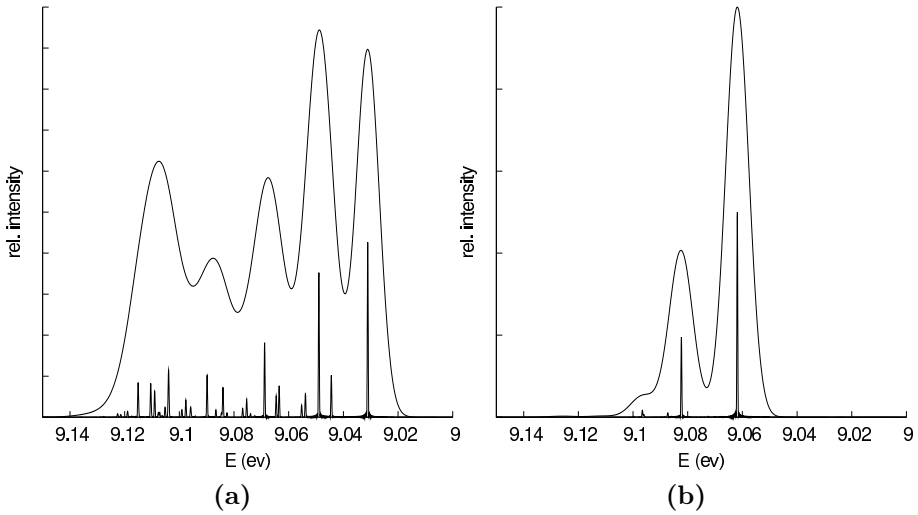

Figure 5.8: ${}^2T_2 \times t_2$ Jahn-Teller spectra of Bi_4^+ including zeroth-order (left) and zeroth-order plus first-order (right) spin-orbit coupling. In both figures only the high-energy ($G_{3/2}$) band is shown.

6 Summary

The central topic of this work is the construction of systematically generalized JT model Hamiltonians for molecules of tetrahedral symmetry and their application in simulations of photoelectron spectra. Recently, Braams, Bowman and coworkers devised an approach to the approximation problem of single-sheeted PE surfaces based on automated scans of *ab initio* data and computational invariant theory. While their results are widely considered as a breakthrough in the construction of PE surfaces of closed-shell systems, the approximation problem of multi-sheeted PE surfaces of open-shell systems remained unsolved. The generalization of the approach of Braams and Bowman to multi-sheeted PE surfaces of systems of high symmetry has been developed in the present thesis. In order to construct multi-sheeted multi-dimensional JT PE surfaces, methods of group theory and the theory of invariant polynomials have been combined to exploit the full symmetry of a molecule. The major achievement of the theoretical part of this work is the development of a new method to obtain matrix expansions of multi-sheeted PE surfaces up to arbitrary order. The derivation of arbitrary-order matrix expansions of multi-sheeted PE surfaces in a diabatic representation is solely based on the molecular symmetry (point-group and/or permutation-inversion symmetry). The multi-sheeted expansion method represents a generalization of the expansion of single adiabatic surfaces and is particularly well-suited for JT PE surfaces.

The first application presented in this work is a high-order expansion of three-sheeted PE surfaces of T_2 symmetry in tetrahedral systems. From the irreducible representations of the permutation group of four elements (S_4), a complete set of generating polynomials has been determined comprising 31 invariant polynomials. This provides a considerable simplified polynomial basis compared to a recently published generating set containing more than 150 terms. From the generating polynomials, a set of symmetry-adapted matrices has been determined which, together with the generating polynomials, permit the expansion of the diabatic model Hamiltonian up to arbitrary order. Analytic expansions of the PE matrix have been determined up

to 6 th order in a basis of internuclear distances and up to 12 th order in the JT active modes using symmetry coordinates, which are based on a space-fixed reference geometry. A large data set of accurate *ab initio* energies has been computed for the three lowest electronic states of T_2 symmetry of the methane cation. The *ab initio* calculations were carried out using the multi-reference configuration-interaction method, where all valence orbitals have been included in the active space of the CASSCF calculation. The parameters in the PE expansion were determined by fitting the adiabatic *ab initio* data to the eigenvalues of the model Hamiltonian. Although in a few special cases the fitting procedure can be simplified to a linear least-squares problem, fitting general JT PE surfaces poses a non-linear optimization problem. In this work, a Marquardt-Levenberg algorithm has been implemented to perform the non-linear least-squares optimization. A Fortran module was implemented which evaluates the approximate electronic energies within the fitted range of coordinates. The new nine-dimensional PE surface has been used for the simulation of Jahn-Teller spectra of the methane cation with the Chebyshev propagation method. Compared to all previous treatments of the JT effect in CH_4^+, which were limited to Hamiltonians expanded up to second order, the full-dimensional three-sheeted PE surface up to 6 th order provides a substantially improved description of the vibronic coupling effects in the methane cation. It was found that the strongest vibronic coupling arises from the t_2 bending mode. Moreover, simulations of the JT spectra indicate that the vibrational structure near the onset of the UV photoelectron spectrum arises from the t_2 bending mode, contrary to previous speculative assignments of the experimental data. Unfortunately, it is not yet possible to compute the photoelectron spectrum with inclusion of all degrees of freedom of the present PE surface with currently available quantum dynamics methods.

The second application of JT theory in this thesis addresses the problem of spin-orbit coupling in JT systems containing heavy atoms. As is well known, many solids containing heavy atoms with unpaired electrons exhibit the JT effect, including materials of high technological importance such as high-temperature superconductors or materials with colossal magnetoresistance. Although relativistic methods are well-established in electronic-structure theory, the lack of appropriately extended theoretical models prevented the examination of SO-induced JT coupling effects in tetrahedral systems. Based on recently developed JT Hamiltonians, the JT effect in ^2E and $^2T_2$ states of the clusters of the series of isoelectronic $X_4{}^+$ (X = P, As, Sb, Bi) clusters of the fifth main group have been investigated. Besides the electrostatic JT

couplings in the electronic ground state of ^2E symmetry and the triply degenerate first excited state of $^2T_2$ symmetry, relativistic JT couplings arising from the SO operator have been evaluated for the first time. The SO-induced JT parameters, which have been determined by relativistic *ab initio* calculations, indicate that for heavier systems, such as Sb_4^+ and Bi_4^+, SO coupling effects can be of the same magnitude as the electrostatic JT effect. Photoelectron spectra have been computed in the electrostatic approximation and with inclusion of the zeroth-order SO splittings as well as first-order relativistic JT couplings. An extension of the Chebyshev wavepacket method to complex-valued Hamiltonians has been implemented to deal with relativistic JT Hamiltonians. In the spectra of the electrostatic model the typical signatures of a very strong JT $T_2 \times t_2$ effect are observed, which are preserved when zero-order SO coupling is included. The first-order SO coupling, on the other hand, cause a significant reduction of the electrostatic JT couplings. From the comparison of the simulations including electrostatic and electrostatic plus SO JT couplings, a detailed picture of the influence of SO effects on the JT spectra could be obtained, including the first characterization of a purely relativistic $^2E \times t_2$ JT effect. The presented results clearly indicate that SO coupling effects play an important role in vibronic-coupling phenomena in molecules with heavy atoms.

Appendices

1 Generating sets of invariant polynomials for YX_4 systems

The complete generating set of polynomials of a YX_4 molecule comprises 31 polynomials. The polynomials were determined from a representation in internuclear distances with the `Singular`-Software and the `finvar`-library [60, 61]. The invariants are expressed in coordinates adapted to irreducible representations. The complete set of invariant polynomials in the JT active coordinates $x_1, y_1, z_1, x_2, y_2, z_2$ are

$$\begin{aligned}
f_1 &= x_1^2 + y_1^2 + z_1^2 \\
f_2 &= x_1 y_1 z_1 \\
f_3 &= x_1^4 + y_1^4 + z_1^4 \\
f_4 &= x_2^2 + y_2^2 + z_2^2 \\
f_5 &= x_2 y_2 z_2 \\
f_6 &= x_2^4 + y_2^4 + z_2^4 \\
f_7 &= x_1 x_2 + y_1 y_2 + z_1 z_2 \\
f_8 &= z_1 x_2 y_2 + y_1 x_2 z_2 + x_1 y_2 z_2 \\
f_9 &= y_1 z_1 x_2 + x_1 z_1 y_2 + x_1 y_1 z_2 \\
f_{10} &= x_1 x_2^3 + y_1 y_2^3 + z_1 z_2^3 \\
f_{11} &= x_1^2 x_2^2 + y_1^2 y_2^2 + z_1^2 z_2^2 \\
f_{12} &= x_1^3 x_2 + y_1^3 y_2 + z_1^3 z_2 \\
f_{13} &= a^2 - ab + b^2 \\
f_{14} &= a^3 - \frac{3}{2}\left(a^2 b + a b^2\right) + b^3
\end{aligned} \tag{1a}$$

$$
\begin{aligned}
f_{15} &= (a-2b)\, x_1^2 + (a+b)\, y_1^2 + (b-2a)\, z_1^2 \\
f_{16} &= a^2 x_1^2 + (a-b)^2\, y_1^2 + b^2 z_1^2 \\
f_{17} &= (a-2b)\, x_1^4 + (a+b)\, y_1^4 + (b-2a)\, z_1^4 \\
f_{18} &= (a-2b)\, x_2^2 + (a+b)\, y_2^2 + (b-2a)\, z_2^2 \\
f_{19} &= a^2 x_2^2 + (a-b)^2\, y_2^2 + b^2 z_2^2 \\
f_{20} &= (a-2b)\, x_2^4 + (a+b)\, y_2^4 + (b-2a)\, z_2^4 \\
f_{21} &= (a-2b)\, x_1 x_2 + (a+b)\, y_1 y_2 + (b-2a)\, z_1 z_2 \\
f_{22} &= a^2 x_1 x_2 + (a-b)^2\, y_1 y_2 + b^2 z_1 z_2 \\
f_{23} &= (a-2b)\, x_1 x_2^3 + (a+b)\, y_1 y_2^3 + (b-2a)\, z_1 z_2^3 \\
f_{24} &= (a-2b)\, x_1^2 x_2^2 + (a+b)\, y_1^2 y_2^2 + (b-2a)\, z_1^2 z_2^2 \\
f_{25} &= (a-2b)\, x_1^3 x_2 + (a+b)\, y_1^3 y_2 + (b-2a)\, z_1^3 z_2 \\
f_{26} &= (a-2b)\, x_1 y_2 z_2 + (a+b)\, y_1 x_2 z_2 + (b-2a)\, z_1 y_2 x_2 \\
f_{27} &= (a-2b)\, x_2 y_1 z_1 + (a+b)\, y_2 x_1 z_1 + (b-2a)\, z_2 y_1 x_1 \\
f_{28} &= a^2 x_1 y_2 z_2 + (a-b)^2\, y_1 x_2 z_2 + b^2 z_1 y_2 x_2 \\
f_{29} &= a^2 x_2 y_1 z_1 + (a-b)^2\, y_2 x_1 z_1 + b^2 z_2 y_1 x_1 .
\end{aligned}
\tag{1b}
$$

Additionally, there exist the following (not JT active) displacements (invariants of first order in the internuclear distances)

$$
\begin{aligned}
s_0 &= \frac{1}{\sqrt{6}} \left(\Delta r_{21} + \Delta r_{31} + \Delta r_{41} + \Delta r_{32} + \Delta r_{42} + \Delta r_{43}\right) \\
s_1 &= \frac{1}{2} \left(\Delta r_1 + \Delta r_2 + \Delta r_3 + \Delta r_4\right).
\end{aligned}
\tag{2}
$$

2 The polarization method

The polarization process is a formal procedure of substituting a set of variables in a polynomial by a another copy of variables with identical symmetry properties [50]. The polarization operators are defined as linear differential operators $D_{ij} (1 \leq i, j \leq m)$, acting on one of m coordinate vectors $\mathbf{v}_j \in V^m = V_1 \oplus \ldots \oplus V_m$ (which transform identically under the symmetric group of n elements, S_n) of dimension n:

$$
\mathrm{D}_{ij}\, p = \sum_{k=1}^{n} v_{i,k} \frac{\partial p}{\partial v_{j,k}}. \tag{3}
$$

This is the derivative of a (invariant) polynomial p with respect to $\mathbf{v}_j$ in the direction of $\mathbf{v}_i$. Hence, the polarization process corresponds to a successive substitution of the variables of a vector space by the variables from another copy of the same vector space. The polarized polynomials are invariants under the group acting on the vector space V^{m+1}. This procedure may be repeated an arbitrary number of times. Weyl has shown for the symmetric group S_n of n elements that if the invariant ring $\mathbb{R}[V_1]^{S_n}$ is generated by a set of polynomials $f_1, \cdots, f_n$, then their polarized forms generate the ring $\mathbb{R}[V_1 \oplus V_2]^{S_n}$ [50]. This holds for an arbitrary number of vectors $\mathbf{v}_i$.

Consider, as an example, the generating polynomial $f^{(1)}(\mathbf{v}_1) = x_1 y_1 z_1$ (Eq. (3.10) with $\mathbf{v}_j = (x_j, y_j, z_j)^\mathsf{T}$) of degree 3 for the T_2 representation of the $T_d \simeq S_4$ group. Polarization yields

$$\mathrm{D}_{21}\, f^{(1)}(\mathbf{v}_1) = x_2 y_1 z_1 + x_1 y_2 z_1 + x_1 y_1 z_2 \tag{4}$$

and similarly

$$\frac{1}{2}\left(\mathrm{D}_{21}\right)^2 f^{(1)}(\mathbf{v}_1) = x_2 y_2 z_1 + x_1 y_2 z_2 + x_2 y_1 z_2. \tag{5}$$

In order to define the mapping between an operator containing the symmetry of a molecular system, the expectation value (this is the actual invariant physical quantity) can be considered as a homogeneous polynomial of degree two in the electronic coordinates (a *2-form*, cf. Eq. 2.4).

$$\mathbf{c}^\mathsf{T}\mathbf{A}\mathbf{c} = \sum_{ij} c_i c_j A_{ij} \tag{6}$$

The resulting polynomial in the coefficients c_i is completely determined by the symmetric matrix $\mathbf{A}$ and, assuming the elements A_{ij} are polynomials in some coordinates $\mathbf{v}$, must be an element of the invariant ring $\mathbb{R}[\mathbf{c} \oplus \mathbf{v}]^G$. If a subspace $\mathbf{w} \leq \mathbf{v}$ of the coordinates on which the elements A_{ij} depend forms a vector space that transforms identically as $\mathbf{c}$, a generating set for the invariant expansion terms in Eq. (3.2) is easily determined by applying twice the polarization operators for $\mathbf{c}$ as shown in Eq. (5). Due to the nature of the polarization operators, the elements A_{ij} are equivalent to the second derivatives w. r. t. c_i and c_j up to a constant factor. This is the main advantage to work with vector spaces that transform as irreducible representations. The complete expansion is obtained from a fundamental set of invariants which contains all distinct irreducible representations. The invariant ring is then

easily extended by polarization and mapped to the respective operator expansion.

An interesting aspect is the structure of the operator expansion. Due to the product structure of the polynomials in the invariant expansion, the operator expansion has the structure of a module. Let $h_{ij}(p),\ i,j \in x,y,z$, be an element of the Hessian of an invariant $p(f_1,\cdots,f_n)$ expressed as a product of invariants f_i. It follows from the product rule of differentiation:

$$h_{ij}(p) = \frac{\partial^2}{\partial x_i \partial x_j} f_1 f_2 \dots f_n = \sum_{k=1}^{n} \frac{\partial^2 f_k}{\partial x_i \partial x_j} \prod_{l \neq k} f_l + \sum_{k \neq m} \left(\frac{\partial f_k}{\partial x_i}\frac{\partial f_m}{\partial x_j} + \frac{\partial f_k}{\partial x_j}\frac{\partial f_m}{\partial x_i} \right) \prod_{l \neq k \neq m} f_l. \tag{7}$$

Finding the generators of a polynomial matrix expansion of a diabatic potential matrix is thus equivalent to finding the first and second partial derivatives of the generating set of polynomials. All matrix elements can be constructed as appropriate products of the first or second derivatives in the respective coordinates with a number of totally-symmetric invariants. Any product of two f_i results in a sum of three matrices with elements

$$h_{ij}(f_k f_l) = a_1 f_k \frac{\partial^2 f_l}{\partial x_i \partial x_j} + a_2 f_l \frac{\partial^2 f_k}{\partial x_i \partial x_j} + a_3 \left(\frac{\partial f_l}{\partial x_i}\frac{\partial f_k}{\partial x_j} + \frac{\partial f_l}{\partial x_j}\frac{\partial f_k}{\partial x_i} \right) \tag{8}$$

where the a_i are independent parameters (to be determined by a least-squares fit to *ab initio* data), since the corresponding matrices form invariant terms in the matrix expansion. Clearly, any product of the h_{ij} with an invariant is a valid expansion term as well, since the factors f_i preserve the symmetry.

3 Matrix expansion of T_2 potential-energy surfaces

As shown in App. 2, every term in the matrix expansion of the JT PE surfaces can be constructed from the first and second derivatives of the invariant polynomials. The general traceless (i. e. JT active) part of the PE expansion can be written as a module over the invariants $\mathbb{R}[f_1,\dots,f_n]$ given in Appendix 1.

$$\mathbf{V} = \mathbb{R}[f_1,\dots,f_n] + \bigoplus_{i=1}^{n} \mathbf{g}_i \mathbb{R}[f_1,\dots,f_n] \tag{9}$$

. The matrices $\mathbf{g}_i$ are

$$\mathbf{g}_1 = \begin{pmatrix} 2x_1^2 - y_1^2 - z_1^2 & 0 & 0 \\ 0 & 2y_1^2 - x_1^2 - z_1^2 & 0 \\ 0 & 0 & 2z_1^2 - x_1^2 - y_1^2 \end{pmatrix}$$

$$\mathbf{g}_2 = \begin{pmatrix} 2x_1^4 - y_1^4 - z_1^4 & 0 & 0 \\ 0 & 2y_1^4 - x_1^4 - z_1^4 & 0 \\ 0 & 0 & 2z_1^4 - x_1^4 - y_1^4 \end{pmatrix}$$

$$\mathbf{g}_3 = \begin{pmatrix} 2x_2^2 - y_2^2 - z_2^2 & 0 & 0 \\ 0 & 2y_2^2 - x_2^2 - z_2^2 & 0 \\ 0 & 0 & 2z_2^2 - x_2^2 - y_2^2 \end{pmatrix}$$

$$\mathbf{g}_4 = \begin{pmatrix} 2x_2^4 - y_2^4 - z_2^4 & 0 & 0 \\ 0 & 2y_2^4 - x_2^4 - z_2^4 & 0 \\ 0 & 0 & 2z_2^4 - x_2^4 - y_2^4 \end{pmatrix} \tag{10a}$$

$$\mathbf{g}_5 = \begin{pmatrix} 2x_1x_2 - y_1y_2 - z_1z_2 & 0 & 0 \\ 0 & 2y_1y_2 - x_1x_2 - z_1z_2 & 0 \\ 0 & 0 & 2z_1z_2 - x_1x_2 - y_1y_2 \end{pmatrix}$$

$$\mathbf{g}_6 = \begin{pmatrix} 2x_1x_2^3 - y_1y_2^3 - z_1z_2^3 & 0 & 0 \\ 0 & 2y_1y_2^3 - x_1x_2^3 - z_1z_2^3 & 0 \\ 0 & 0 & 2z_1z_2^3 - x_1x_2^3 - y_1y_2^3 \end{pmatrix}$$

$$\mathbf{g}_7 = \begin{pmatrix} 2x_1^2x_2^2 - y_1^2y_2^2 - z_1^2z_2^2 & 0 & 0 \\ 0 & 2y_1^2y_2^2 - x_1^2x_2^2 - z_1^2z_2^2 & 0 \\ 0 & 0 & 2z_1^2z_2^2 - x_1^2x_2^2 - y_1^2y_2^2 \end{pmatrix}$$

$$\mathbf{g}_8 = \begin{pmatrix} 2x_1^3x_2 - y_1^3y_2 - z_1^3z_2 & 0 & 0 \\ 0 & 2y_1^3y_2 - x_1^3x_2 - z_1^3z_2 & 0 \\ 0 & 0 & 2z_1^3z_2 - x_1^3x_2 - y_1^3y_2 \end{pmatrix}$$

$$
\begin{aligned}
\mathbf{g}_9 &= \begin{pmatrix} 0 & z_1 & y_1 \\ z_1 & 0 & x_1 \\ y_1 & x_1 & 0 \end{pmatrix} \\
\mathbf{g}_{10} &= \begin{pmatrix} 0 & x_1y_1 & x_1z_1 \\ x_1y_1 & 0 & y_1z_1 \\ x_1z_1 & y_1z_1 & 0 \end{pmatrix} \\
\mathbf{g}_{11} &= \begin{pmatrix} 0 & z_1^3 & y_1^3 \\ z_1^3 & 0 & x_1^3 \\ y_1^3 & x_1^3 & 0 \end{pmatrix} \\
\mathbf{g}_{12} &= \begin{pmatrix} 0 & z_2 & y_2 \\ z_2 & 0 & x_2 \\ y_2 & x_2 & 0 \end{pmatrix} \\
\mathbf{g}_{13} &= \begin{pmatrix} 0 & x_2y_2 & x_2z_2 \\ x_2y_2 & 0 & y_2z_2 \\ x_2z_2 & y_2z_2 & 0 \end{pmatrix} \\
\mathbf{g}_{14} &= \begin{pmatrix} 0 & z_2^3 & y_2^3 \\ z_2^3 & 0 & x_2^3 \\ y_2^3 & x_2^3 & 0 \end{pmatrix} \qquad \text{(10b)} \\
\mathbf{g}_{15} &= \begin{pmatrix} 0 & x_1y_2 + x_2y_1 & x_1z_2 + x_2z_1 \\ x_1y_2 + x_2y_1 & 0 & y_1z_2 + y_2z_1 \\ x_1z_2 + x_2z_1 & y_1z_2 + y_2z_1 & 0 \end{pmatrix} \\
\mathbf{g}_{16} &= \begin{pmatrix} 0 & x_1x_2^2 & y_1y_2^2 \\ x_1x_2^2 & 0 & z_1z_2^2 \\ y_1y_2^2 & z_1z_2^2 & 0 \end{pmatrix} \\
\mathbf{g}_{17} &= \begin{pmatrix} 0 & x_1^2x_2 & y_1^2y_2 \\ x_1^2x_2 & 0 & z_1^2z_2 \\ y_1^2y_2 & z_1^2z_2 & 0 \end{pmatrix} \\
\mathbf{g}_{18} &= \begin{pmatrix} a-2b & 0 & 0 \\ 0 & a+b & 0 \\ 0 & 0 & b-2a \end{pmatrix} \\
\mathbf{g}_{19} &= \begin{pmatrix} a^2+2ab-2b^2 & 0 & 0 \\ 0 & a^2-4ab+b^2 & 0 \\ 0 & 0 & b^2+2ab-2a^2 \end{pmatrix}.
\end{aligned}
$$

4 Symmetry-adapted coordinates

Symmetry-adapted coordinates are coordinates of a vector space on which a representation of a molecular symmetry group acts. Usually, irreducible representations are considered in JT theory. The first step in the formal derivation of symmetry-adapted coordinates is the definition of a set SALCs in a suitable basis. SALCs form the basis functions of the vector space associated with the symmetry-adapted coordinates. Valid SALCs must be closed under the action of the group representation and the typical approach is to reduce a group representation w. r. t. internuclear distances to linear combinations that form SALCs of irreducible representations. An arbitrary point in a linear vector space is then given by the linear form (cf. Sec. 2.3)

$$L(\mathbf{s}, \mathbf{S}) = \langle \mathbf{s} \mid \mathbf{S} \rangle = \sum_{i}^{n} s_i S_i. \tag{11}$$

However the shape of molecules with more than three identical nuclei is not uniquely defined by the internuclear distances of their SALCs. Therefore, all calculations that require a transformation of symmetry to Cartesian coordinates must be performed with different (not rotation/reflection-invariant) basis functions. We used the usual symmetry labels of molecular point groups, first introduced by Mulliken [126].

4.1 X_4 molecules

The six internuclear distances of a homonuclear four-atomic molecules form a basis of a six-dimensional faithful representation Γ of the molecular symmetry group T_d. The representation Γ describes the full permutation symmetry of the of four identical nuclei and reduces to

$$\Gamma = A_1 \oplus E \oplus T_2. \tag{12}$$

Transforming the internuclear distances into a set of symmetry-adapted linear combinations (SALCs) as a basis of the irreducible representations A_1, E and T_2 yields

the coordinates:

$$
\begin{aligned}
s_1 &= \frac{1}{\sqrt{6}}(\Delta r_{12} + \Delta r_{43} + \Delta r_{13} + \Delta r_{24} + \Delta r_{14} + \Delta r_{23}) \\
s_a &= \frac{1}{2}(\Delta r_{13} + \Delta r_{24} - \Delta r_{14} - \Delta r_{23}) \\
s_b &= \frac{1}{2\sqrt{3}}(2\Delta r_{12} + 2\Delta r_{43} - \Delta r_{13} - \Delta r_{24} - \Delta r_{14} - \Delta r_{23}) \\
s_x &= \frac{1}{\sqrt{2}}(\Delta r_{12} - \Delta r_{34}) \\
s_y &= \frac{1}{\sqrt{2}}(\Delta r_{14} - \Delta r_{23}) \\
s_z &= \frac{1}{\sqrt{2}}(\Delta r_{13} - \Delta r_{24})
\end{aligned}
\tag{13}
$$

The irreducible representations in this basis are given by orthogonal matrices and form matrix groups of order 1, 6 and 24 for the A_1, E and T_2 representations, respectively. All these matrix representations occur in a number of different point groups, thus the formal aspects of the group theoretical treatment of JT problems apply to a wide range of molecules in various symmetry groups and with different definitions of symmetry coordinates. As an example, the matrices of the E representation are identical with the matrices of the E representation of the point group C_{3v} as well as with the E' representation of the D_{3h} molecular point group. In fact, the number of different irreducible representations, which are the objects of practical interest in JT problems, can be reduced to 14 for all 32 molecular point groups [46].

For the purpose of quantum dynamics in bound states, i. e. in the vicinity of the molecular equilibrium geometry, a set of SALCs in Cartesian coordinates is more appropriate. Firstly, the kinetic-energy operator has a particularly convenient (diagonal) form in symmetry-adapted Cartesian coordinates. This is an important simplification in consideration of an application in quantum dynamics. Additionally, the mapping between internuclear distances and the shape of the molecule, or more generally the geometry of four points in 3D space, is not unique [64]. Consequently, *ab initio* calculations which rely on the Cartesian coordinates can not be performed along all degrees of freedom using internuclear distances. The drawback of this choice is clearly the dependence of the coordinate system on a given reference geometry accompanied with the loss of invariance of the PE surface under overall rotations.

The construction of a set of SALCs in terms of Cartesian displacement vectors is easily accomplished with regard to Eq. (13). If the impact of the SALCs on a

single atom is examined, each symmetry-adapted displacement coordinate acts as a linear translation described by a Cartesian vector $\mathbf{r}$ whose magnitude is proportional to the respective symmetry coordinate. Let $\mathbf{r}_{ij}$ be the vector of unit length from nucleus i to nucleus j at the tetrahedral reference geometry.

$$\mathbf{r}_{ij} = \frac{\mathbf{r}_j - \mathbf{r}_i}{||\mathbf{r}_j - \mathbf{r}_i||} = -\mathbf{r}_{ji} \tag{14}$$

Symmetry-adapted linear combinations are now constructed by replacing the internuclear distances in Eq. (13) with the corresponding vectors and taking the sum over all vectors that involve the considered atom. The sign of the vector is determined by the index of the atom: If the vector points to the respective nucleus, i. e. the atom's index is the first, the sign must be inverted. As an example the impact of a displacement along s_b on nucleus 2 is analyzed. The terms in the definition of s_b that include the index 2 are $r_{12},\ r_{23}$ and r_{24}. Replacing those with the corresponding vectors and inverting the sign of r_{23} and r_{24} yields the sum

$$\frac{1}{2\sqrt{3}}\left(2\mathbf{r}_{12} + \mathbf{r}_{23} + \mathbf{r}_{24}\right) \tag{15}$$

and multiplication with a value d results in the displacement vector for atom 2 for the symmetry coordinate $s_b = d$. It is straight forward to find the complete set of Cartesian symmetry coordinates following these rules. Most conveniently the transformation to SALCs is written as a matrix-vector product.

$$\mathbf{A}\mathbf{s} + \mathbf{r}^{(0)} = \mathbf{r} \tag{16}$$

$$\mathbf{A} = \begin{pmatrix} -\frac{1}{\sqrt{6}}(\mathbf{r}_{12}+\mathbf{r}_{13}+\mathbf{r}_{14}) & \frac{1}{2}(\mathbf{r}_{14}-\mathbf{r}_{13}) & \frac{1}{2\sqrt{3}}(-2\mathbf{r}_{12}+\mathbf{r}_{13}+\mathbf{r}_{14}) & -\frac{1}{2}\mathbf{r}_{12} & -\frac{1}{2}\mathbf{r}_{14} & -\frac{1}{2}\mathbf{r}_{13} \\ \frac{1}{\sqrt{6}}(\mathbf{r}_{12}-\mathbf{r}_{23}-\mathbf{r}_{24}) & \frac{1}{2}(\mathbf{r}_{23}-\mathbf{r}_{24}) & \frac{1}{2\sqrt{3}}(2\mathbf{r}_{12}+\mathbf{r}_{23}+\mathbf{r}_{24}) & \frac{1}{2}\mathbf{r}_{12} & \frac{1}{2}\mathbf{r}_{14} & \frac{1}{2}\mathbf{r}_{13} \\ \frac{1}{\sqrt{6}}(\mathbf{r}_{13}+\mathbf{r}_{23}-\mathbf{r}_{34}) & \frac{1}{2}(\mathbf{r}_{13}-\mathbf{r}_{23}) & \frac{1}{2\sqrt{3}}(-2\mathbf{r}_{34}-\mathbf{r}_{13}-\mathbf{r}_{23}) & \frac{1}{2}\mathbf{r}_{34} & -\frac{1}{2}\mathbf{r}_{23} & \frac{1}{2}\mathbf{r}_{13} \\ \frac{1}{\sqrt{6}}(\mathbf{r}_{14}+\mathbf{r}_{24}+\mathbf{r}_{34}) & \frac{1}{2}(\mathbf{r}_{24}-\mathbf{r}_{14}) & \frac{1}{2\sqrt{3}}(2\mathbf{r}_{34}-\mathbf{r}_{14}-\mathbf{r}_{24}) & -\frac{1}{2}\mathbf{r}_{34} & \frac{1}{2}\mathbf{r}_{14} & -\frac{1}{2}\mathbf{r}_{24} \end{pmatrix}$$

$$\mathbf{s} = \begin{pmatrix} s_1 & s_a & s_b & s_x & s_y & s_z \end{pmatrix}^{\mathsf{T}}$$

$$\mathbf{r}^{(0)} = \mathbf{r}_1^{(0)} \oplus \mathbf{r}_2^{(0)} \oplus \mathbf{r}_3^{(0)} \oplus \mathbf{r}_4^{(0)}$$

$$\mathbf{r} = \mathbf{r}_1 \oplus \mathbf{r}_2 \oplus \mathbf{r}_3 \oplus \mathbf{r}_4$$

In Eq. (16) $\mathbf{s}$ denotes a vector of six symmetry coordinates, $\mathbf{r}^{(0)}$ is the direct sum of the Cartesian coordinate vectors at the reference geometry and $\mathbf{r}$ corresponds to

the displaced Cartesian coordinates of all four nuclei, also written as a direct sum.

The columns in the 12×6 matrix $\mathbf{A}$ are the normalized eigenvectors of the Hessian matrix of any homonuclear tetrahedral (X_4) molecule. The pseudo-inverse of $\mathbf{A}$ is the transposed matrix $\mathbf{A}^\mathsf{T}$

$$\mathbf{A}^\mathsf{T}\mathbf{A} = \mathbf{I}_6 \tag{17}$$

and $\mathbf{I}_6$ denotes the identity matrix of rank 6. Moreover, the SALCs defined by Eq. (16) are closely related to the normal modes of the molecule. Depending on the specific set of normal modes (mass weighted, dimensionless etc.), each normal mode is related to the symmetry coordinate s_i of the same symmetry by a scaling factor. In contrast, the transformation between Cartesian normal modes and internuclear distances as they appear in Eq. (13) is non-linear and in general not invertible. In regard to the discrete grid representation of a wave-packet in quantum dynamics which is usually defined by the coordinates of the kinetic-energy operator (i. e. normal modes in our approach) it is therefore favorable to use Cartesian symmetry coordinates according to Eq. (16).

4.2 YX_4 molecules

In YX_4 molecules, there are four Y-X bonds which form a standard basis of the S_4 group (the bond lengths do not depend on each other and are directly related to the permutation of X-atoms). The four Y-X bonds and the six X-X distances (or X-Y-X angles) form the basis of a 10 dimensional reducible representation Γ of T_d. In what follows, these are labeled as r_i $i = 1, 2, 3, 4$ for the Y-X_i and r_{ij} $i, j = 1, \ldots, 4;\ j < i$ for the X_j-X_i distances. Clearly the sets r_i and r_{ij} belong to separate orbits under the transformations of the symmetric group S_4 and, therefore, can be treated as independent four- and six-dimensional vector spaces Γ_4 and Γ_6. The decomposition into irreducible representations reads

$$\Gamma = 2A_1 \oplus E \oplus 2T_2 \tag{18}$$

$$\Gamma_4 = A_1 \oplus T_2 \tag{19}$$

$$\Gamma_6 = A_1 \oplus E \oplus T_2. \tag{20}$$

Hence, the 10-dimensional representation Γ is decomposed into five irreducible representations. Accordingly, the basis of internuclear distances is transformed into 10 SALCs for $3N - 6 = 9$ independent degrees of freedom.

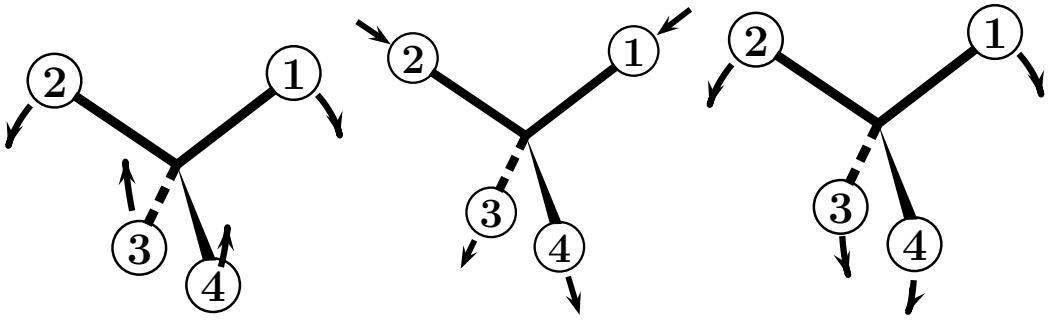

Figure 1: Symmetry-adapted displacements of E (left), T_2 stretch (center) and T_2 bend (right) type in tetrahedral YX_4 molecules. If the Cartesian z-axis is aligned along the vertical quenching/stretching direction, the shown displacements correspond to the SALCs S_{2a}, S_{3z}, S_{4z}, respectively.

The symmetry coordinates of YX_4 molecules and in particular for methane have been discussed by several authors [44, 57, 63, 64, 127]. For the stretching coordinates we use the well-known symmetry adapted linear combinations (SALCs). Applying projection operators to a basis of displacements along the CH bond-lengths (CH_i=r_i) yields the coordinates

$$\begin{aligned} \phi_1 &= 3\Delta r_1 - \Delta r_2 - \Delta r_3 - \Delta r_4 & \phi_2 &= 3\Delta r_2 - \Delta r_1 - \Delta r_3 - \Delta r_4 \\ \phi_3 &= 3\Delta r_3 - \Delta r_1 - \Delta r_2 - \Delta r_4 & \phi_4 &= 3\Delta r_4 - \Delta r_1 - \Delta r_2 - \Delta r_3 \end{aligned} \tag{21}$$

which are transformed to an orthonormal basis by a unitary transformation [44].

$$\mathbf{A}^{\mathrm{CH}} = \frac{1}{2}\begin{pmatrix} 1 & 1 & 1 & 1 \\ -1 & 1 & -1 & 1 \\ 1 & -1 & -1 & 1 \\ -1 & -1 & 1 & 1 \end{pmatrix} \tag{22}$$

$$\mathbf{s} = \mathbf{A}^{\mathrm{CH}}\boldsymbol{\phi} \tag{23}$$

$$\begin{aligned} s_1 &= \frac{1}{2}\left(\Delta r_1 + \Delta r_2 + \Delta r_3 + \Delta r_4\right) \\ s_{3x} &= \frac{1}{2}\left(-\Delta r_1 + \Delta r_2 - \Delta r_3 + \Delta r_4\right) \\ s_{3y} &= \frac{1}{2}\left(\Delta r_1 - \Delta r_2 - \Delta r_3 + \Delta r_4\right) \\ s_{3z} &= \frac{1}{2}\left(-\Delta r_1 - \Delta r_2 + \Delta r_3 + \Delta r_4\right) \end{aligned} \tag{24}$$

The Δr_i terms are defined as

$$\Delta r_i = \left|\left| r_i - r_i^{(0)} \right|\right| \tag{25}$$

and describe the elongation or contraction of the i th CH bond with respect to the bond length at a reference geometry $r_i^{(0)}$. The displacements are illustrated in Fig. 1. It should be noted that the signs in the expression (24) depend on the numbering of the hydrogen atoms.

The remaining six SALCs are obtained by the linear transformation

$$\mathbf{A}^{\mathrm{HH}} = \begin{pmatrix} \frac{1}{\sqrt{6}} & \frac{1}{\sqrt{6}} & \frac{1}{\sqrt{6}} & \frac{1}{\sqrt{6}} & \frac{1}{\sqrt{6}} & \frac{1}{\sqrt{6}} \\ \frac{1}{\sqrt{3}} & -\frac{1}{2\sqrt{3}} & -\frac{1}{2\sqrt{3}} & -\frac{1}{2\sqrt{3}} & -\frac{1}{2\sqrt{3}} & \frac{1}{\sqrt{3}} \\ -\frac{1}{2\sqrt{3}} & \frac{1}{\sqrt{3}} & -\frac{1}{2\sqrt{3}} & -\frac{1}{2\sqrt{3}} & \frac{1}{\sqrt{3}} & -\frac{1}{2\sqrt{3}} \\ 0 & \frac{1}{\sqrt{2}} & 0 & 0 & -\frac{1}{\sqrt{2}} & 0 \\ 0 & 0 & -\frac{1}{\sqrt{2}} & -\frac{1}{\sqrt{2}} & 0 & 0 \\ \frac{1}{\sqrt{2}} & 0 & 0 & 0 & 0 & -\frac{1}{\sqrt{2}} \end{pmatrix} \tag{26}$$

of the six internuclear distances between the hydrogen atoms. The corresponding coordinates, in terms of displacements from the equilibrium geometry, are

$$\begin{aligned} \Delta r_{ij} &= ||\mathbf{r}_i - \mathbf{r}_j|| - \left|\left| \mathbf{r}_i^{(0)} - \mathbf{r}_j^{(0)} \right|\right| \\ (s_0, s_{2a}, s_{2b}, s_{4x}, s_{4y}, s_{4z})^{\mathsf{T}} &= \mathbf{A}^{\mathrm{HH}} (\Delta r_{21}, \Delta r_{31}, \Delta r_{41}, \Delta r_{32}, \Delta r_{42}, \Delta r_{43})^{\mathsf{T}}. \end{aligned} \tag{27}$$

It turned out, however, that specifically the bending coordinates associated with the six internuclear distances (or angles) of the hydrogen atoms lead to deficiencies in the description of nuclear geometries [57, 63, 64]. Most importantly, the standard symmetry coordinates in terms of internuclear distances or valence angles do not uniquely determine the shape of the molecule and therefore no unique transformation from symmetry to Cartesian coordinates exists. Since the ambiguous points are in general not energetically degenerate we introduce an alternative set of symmetry coordinates based on infinitesimal rotations in order to map a set of symmetry coordinates unambiguously to a molecular geometry. This is essential for all *ab initio* calculations and leads to "well-shaped" PE surfaces for polynomial approximations in a diabatic representation. The same coordinates were also used to construct PE surfaces for the six-dimensional $T_2 \times t_2 + t_2$ and $T_2 \times e$ subproblems as a proof-of-concept.

The bending motions in a YX_4 molecule are expressed with respect to SALCs of a_1, e and t_2 symmetry, where "of Γ symmetry" is used synonymously to "forms a basis of the irreducible representation Γ". Assuming fixed values for the stretching coordinates, the four X atoms within a centrally connected YX_4 molecule can be considered to move on the surface of a sphere. Displacements of the X atoms along the bending coordinates are thus conveniently described as rotations of the position vectors in three-dimensional Euclidean space.

Let $\mathbf{v}_{ij}$ be the normalized vector product of the position vectors $\mathbf{X}_i^{(0)}$ and $\mathbf{X}_j^{(0)}$ at the tetrahedral reference geometry:

$$\mathbf{v}_{ij} = \frac{\mathbf{X}_i^{(0)} \times \mathbf{X}_j^{(0)}}{\left\| \mathbf{X}_i^{(0)} \times \mathbf{X}_j^{(0)} \right\|_2} \qquad \mathbf{v}_{ij} = -\mathbf{v}_{ji} \tag{28}$$

Using the permutation (anti-) symmetry, the complete set for a five-atomic tetrahedral molecule comprises six (not linearly independent) elements. The vectors $\mathbf{v}_{ij}$ are now used to define a basis of rotation vectors that act on the four X atoms and describe symmetry adapted displacements in the infinitesimal limit.

$$\begin{aligned}
\mathbf{w}_1 &= (s_{4z} + s_{2a})\mathbf{v}_{21} + (s_{4x} + s_{2b})\mathbf{v}_{31} - s_{4y}\mathbf{v}_{41} \\
\mathbf{w}_2 &= -(s_{4z} + s_{2a})\mathbf{v}_{21} + s_{4y}\mathbf{v}_{32} + (s_{2b} - s_{4x})\mathbf{v}_{42} \\
\mathbf{w}_3 &= -s_{4y}\mathbf{v}_{32} - (s_{4x} + s_{2b})\mathbf{v}_{31} + (s_{2a} - s_{4z})\mathbf{v}_{43} \\
\mathbf{w}_4 &= (s_{4x} - s_{2b})\mathbf{v}_{42} + s_{4y}\mathbf{v}_{41} + (s_{4z} - s_{2a})\mathbf{v}_{43},
\end{aligned} \tag{29}$$

where s_{4x}, s_{4y}, s_{4z} and s_{2a}, s_{2b} are coordinates of T_2 and E symmetry, respectively (see Fig. 1). In what follows, it is essential to distinguish between symmetry adapted basis functions and the corresponding coordinates since it is convenient for tetrahedral systems to express the coordinates of E symmetry in a non-orthogonal basis. To clarify this we use the capital-letter S to denote SALCs of basis functions and the lowercase-letter s for the dual space of symmetry coordinates.

The vectors $\mathbf{w}_i$ define the displacements as sums of symmetry-adapted infinitesimal rotations and completely separate overall rotations of the molecule, since

$$\sum_i \mathbf{w}_i = 0 \tag{30}$$

for arbitrary values of the symmetry coordinates. It is straightforward to verify the symmetry properties under permutation of like nuclei.

An explicit rotation matrix is obtained from SALCs of rotation vectors by Rodriguez' formula, where the magnitude of displacement α_i is given by the 2-norm of the rotation vector ($\alpha_i = \|\mathbf{w}_i\|_2$).

$$\mathbf{X}_i = \mathbf{X}_i^{(0)} \cos\alpha_i + (\mathbf{w}_i \times \mathbf{X}_i^{(0)}) \sin\alpha_{ij} + \mathbf{w}_i(\mathbf{w}_i \cdot \mathbf{X}_i^{(0)})(1 - \cos\alpha_i) \qquad (31)$$

The actual displacements are thus accomplished by four rotation matrices which depend on the symmetry adapted coordinates and a reference geometry. This permits the calculation of cuts along specific symmetry coordinates, whereas e. g. the stretching coordinates remain at fixed values and the bending coordinates are varied.

5 Elements of the $T_2 \times t_2$ and $T_2 \times (t_2 + t_2)$ JT PE matrices

tot. deg.	2	3	4	5	6	7	8	9
x	2 0	1	4 2 0 0	3 1	6 4 2 2 0 0	5 3 1 1	8 6 4 4 2 2 0 0 0	7 5 3 3 1 1
yz	0 0	1	0 0 2 0	1 1	0 0 2 0 2 0	1 1 3 1	0 0 2 0 2 0 4 2 0	1 1 3 1 3 1
$y^2 + z^2$	0 1	0	0 1 0 2	0 1	0 1 0 2 1 3	0 1 0 2	0 1 0 2 1 3 0 2 4	0 1 0 2 1 3

tot. deg.	10	11	12
x	10 8 6 6 4 4 2 2 2 0 0 0	9 7 5 5 3 3 1 1 1	12 10 8 8 6 6 4 4 4 2 2 2 0 0 0 0
yz	0 0 2 0 2 0 4 2 0 4 2 0	1 1 3 1 3 1 5 3 1	0 0 2 0 2 0 4 2 0 4 2 0 6 4 2 0
$y^2 + z^2$	0 1 0 2 1 3 0 2 4 1 3 5	0 1 0 2 1 3 0 2 4	0 1 0 2 1 3 0 2 4 1 3 5 0 2 4 6

Table 1: Powers of polynomial factors in the expansion terms of the diagonal element h_{11} of the PE matrix up to 12 th order. The matrix elements h_{22} and h_{33} are obtained by permuting x and y or x and z, respectively. The table header indicates the total degree of the polynomial.

tot. deg.	1	2	3		4		5				6				7						8						9								
x	1	0	3	1	2	0	5	3	1	1	4	2	0	0	7	5	3	3	1	1	6	4	2	2	0	0	9	7	5	5	3	3	1	1	1
yz	0	1	0	0	1	1	0	0	2	0	1	1	3	1	0	0	2	0	2	0	1	1	3	1	3	1	0	0	2	0	2	0	4	2	0
$y^2 + z^2$	0	0	0	1	0	1	0	1	0	2	0	1	0	2	0	1	0	2	1	3	0	1	0	2	1	3	0	1	0	2	1	3	0	2	4

tot. deg.	10										11											12												
x	8	6	4	4	2	2	0	0	0		11	9	7	7	5	5	3	3	3	1	1	1	10	8	6	6	4	4	2	2	2	0	0	0
yz	1	1	3	1	3	1	5	3	1		0	0	2	0	2	0	4	2	0	4	2	0	1	1	3	1	3	1	5	3	1	5	3	1
$y^2 + z^2$	0	1	0	2	1	3	0	2	4		0	1	0	2	1	3	0	2	4	1	3	5	0	1	0	2	1	3	0	2	4	1	3	5

Table 2: Powers of polynomial factors in expansion terms of the off-diagonal element h_{23} of the PE matrix up to 12 th order. The matrix elements h_{13} and h_{12} are obtained by permuting x and y or x and z, respectively.

tot. deg.	2		3			4														
x_1	1	0	1	1	0	0	3	2	2	2	1	1	1	1	0	0	0	0	0	0	0	0
$y_1 z_1$	0	0	0	0	1	0	0	0	0	0	0	0	0	0	1	1	0	0	0	0	0	0
$y_1^2 + z_1^2$	0	0	0	0	0	0	0	0	0	0	1	0	0	0	0	0	1	1	1	0	0	0
x_2	1	0	0	0	1	1	1	2	0	0	1	3	1	1	0	0	2	0	0	2	0	0
$y_2 z_2$	0	0	1	0	0	0	0	0	0	0	0	0	0	0	1	0	0	0	0	0	1	0
$y_2^2 + z_2^2$	0	0	0	0	0	0	0	0	1	0	0	0	1	0	0	0	0	1	0	0	0	1
$y_1 z_2 + z_1 y_2$	0	0	0	1	0	1	0	0	0	0	0	0	0	0	1	0	0	0	0	1	0	0
$y_1 y_2 + z_1 z_2$	0	1	0	0	0	0	0	0	0	1	0	0	0	1	0	0	0	0	1	1	0	1

Table 3: Diagonal matrix element h_{11} as products of powers of generating polynomials for two t_2 coordinate vectors. The matrix elements h_{22} and h_{33} are obtained by permuting $(x_1, x_2) \leftrightarrow (y_1, y_2)$ or $(x_1, x_2) \leftrightarrow (z_1, z_2)$, respectively.

tot. deg.	2	3					4													
x_1	0	2	1	1	1	0	0	2	2	1	1	1	0	0	0	0	0	0	0	0
$y_1 z_1$	0	0	0	0	0	0	0	0	0	1	0	0	1	1	1	0	0	0	0	0
$y_1^2 + z_1^2$	0	0	0	0	0	1	0	0	0	0	0	0	0	0	0	1	1	0	0	0
x_2	0	1	2	0	0	1	1	0	0	1	1	1	2	0	0	0	0	2	0	0
$y_2 z_2$	0	0	0	0	0	0	0	1	0	0	1	0	0	0	0	1	0	0	1	0
$y_2^2 + z_2^2$	0	0	0	1	0	0	0	0	0	0	0	0	1	0	0	1	0	0	1	
$y_1 z_2 + z_1 y_2$	1	0	0	0	0	0	0	0	1	0	0	1	0	0	0	0	0	1	0	1
$y_1 y_2 + z_1 z_2$	0	0	0	0	1	0	1	0	0	0	0	0	0	0	1	0	0	0	1	0

Table 4: Off-diagonal element h_{23} in the PE expansion as products of powers of generating polynomials for two t_2 coordinate vectors. The matrix elements h_{13} and h_{12} are obtained by permuting $(x_1, x_2) \leftrightarrow (y_1, y_2)$ or $(x_1, x_2) \leftrightarrow (z_1, z_2)$, respectively.

6 Convoluted Jahn-Teller spectra of CH_4^+

A crude approximation of the overall multi-mode JT vibronic spectrum can be obtained as a convolution of the $T_2 \times t_2$ (bending), $T_2 \times t_2$ (stretching) and $T_2 \times e$ vibronic spectra. This approximation is tantamount to the neglect of the commutators of the partial JT Hamiltonians. While this approximation is rather crude, the convoluted spectrum gives an indication of the expected line density and the width of the bandshape. The single totally symmetric stretching mode of CH_4^+ is not included in this simulation. For comparison, the experimental photoelectron spectrum of CH_4 from Ref. [23] is shown in Fig. 3.

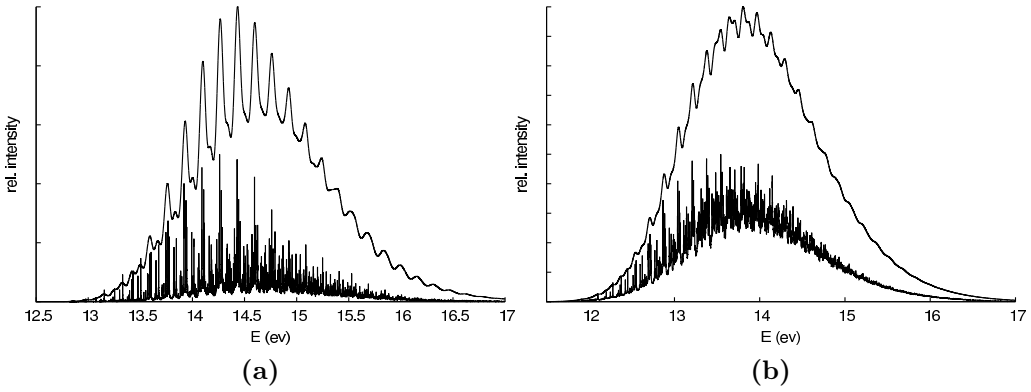

Figure 2: Convoluted $[T_2 \times e] \otimes [T_2 \times t_2]$ JT spectrum of CH_4^+ in the bending normal modes (left) and $[T_2 \times e] \otimes [T_2 \times t_2] \otimes [T_2 \times t_2]$ spectrum (right).

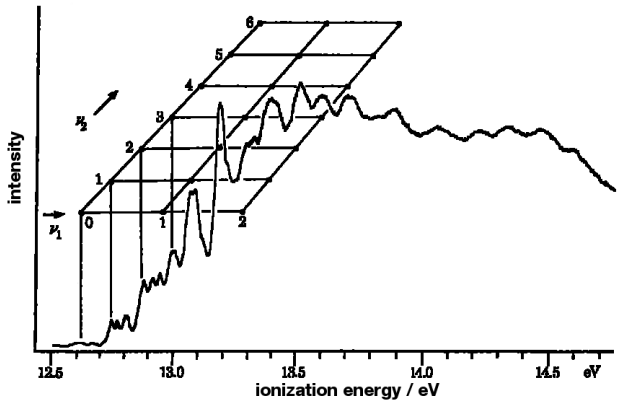

Figure 3: Experimental photoelectron spectrum of CH_4 (from Ref. [23]).

Bibliography

[1] M. Born and R. Oppenheimer, Ann. Phys. **389**, 457 (1927).

[2] M. Born and K. Huang, *Dynamical Theory of Crystal Lattices*, 2nd ed. (Clarendon Press, Oxford, 1962).

[3] H. A. Jahn and E. Teller, Proc. Roy. Soc. A **161**, 220 (1937).

[4] H. A. Jahn, Proc. Roy. Soc. A **164**, 117 (1938).

[5] I. B. Bersuker, *The Jahn-Teller Effect* (Cambridge University Press, Cambridge, UK, 2006).

[6] H. Köppel, L. S. Cederbaum, and S. Mahapatra, in *Handbook of High-resolution Spectroscopy*, edited by M. Quack and F. Merkt (Wiley, New York, 2011).

[7] I. B. Bersuker, Chem. Rev. **101**, 1067 (2001).

[8] B. E. Applegate, T. A. Barckholtz, and T. A. Miller, Chem. Soc. Rev. **32**, 38 (2003).

[9] *The Jahn-Teller Effect: Fundamentals and Implications for Physics and Chemistry*, edited by H. Köppel, D. R. Yarkony, and H. Barentzen (Springer, Berlin, 2010).

[10] *Conical Intersections: Electronic Structure, Dynamics & Spectroscopy*, edited by W. Domcke, D. R. Yarkony, and H. Köppel (World Scientific, Singapore, 2004).

[11] H. Köppel, W. Domcke, and L. S. Cederbaum, Adv. Chem. Phys. **57**, 59 (1984).

[12] T. A. Barckholtz and T. A. Miller, J. Phys. Chem. A **103**, 2321 (1999).

[13] U. Höper, P. Botschwina, and H. Köppel, J. Chem. Phys. **112**, 4132 (2000).

[14] T. Ichino, S. W. Wren, K. M. Vogelhuber, A. J. Gianola, W. C. Lineberger, and J. F. Stanton, J. Chem. Phys. **129**, 084310 (2008).

[15] J. J. Dillon and D. R. Yarkony, J. Chem. Phys. **131**, 134303 (2009).

[16] S. Mahapatra, L. S. Cederbaum, and H. Köppel, J. Chem. Phys. **111**, 10452 (1999).

[17] H. Köppel, M. Döscher, I. Bâldea, H.-D. Meyer, and P. G. Szalay, J. Chem. Phys. **117**, 2657 (2002).

[18] A. Viel and W. Eisfeld, J. Chem. Phys. **120**, 4603 (2004).

[19] R. Dixon, Mol. Phys. **20**, 113 (1971).

[20] D. Opalka and W. Domcke, J. Chem. Phys. **132**, 154108 (2010).

[21] D. Opalka and W. Domcke, Chem. Phys. Lett. **494**, 134 (2010).

[22] J. W. Rabalais, T. Bergmark, L. O. Werme, L. Karlsson, and K. Siegbahn, Phys. Scr. **3**, 13 (1971).

[23] A. W. Potts and W. C. Price, Proc. Roy. Soc. A **326**, 165 (1972).

[24] R. Signorell and F. Merkt, J. Chem. Phys. **110**, 2309 (1999).

[25] H. J. Wörner and F. Merkt, Angew. Chem. Int. Ed. **48**, 6404 (2009).

[26] A. J. Millis, B. I. Shraiman, and R. Mueller, Phys. Rev. Lett. **77**, 175 (1996).

[27] M. Baldini, V. V. Struzhkin, A. F. Goncharov, P. Postorino, and W. L. Mao, Phys. Rev. Lett. **106**, 066402 (2011).

[28] A. F. Hebard, M. J. Rosseinsky, R. C. Haddon, D. W. Murphy, S. H. Glarum, T. T. M. Palstra, A. P. Ramirez, and A. R. Kortan, Nature **350**, 600 (1991).

[29] L. Bogani and W. Wernsdorfer, Nature Materials **7**, 179 (2008).

[30] B. Tsukerblat, S. Klokishner, and A. Palii, in *The Jahn-Teller Effect: Fundamentals and Implications for Physics and Chemistry*, edited by H. Köppel, D. R. Yarkony, and H. Barentzen (Springer, Berlin, 2010) pp. 555–619.

[31] W. Domcke, S. Mishra, and L. V. Poluyanov, Chem. Phys. **322**, 405 (2006).

[32] L. V. Poluyanov and W. Domcke, J. Chem. Phys. **129**, 224102 (2008).

[33] L. V. Poluyanov and W. Domcke, Chem. Phys. **374**, 86 (2010).

[34] S. Elbel, J. Kudnig, M. Grodzicki, and H. J. Lempka, Chem. Phys. Lett. **109**, 312 (1984).

[35] J. M. Dyke, S. Elbel, A. Morris, and J. C. H. Stevens, J. Chem. Soc., Faraday Trans. 2 **82**, 637 (1986).

[36] J. M. Dyke, A. Morris, and J. C. H. Stevens, Chem. Phys. **102**, 29 (1986).

[37] L.-S. Wang, B. Niu, Y. T. Lee, D. A. Shirley, E. Ghelichkhani, and E. R. Grant, J. Chem. Phys. **93**, 6318 (1990).

[38] L.-S. Wang, B. Niu, Y. T. Lee, D. A. Shirley, E. Ghelichkhani, and E. R. Grant, J. Chem. Phys. **93**, 6327 (1990).

[39] G. A. Worth and L. S. Cederbaum, Annu. Rev. Phys. Chem. **55**, 127 (2004).

[40] C. A. Mead and D. G. Truhlar, J. Chem. Phys. **77**, 6090 (1982).

[41] B. K. Kendrick, C. A. Mead, and D. G. Truhlar, Chem. Phys. Lett. **330**, 629 (2000).

[42] *Geometric Phases in Physics*, edited by A. Shapere and F. Wilczek (World Scientific, Singapore, 1989).

[43] B. K. Kendrick, in *Conical Intersections*, edited by W. Domcke, D. R. Yarkony, and H. Köppel (World Scientific, Singapore, 2004) pp. 521–553.

[44] F. A. Cotton, *Chemical Applications of Group Theory*, 3rd ed. (Wiley, New York, 1990).

[45] D. Gay and E. Ascher, Linear and Multilinear Algebra **18**, 91 (1985).

[46] E. Ascher and D. Gay, J. Phys. A: Math. Gen. **18**, 397 (1985).

[47] P. R. Bunker and P. Jensen, *Molecular Symmetry and Spectroscopy*, 2nd ed. (NRC Research Press, Ottawa, Ontario, Canada, 1998).

[48] H. Derksen and G. Kemper, *Computational Invariant Theory* (Springer, Berlin, 2002).

[49] E. Noether, Math. Ann. **77**, 89 (1915).

[50] H. Weyl, *The Classical Groups. Their Invariants and Representations* (Princeton Univ. Press, Princeton, 1946).

[51] T. Molien, Sitzungsber. König. Preuss. Akad. Wiss., 1152 (1897).

[52] N. J. A. Sloane, Am. Math. Mon. **84**, 82 (1977).

[53] A. Schmelzer and J. N. Murrell, Int. J. Quantum Chem. **28**, 287 (1985).

[54] A. G. McLellan, J. Phys. C: Solid State Phys. **7**, 3326 (1974).

[55] P. Cassam-Chenai and F. Patras, J. Math. Chem. **44**, 938 (2008).

[56] B. J. Braams and J. M. Bowman, Int. Rev. Phys. Chem. **28**, 577 (2009).

[57] M. A. Collins and D. F. Parsons, J. Chem. Phys. **99**, 6756 (1993).

[58] M. D. Neusel, *Invariant Theory*, Vol. 36 (AMS, Providence, RI, 2007).

[59] "GAP – Groups, Algorithms, and Programming, Version 4.4.12," (2008).

[60] G.-M. Greuel, G. Pfister, and H. Schönemann, "SINGULAR 3.0.4 — A computer algebra system for polynomial computations," (2007), http://www.singular.uni-kl.de.

[61] A. E. Heydtmann, "finvar.lib: A SINGULAR 3.0.4 library for computing invariant rings of finite groups," (2008).

[62] H. Weyl, *The Theory of Groups and Quantum Mechanics* (Dover Publications, New York, 1931).

[63] X.-G. Wang and T. Carrington, Jr., J. Chem. Phys. **118**, 6260 (2003).

[64] M. Boutin and G. Kemper, Adv. Appl. Math. **32**, 709 (2004).

[65] W. Heisenberg, Z. Phys. A **39**, 499 (1926).

[66] W. Pauli, Z. Phys. A **43**, 601 (1927).

[67] G. Breit, Phys. Rev. **34**, 553 (1929).

[68] H. A. Bethe and E. E. Salpeter, *Quantum Mechanics for One- and Two-Electron Atoms* (Springer, Berlin, 1957).

[69] P. A. M. Dirac, Proc. Roy. Soc. A **117**, 610 (1928).

[70] L. L. Foldy and S. A. Wouthuysen, Phys. Rev. **78**, 29 (1950).

[71] S. P. McGlynn, T. Azumi, and M. Kinoshita, *Molecular Spectroscopy of the Triplet State* (Prentice-Hall, Englewood Cliffs, N.J., 1969).

[72] A. Berning, M. Schweizer, H.-J. Werner, P. J. Knowles, and P. Palmieri, Mol. Phys. **98**, 1823 (2000).

[73] L. V. Poluyanov and W. Domcke, Chem. Phys. **352**, 125 (2008).

[74] P. Mondal, D. Opalka, L. V. Poluyanov, and W. Domcke, Chem. Phys. **387**, 56 (2011).

[75] E. P. Wigner, *Group Theory and its Application to the Quantum Mechanics of Atomic Spectra* (Academic Press, New York, 1959).

[76] H. A. Kramers, Koniklije Nederlandse Akademie van Wetenschapen **33**, 959 (1930).

[77] C. J. Bradley and A. P. Cracknell, *The Mathematical Theory of Symmetry in Solids* (Clarendon Press, Oxford, 1972).

[78] L. V. Poluyanov and W. Domcke, in *The Jahn-Teller Effect: Fundamentals and Implications for Physics and Chemistry*, edited by H. Köppel, D. R. Yarkony, and H. Barentzen (Springer, Berlin, 2010) pp. 77–97.

[79] D. J. Tannor, *Introduction to quantum mechanics: a time-dependent perspective* (University Science Books, Sausalito, 2006).

[80] J. P. Boyd, *Chebyshev and Fourier Spectral Methods*, 2nd ed. (Dover Publications, New York, 2001).

[81] H. Tal-Ezer and R. Kosloff, J. Chem. Phys. **81**, 3967 (1984).

[82] C. Leforestier, R. H. Bisseling, C. Cerjan, M. Feit, R. Friesner, A. Guldberg, A. Hammerich, G. Jolicard, W. Karrlein, H.-D. Meyer, N. Lipkin, O. Roncero, and R. Kosloff, J. Comput. Phys. **94**, 59 (1991).

[83] S. K. Gray, J. Chem. Phys. **96**, 6543 (1992).

[84] G. G. Balint-Kurti, Theor. Chem. Acc. **127**, 1 (2010).

[85] J. C. Light and T. Carrington, Adv. Chem. Phys. **114**, 263 (2000).

[86] E. T. Whittaker, Proc. Soc. Roy. Edinburgh **135**, 181 (1915).

[87] D. O. Harris, G. G. Engerholm, and W. D. Gwinn, J. Chem. Phys. **43**, 1515 (1965).

[88] J. Echave and D. C. Clary, Chem. Phys. Lett. **190**, 225 (1992).

[89] E. Anderson, Z. Bai, C. Bischof, S. Blackford, J. Demmel, J. Dongarra, J. Du Croz, A. Greenbaum, S. Hammarling, A. McKenney, and D. Sorensen, *LAPACK Users' Guide*, 3rd ed. (Society for Industrial and Applied Mathematics, Philadelphia, PA, 1999).

[90] D. W. Robinson, Math. Mag. **32**, 213 (1959).

[91] H. Aslaksen, S.-P. Chan, and T. Gulliksen, Appl. Algebra Eng. Comm. Comput. **7**, 53 (1996).

[92] A. Ceulemans, D. Beyens, and L. G. Vanquickenborne, J. Am. Chem. Soc. **106**, 5824 (1984).

[93] U. Öpik and M. H. L. Pryce, Proc. Roy. Soc. A **238**, 425 (1957).

[94] S. Muramatsu and T. Iida, J. Phys. Chem. Solids **31**, 2209 (1970).

[95] A. Ceulemans, J. Chem. Phys. **87**, 5374 (1987).

[96] J. Arents and L. C. Allen, J. Chem. Phys. **53**, 73 (1970).

[97] R. F. Frey and E. R. Davidson, J. Chem. Phys. **88**, 1775 (1988).

[98] M. N. Paddon-Row, D. J. Fox, J. A. Pople, K. N. Houk, and D. W. Pratt, J. Am. Chem. Soc. **107**, 7696 (1985).

[99] W. Meyer, J. Chem. Phys. **58**, 1017 (1973).

[100] L. B. Knight, J. Steadman, D. Feller, and E. R. Davidson, J. Am. Chem. Soc. **106**, 3700 (1984).

[101] H. J. Wörner, R. van der Veen, and F. Merkt, Phys. Rev. Lett. **97**, 173003 (2006).

[102] H. J. Wörner, X. Qian, and F. Merkt, J. Chem. Phys. **126**, 144305 (2007).

[103] T. H. Dunning, Jr., J. Chem. Phys. **90**, 1007 (1989).

[104] I. B. Bersuker and V. Polinger, *Vibronic Interactions in Molecules and Crystals* (Springer, Berlin, 1989).

[105] H. Koizumi, I. B. Bersuker, J. E. Boggs, and V. Z. Polinger, J. Chem. Phys. **112**, 8470 (2000).

[106] G. Bieri and L. Åsbrink, J. Electron Spectrosc. Relat. Phenom. **20**, 149 (1980).

[107] H.-D. Meyer, U. Manthe, and L. S. Cederbaum, Chem. Phys. Lett. **165**, 73 (1990).

[108] H. Wang and M. Thoss, J. Chem. Phys. **119**, 1289 (2003).

[109] D. Opalka, M. Segado, L. V. Poluyanov, and W. Domcke, Phys. Rev. A **81**, 042501 (2010).

[110] R. Meiswinkel and H. Köppel, Chem. Phys. Lett. **201**, 449 (1993).

[111] A. Wolf, M. Reiher, and B. A. Hess, in *Relativistic Electronic Structure Theory Part 1: Fundamentals*, edited by P. Schwerdtfeger (Elsevier, Amsterdam, 2002) Chap. 11, pp. 622–663.

[112] B. A. Hess and C. M. Marian, in *Computational Molecular Spectroscopy*, edited by P. Jensen and P. R. Bunker (Wiley, New York, 2000) Chap. 6, pp. 152–219.

[113] R. Englman, *The Jahn-Teller Effect in Molecules and Crystals* (Wiley, New York, 1972).

[114] M. D. Sturge, Solid State Phys. **20**, 91 (1967).

[115] H. Bethe, Ann. Phys. **395**, 133 (1929).

[116] M. Hamermesh, *Group Theory and Its Application to Physical Problems* (Addison-Wesley, Reading, UK, 1962).

[117] W. Moffitt and W. Thorson, Phys. Rev. **108**, 1251 (1957).

[118] B. O. Roos, Adv. Chem. Phys. **69**, 399 (1987).

[119] D. E. Woon and T. H. Dunning, J. Chem. Phys. **98**, 1358 (1993).

[120] B. Metz, H. Stoll, and M. Dolg, J. Chem. Phys. **113**, 2563 (2000).

[121] K. A. Peterson, J. Chem. Phys. **119**, 11099 (2003).

[122] H.-J. Werner, P. J. Knowles, R. Lindh, F. R. Manby, M. Schütz, P. Celani, T. Korona, A. Mitrushenkov, G. Rauhut, T. B. Adler, R. D. Amos, A. Bernhardsson, A. Berning, D. L. Cooper, M. J. O. Deegan, A. J. Dobbyn, F. Eckert, E. Goll, C. Hampel, G. Hetzer, T. Hrenar, G. Knizia, C. Köppl, Y. Liu, A. W. Lloyd, R. A. Mata, A. J. May, S. J. McNicholas, W. Meyer, M. E. Mura, A. Nicklass, P. Palmieri, K. Pflüger, R. Pitzer, M. Reiher, U. Schumann, H. Stoll, A. J. Stone, R. Tarroni, T. Thorsteinsson, M. Wang, and A. Wolf, "Molpro, version 2008.3, a package of ab initio programs," (2008), see http://www.molpro.net.

[123] J. C. Slonczewski, Phys. Rev. **131**, 1596 (1963).

[124] H. Köppel, E. Haller, L. S. Cederbaum, and W. Domcke, Mol. Phys. **41**, 669 (1980).

[125] F. S. Ham, Phys. Rev. **138**, A1727 (1965).

[126] R. S. Mulliken, J. Chem. Phys. **23**, 1997 (1955).

[127] J. Wilson, E. Bright, J. C. Decius, and P. C. Cross, *Molecular Vibrations* (Dover Publications, New York, 1955).

Acknowledgments

I would like to express my gratitude to the supervisor of this thesis, Prof. W. Domcke, for his scientific advice and support throughout this work. It is his personal merit that the "Institut für Theoretische Chemie" is such a pleasant environment for scientific work. I am also indebted to many friends and colleagues for inspiring conversations, which renders a complete list of honorary mentions virtually impossible. However I would like to make a special reference to Dr. Christoph Scheurer and Mrs. Ruth Mösch for many valuable discussions and their unbureaucratic administrative management.